Front. Mech. Eng. 2023, 18(2): 28
https://doi.org/10.1007/s11465-022-0744-9

REVIEW ARTICLE

Energy field-assisted high-speed dry milling green machining technology for difficult-to-machine metal materials

Jin ZHANG[a,b], Xuefeng HUANG[a,b], Xinzhen KANG[a,b], Hao YI[a,b], Qianyue WANG[a,b], Huajun CAO (✉)[a,b]

[a] *College of Mechanical and Vehicle Engineering, Chongqing University, Chongqing 400044, China*
[b] *State Key Laboratory of Mechanical Transmissions, Chongqing University, Chongqing 400044, China*

✉ *Corresponding author. E-mail: hjcao@cqu.edu.cn (Huajun CAO)*

ABSTRACT Energy field-assisted machining technology has the potential to overcome the limitations of machining difficult-to-machine metal materials, such as poor machinability, low cutting efficiency, and high energy consumption. High-speed dry milling has emerged as a typical green processing technology due to its high processing efficiency and avoidance of cutting fluids. However, the lack of necessary cooling and lubrication in high-speed dry milling makes it difficult to meet the continuous milling requirements for difficult-to-machine metal materials. The introduction of advanced energy-field-assisted green processing technology can improve the machinability of such metallic materials and achieve efficient precision manufacturing, making it a focus of academic and industrial research. In this review, the characteristics and limitations of high-speed dry milling of difficult-to-machine metal materials, including titanium alloys, nickel-based alloys, and high-strength steel, are systematically explored. The laser energy field, ultrasonic energy field, and cryogenic minimum quantity lubrication energy fields are introduced. By analyzing the effects of changing the energy field and cutting parameters on tool wear, chip morphology, cutting force, temperature, and surface quality of the workpiece during milling, the superiority of energy-field-assisted milling of difficult-to-machine metal materials is demonstrated. Finally, the shortcomings and technical challenges of energy-field-assisted milling are summarized in detail, providing feasible ideas for realizing multi-energy field collaborative green machining of difficult-to-machine metal materials in the future.

KEYWORDS difficult-to-machine metal material, green machining, high-speed dry milling, laser energy field-assisted milling, ultrasonic energy field-assisted milling, cryogenic minimum quantity lubrication energy field-assisted milling

1 Introduction

With continuous improvements in advanced manufacturing fields such as aerospace, rail transit, and clean energy equipment production, various high-performance alloys (e.g., nickel-based alloys, titanium alloys, and high-strength steels) are widely used. However, they are regarded as typical difficult-to-machine metal materials because of their good toughness, high strength, and excellent wear resistance, which pose a serious challenge to the high-performance manufacturing process of high-efficiency and precision machining [1–3].

Received July 13, 2022; accepted November 29, 2022

The poor machinability of difficult-to-machine metal materials is reflected in the following:

① Chemical level

For titanium alloys containing Ti, Mo, Cr, and V, highly chemically active metal elements can reduce machinability [4]. Furthermore, the α phase formed in the organization of the alloy structure is a hexagonal lattice structure, which increases cutting difficulty.

For nickel-based alloys, which exhibit a single austenite structure organization, Al, Ti, and other oxygen-friendly elements promote the oxidation of materials at high temperatures, resulting in tool adhesion. In addition, the strengthening phases (intermetallic compounds, borides, and carbides) in the alloy materials form hard particles, resulting in increased tool wear [5].

The contents of Cr, Mn, Si, Ni, and other elements are high in high-strength steel, which has a tempered martensite structure. Different v_c (cutting speed) values correspond to different chip morphologies and play a leading role in improving performance. The addition of Cr can change the hardness, strength, and toughness of steel; the presence of Mn can influence its hot machinability, and the addition of Si can improve its tensile and yield strength. The addition of Ni can simultaneously improve the strength and hardness of metal materials and increase the cutting force and processing energy consumption [6].

② Thermal conductivity

Compared with 45 steel, the thermal conductivity of titanium alloys is reduced by 80%, which can easily lead to plastic deformation in the shear zone and at high temperatures, thus aggravating tool wear and causing work hardening [7].

The thermal conductivity of nickel-based alloys is low, and heat aggregation during the processing of such alloys can easily occur, resulting in high local temperatures, which causes surface stress, a considerable temperature gradient in the workpiece, and a work-hardening problem [8].

The thermal conductivity of high-strength steel is low (only 40% of that of 45 steel), which hinders the transmission of the cutting heat, resulting in the phenomenon that the temperature of the tool-workpiece contact surface can be too high, thus leading to the work-hardening problem of the workpiece surface [9].

③ Cutting machinability

Titanium alloy cutting, which is a typical shear machining process, is inclined to produce large shear angles [10] and the 'negative shrinkage' phenomenon, which has a negative impact on the machining process. Compared with 45 steel, the machinability of titanium alloys is in the range of 0.15–0.5 [11].

Because of the increase in heat accumulation, cracks or burns on the surface of the workpiece can easily occur, which makes it difficult to ensure the quality and integrity of the machined surface during the cutting process of nickel-based alloys. Compared to 45 steel, the machinability of nickel-based alloys is less than 0.15 [12].

The plastic deformation of high-strength steel materials is large, and because of the severe friction during the machining process, it is easy to produce chip tumors. Furthermore, the uneven stress distribution causes severe tool tip wear, which leads to instability in the machining process and reduces the cutting efficiency. Compared with 45 steel, the machinability of high-strength steel is in the range of 0.5–0.65 [13].

High-speed cutting has the advantages of improving machining efficiency and reducing production costs and is also used in the field of difficult-to-machine metal materials [14–17]. Because the deformation zone of materials subjected to high-speed cutting is usually accompanied by strong strain, a high strain rate, and high temperatures [18–20], traditional cooling and lubrication of the cutting deformation zone by pouring cutting fluid is necessary during the cutting process [21,22]. Compared with conventional milling (CM), the friction between the workpiece and the tool is more intense in the high-speed milling process, and the time at which the deformation zone remains in a high-temperature state is longer. The heat of the cutting fluid is uneven, and local droplets can start boiling [23]. A large number of microbubbles are blocked by an oil film, resulting in an increase in the heat transfer resistance and a decrease in the heat exchange efficiency [24]. In addition, the extensive use of cutting fluid not only endangers the health of operators (cancer, asthma, and skin diseases) but also seriously pollutes the environment (air, soil, and water) and increases the economic cost of processing waste liquid and chips; the cost of cutting fluid from purchase to processing accounts for 16% to 30% of the total cost of manufacturing difficult-to-machine metal materials, which is much higher than the tool cost of only 7% [25–29]. Therefore, new green and low-carbon processing technologies that can replace pouring and cutting should be explored.

High-speed dry milling (HSDM) is regarded as a typical green and efficient machining technology because it not only improves the machining efficiency but also eliminates the use of cutting fluids [30–33]. The development of tool coatings and high-speed dry cutting machine tools has enabled the use of HSDM for machining [34–36]. Lu et al. [37] used coated tools for the HSDM of hardened steel and found that the cutting force decreased and the tool life increased. The Chongqing Machine Tool Group, jointly with Chongqing University, pioneered high-speed dry cutting machine tools such as YS3116CNC7 and Y3120CNC7, which improved the production efficiency of machine tools and reduced the manufacturing cost of workpieces [38]. Considering the inherent characteristics of difficult-to-machine metal materials, coupled with the high cutting speed and lack of cutting fluid necessary for cooling and lubrication in the HSDM manufacturing process, the friction between the tool and the workpiece and between the tool and the chip is extremely intense, resulting in an increase in the temperature of both the tool and workpiece, which affects the machining accuracy of the workpiece [39,40]. Consequently, the HSDM of difficult-to-machine metal materials can achieve the desired effect only in a specific process-feasible regime, and it is difficult to achieve full-condition adaptation [22]. Therefore, research on innovative HSDM processes is crucial.

Thermal-assisted machining (TAM) was proposed in the 1950s [41]. Its advantage is that preheating can not only reduce the ultimate strength of materials but also promote plastic deformation of hard materials during processing. The advantages of TAM also include improved manufacturing performance, machining

efficiency, and quality of difficult-to-machine metal materials by increasing the temperature of the cutting zone through an external heat source. Under ideal conditions, the shear band of the material instantaneously reaches the ideal temperature, and most of the heat is removed by the chip, thereby avoiding heat generation in the shear zone [42]. For the positive contribution of TAM technology to the cutting process, the heat source should be local, fast, and controllable. Lasers, induction coils, plasma, and oxyacetylene torches have been widely used [43–45]. Because improper selection of a heat source will lead to adverse changes in the microstructure after machining [46,47], researchers have mainly focused on the two commonly used heating methods of plasma and laser in machining. Considering that the laser has the advantages of a precise and controllable local area, no need for protective gas, and high spatial accessibility, it has emerged as the most promising auxiliary heat source for the processing of difficult-to-machine metal materials, and subsequent research has mainly focused on laser-assisted processing technology [42].

The implementation process of laser energy field-assisted milling (LAM) uses a laser to preheat the workpiece locally in advance to achieve material softening and change the material properties of the shear zone that is ready to be removed, which can improve the manufacturing performance of difficult-to-machine metal materials under temperature-assisted conditions [48]. At present, lasers widely used for difficult-to-machine metal materials mainly include carbon dioxide (CO_2) lasers, high-power semiconductor lasers (HPDL), and neodymium-doped yttrium aluminum garnet (Nd:YAG) lasers [42]. As each of the three lasers has its own merits, it is necessary to make reasonable choices according to the properties of the materials to be processed. After the material area to be removed is heated by laser assistance, the subsequent machining process can reduce the cutting force, prolong the tool life, improve the material removal rate, reduce cutting energy consumption, reduce manufacturing costs, and optimize the surface quality of the workpiece [49–51]. However, the difficulty of LAM machining is the precise control of the preheating temperature of the workpiece. Studies have shown that the laser power, heat source size, laser scanning speed, and heating position have a significant influence on the preheating temperature of the material [52,53]. Therefore, to obtain ideal results in the shear region of difficult-to-machine metal materials, laser energy field-assisted machining parameters should be reasonably selected [54].

The introduction of a laser energy field in CM machining prolongs the entire machining cycle, and ultrasonic vibration energy field-assisted milling (UVAM) with intermittent cutting characteristics can improve the material removal rate, which can compensate for the disadvantage of the long machining cycle of LAM. Therefore, UVAM is important. In the UVAM process, electrical signals are converted into ultrasonic frequency vibrations, which act along a certain direction on the workpiece or tool [55,56] to realize tool-workpiece separation so that the cutting area is periodically opened to ensure that the traditional cutting fluid enters the cutting area and provides rapid cooling at high temperatures [57]. Furthermore, during the processing of difficult-to-machine metal materials, the chip removes most of the heat, and ultrasonic separation can ensure rapid chip breaking [58–60], thereby avoiding the accumulation of heat on the tool and workpiece. UVAM also exhibits an acoustic softening effect [61]. In addition to the above advantages, UVAM can also reduce the cutting force [62,63], improve the material removal rate [64], optimize the surface quality of the workpiece [65,66], extend the tool life [67,68], reduce the manufacturing costs, and achieve green and low-carbon machining [69] by regularly changing the contact state between the workpiece and tool [70,71]. However, the vibration frequency and amplitude of UVAM significantly influence the machining process. Therefore, to maintain the advantages of UVAM, it is necessary to control the vibration frequency and amplitude reasonably.

The minimum quantity lubrication (MQL) technology can effectively solve the heat transfer problem of difficult-to-machine metal materials in HSDM. In 1997, Klocke and Eisenblätter [72] proposed an economical and environmentally friendly MQL technology. In this process, a very small amount of atomized droplets is sprayed into the cutting area with high-pressure gas for lubrication [73], and any cutting heat position is reached with the help of the trachea, which can effectively reduce the cutting force and cutting heat, prolong the tool life, and optimize the surface quality of the workpiece [74,75]. However, under some specific conditions, micro-lubrication technology has some shortcomings: When using MQL to assist in the high-speed cutting of difficult-to-machine metal materials, excessive heat production leads to the rupture of the lubricating oil film, resulting in insufficient cooling in the cutting area and lubrication failure [76,77]. In addition, the cooling performance of micro-lubrication technology with high-pressure atomization airflow is limited, and a performance gap remains between this technology and traditional pouring cutting [78,79]. Therefore, further research on MQL technology is needed.

Nanofluid minimum quantity lubrication (NMQL) technology is an enhancement of MQL technology that is realized by adding nanoparticles in proportion to the MQL fluid. Compared with ordinary MQL, the thermal conductivity of nanofluids is higher, which is due to the addition of nanoparticles with excellent antifriction and antiwear properties [80], thereby reducing the heat transfer resistance and improving the heat exchange efficiency and material removal rate. In addition, nanoparticles with small volumes undergo Brownian

motion in the base fluid, which can improve lubrication [81]. Compared to MQL, the lubrication advantages of NMQL have been confirmed in many studies [82–86]. However, when the cutting temperature is high (600–1000 °C), the heat transfer efficiency of the nanoparticles is still limited [87]. Although the cutting temperature is reduced for titanium alloys [88], nickel-based alloys [89], high-strength steel [90], and other difficult-to-machine metal materials, the range of the cooling amplitude is small, and defects such as burns and adhesion on the surface of the workpiece still occur. Therefore, the heat-exchange problem in the NMQL-assisted cutting process of difficult-to-cut materials remains.

Cryogenic technology is generally used to solve the problem of heat transfer in the cutting process by injecting a liquid/gaseous medium into the shear deformation zone [91]. Currently, the main cryogenic media used for difficult-to-machine metal materials include liquid nitrogen (LN_2) [92], liquid carbon dioxide (LCO_2) [93], supercritical carbon dioxide ($SCCO_2$) [94], and cold air (CA) [95]. Cryogenic processing can not only improve the material removal rate but also effectively prolong tool life [96]; thus, the cryogenic manufacturing cost is far lower than the traditional pouring processing cost [97,98]. Different temperature thresholds can be realized using different liquid/gaseous media to avoid insufficient cooling or excessive cooling hardening. However, the lubrication performance of cryogenic technology is insufficient, and its friction reduction and wear resistance characteristics must be improved [99].

In view of the high-performance manufacturing process of difficult-to-machine metal materials, the currently best-recognized method is the combination of the cryogenic cold medium, MQL (NMQL), and milling, which is referred to as cryogenic minimum quantity lubrication energy field-assisted milling (CMQLAM). CMQLAM not only reduces the temperature of the shear zone but also retains the lubrication ability of MQL (NMQL). Apart from being a green low-carbon technology, its advantages include adequate cooling, reducing cutting force, optimizing the surface quality of the workpiece, extending tool life, and reducing manufacturing costs [100–102]. Considering that the cryogenic medium type, gas pressure, and MQL flow rate affect the performance of CMQLAM, it is necessary to reasonably regulate these three parameters to obtain the optimal effect of CMQLAM. Figure 1 shows the overall structure of this review.

It has been widely reported that the processing performance of HSDM can be improved using LAM, UVAM, or CMQLAM alone. However, it is difficult to select an appropriate auxiliary process from multiple energy fields and to realize machining under various harsh conditions. Based on this, this paper reviews the latest research progress of energy-field-assisted green machining technology for difficult-to-machine metal materials; summarizes the operating mechanisms, technical difficulties, and application status of HSDM, LAM, UVAM, and CMQLAM for difficult-to-machine metal materials; and compares and analyzes the effects on cutting force, heat, chip morphology, tool life, specific cutting energy, material removal rate, and surface quality of titanium alloy, nickel-based alloy, and high-strength steel compared with traditional milling under energy-field-assisted conditions. The development direction of energy-field-assisted green machining technology is reported in this paper to provide a reference for multi-energy-field composite-assisted green machining technology.

2 HSDM of difficult-to-machine metal materials

Compared with CM pouring cutting, HSDM is a near-zero-emission green processing technology that eliminates the environmental pollution and occupational health hazards caused by cutting oil and avoids the cleaning process of cutting oil adhering to the surface of the workpiece and some iron chips. Under appropriate process conditions with high-performance coated tools, HSDM can reduce the cutting force, temperature, surface roughness, and tool wear. According to the cutting speed ranges of the HSDM, difficult-to-machine metal materials can be divided into three parts. The logical structure of the classification is shown in Fig. 2.

For HSDM of titanium alloys, after finding that the effect of cutting parameter optimization on tool wear was not clear, chemical vapor deposition (CVD) and physical vapor deposition (PVD) tool coatings were utilized to compare the cutting effect of HSDM. The PVD coating was more suitable for HSDM. In addition, the effect of the AlTiN and TiAlSiN multi-nanocomposite structure coatings were analyzed. The results showed that the quaternary TiAlSiN coating not only resulted in uniform chips but also had high oxidation resistance, significantly prolonging tool life.

To analyze the HSDM of high-strength steel, first, friction and wear experiments showed that HSDM could reduce the wear of the machined surface to a greater extent than CM. Second, the optimal cutting parameters were obtained when using the CVD coating of Al_2O_3 + TiC. Subsequently, three other optimal TiN/TiCN/TiAlN coatings and their cutting parameters were obtained. Finally, using the TiCN-NbC coating, the influence of cutting parameters on the surface roughness, microhardness, and residual stress of the workpiece was analyzed.

For the HSDM of nickel-based alloys, first, the influence of cutting parameters on the cutting force was investigated based on (Al, Ti)N-coated tools. Second, the effect of cutting parameters on tool wear was studied

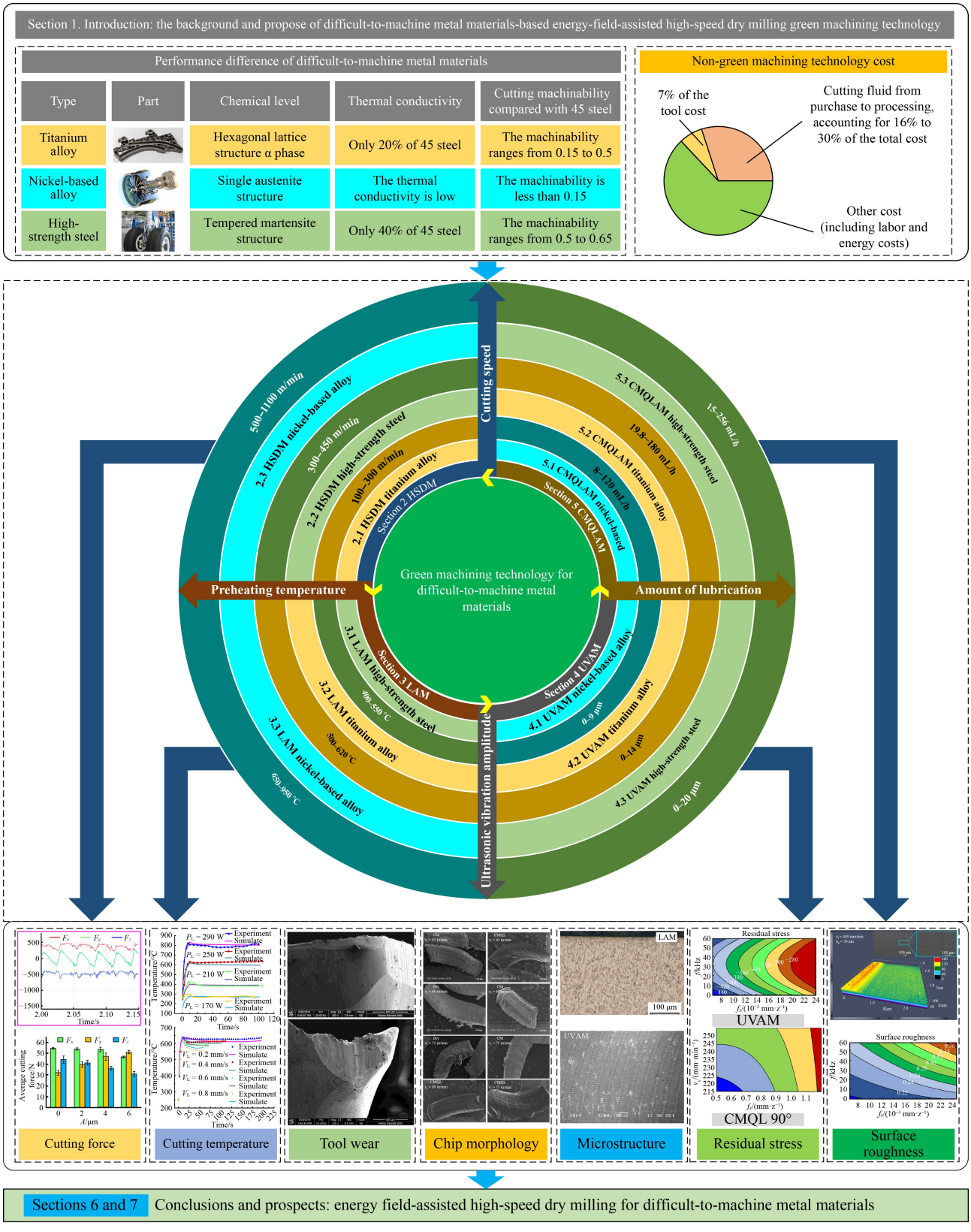

Fig. 1 Overall structure of this review. HSDM: high-speed dry milling, LAM: laser-assisted milling, UVAM: ultrasonic vibration-assisted milling, CMQLAM: cryogenic minimum quantity lubrication energy field-assisted milling.

using TiN/TiAlN-coated tools. Third, the influence of cutting parameters on the cutting force and tool wear was analyzed using polycrystalline cubic boron nitride (PCBN) tools. Furthermore, the influences of cutting

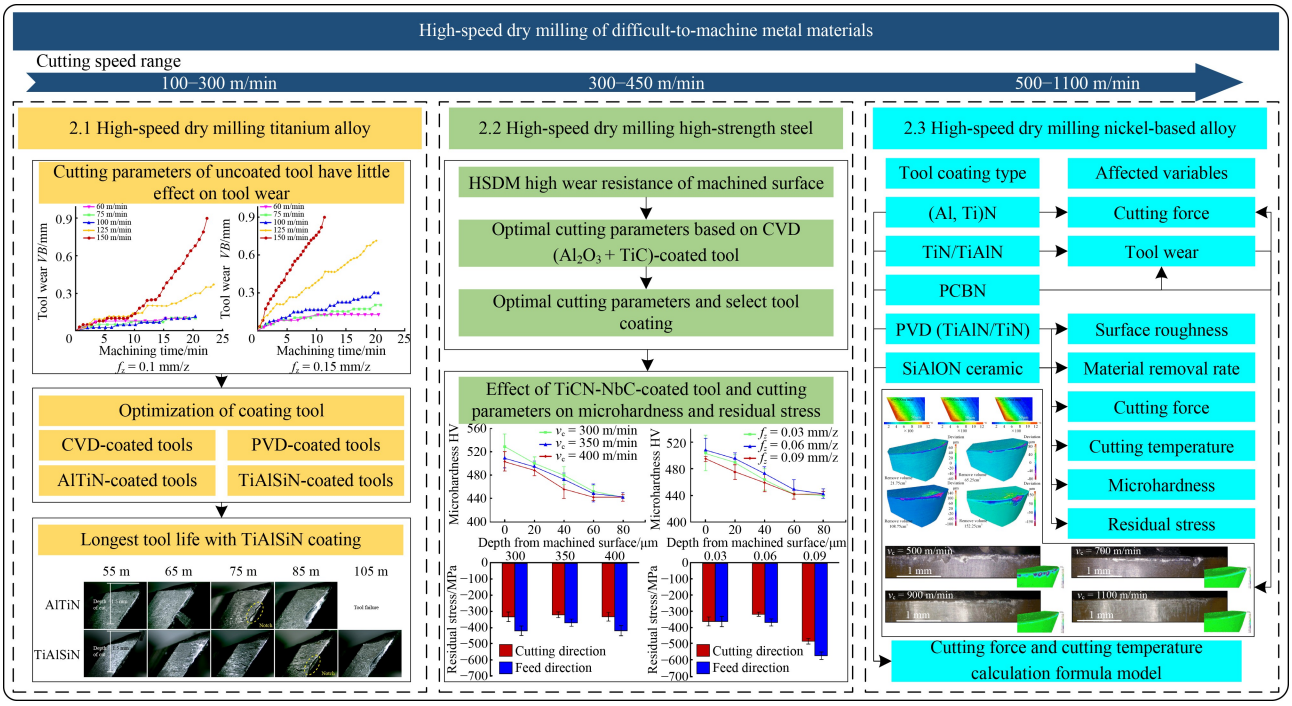

Fig. 2 Logical structure of high-speed dry milling difficult-to-machine metal materials. CVD: chemical vapor deposition, PVD: physical vapor deposition, HSDM: high-speed dry milling.

parameters on the surface roughness when using TiAlN/TiN PVD nano-multilayer coated tools were analyzed. In addition, the effects of cutting parameters on the material removal rate, cutting temperature, microhardness, and residual stress were briefly described for the application of the SiAlON ceramic tool. The effects of this tool and the PVD nano-multilayer coated tool on the surface roughness were compared, and it was found that the SiAlON ceramic tool could obtain better surface roughness. The effects of cutting parameters on the surface roughness, cutting temperature, cutting force, and microhardness were analyzed in detail based on the use of SiAlON ceramic tools. Finally, to gain a real-time perception of the cutting force and cutting temperature, a detailed calculation formula for the cutting force and cutting temperature was established based on SiAlON ceramic tools, and its accuracy was verified.

2.1 HSDM of titanium alloy

The cutting parameters have a significant impact on the entire machining process. Krishnaraj et al. [104] conducted an HSDM experiment on Ti–6Al–4V (TC4). Based on the Taguchi experimental design, the effects of v_c, v_f (feed speed), and α_p (axial cutting depth) on the cutting force, temperature, and surface roughness were analyzed. The experimental results show that f_z (feed per tooth) and α_p have the greatest impact on the cutting force, whereas v_c has a significant influence on the cutting temperature and surface roughness. Within the selected range of these cutting parameters, when v_c, v_f, and α_p were 150 m/min, 0.075 mm/r, and 0.75 mm, respectively (for cutting titanium alloy, the high-speed cutting range was reached when v_c was 100 m/min [103]), the cutting effect was the best, and the machining efficiency was the highest [104]. However, the influence of cutting parameters on the tool life and tool wear has not been studied.

Based on the above research, Ginting and Nouari [105] studied the process capability of the HSDM of Ti-6242S with ordinary uncoated cemented carbide tools. The impact of v_c and f_z on tool wear was investigated. By observing Fig. 3(a) [105], the author found that when v_c and f_z were 150 m/min and 0.1 mm/z, respectively, the tool could work for 22.4 min. When f_z increased to 0.15 mm/z, the tool life decreased by a factor of two, indicating that f_z had a great influence on the tool life. Irrespective of whether f_z was 0.1 or 0.15 mm/z, the tool wear increased with increasing v_c, which suggests that v_c was another important factor affecting tool life. The tool wear and chip morphology were analyzed using the finite element method (FEM) and scanning electron microscopy (SEM). It was observed that the tool-wear mechanism would be transformed from abrasive wear to adhesive wear if the value of v_c increased. The chip gradually obtained a large serrated curvature when f_z was 0.15 mm/z and v_c ranged from 60–150 m/min, also indicating that the radius of the chip curvature was directly affected by the v_c value [105]. Based on the above studies, the optimal machining effect can be

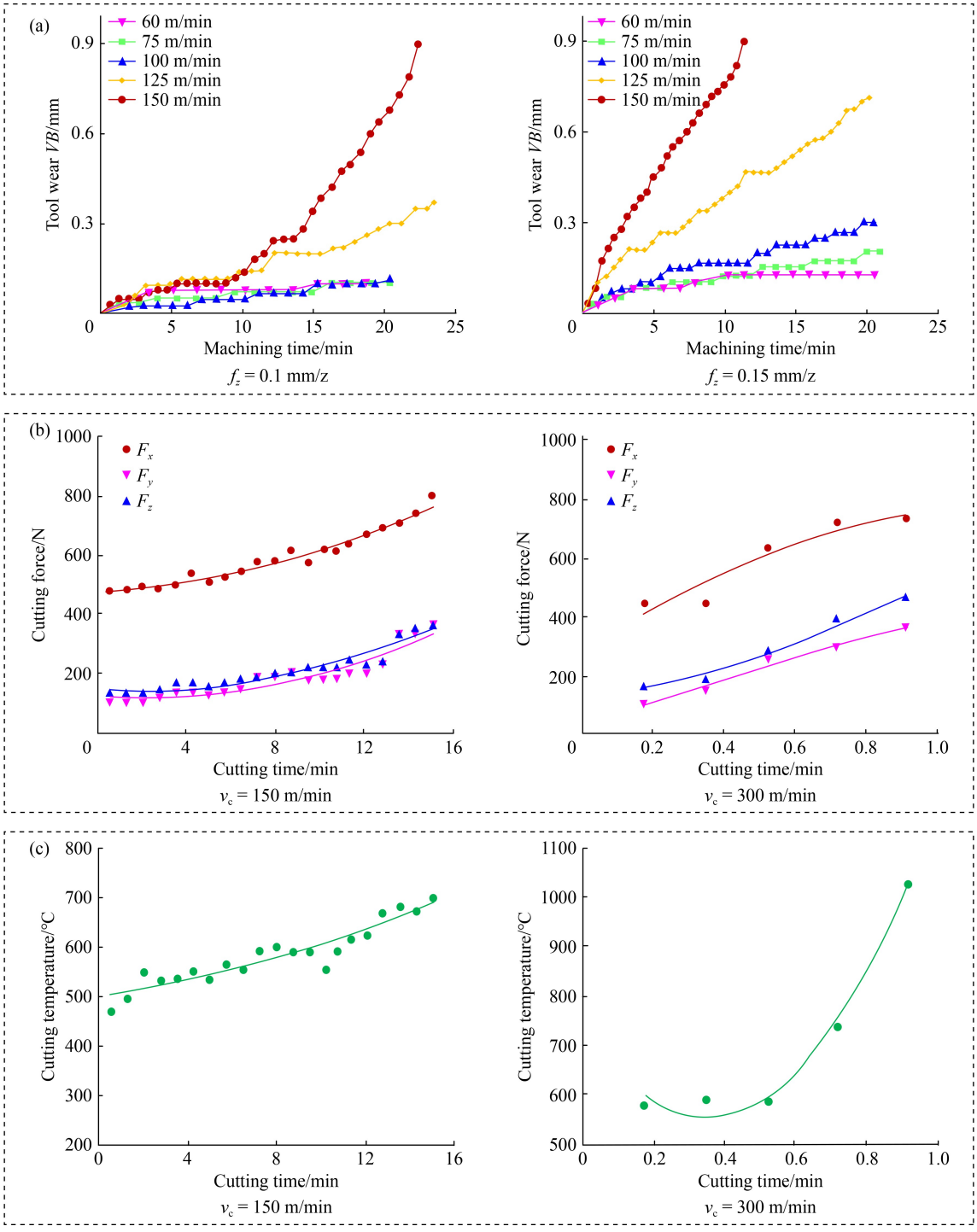

Fig. 3 Influence of cutting parameters on tool wear, cutting force and temperature: (a) effect of v_c and f_z on tool wear [105], (b) cutting force under different v_c [106], and (c) cutting temperature under different v_c [106]. Reproduced with permissions from Refs. [105,106] from Elsevier and Springer Nature.

obtained by appropriately adjusting the process parameters. The influence of changing the parameters on tool wear was not obvious. Therefore, it is necessary to further explore the influence of other methods (such as tool coating) on tool wear.

The influence of cutting force and temperature on the surface quality of TC4 during the HSDM process at different v_c values was systematically investigated by Li et al. [106]. They used CVD-coated tools (Ti(C, N)-Al_2O_3) for HSDM of TC4. The results showed that with the increase in v_c and f_z, tool wear aggravated, and tool life decreased sharply. The reason for the tool injury would transform from cutting load into thermal damage with increasing v_c value. With the development of the

machining process, it was found that the cutting force (Fig. 3(b) [106]) and temperature (Fig. 3(c) [106]) were the main factors affecting the tool wear [106]. Furthermore, the authors found that the average cutting force decreased significantly with increasing v_c, and the reason for the observed reduction was attributed to the thermal softening of the workpiece caused by the increase in cutting temperature. Based on the SEM results, the surface microstructure and grain orientation changed with different feed directions, as shown in Fig. 4(a) [107]. The authors also observed chip morphology during the HSDM processing of TC4 and found that chip morphology corresponded to different v_c values. At the same SEM doubling rate, the number of lamellae also changed. With an increase in v_c, the number of lamellae decreased, but the lamellar structure became clearer, as shown in Fig. 4(b) [108]. By observing the serrated chip morphology in Fig. 4(c) [108], it was found that the degree of serration increased with increasing v_c, which is more conducive to chip breaking [108]. Although these

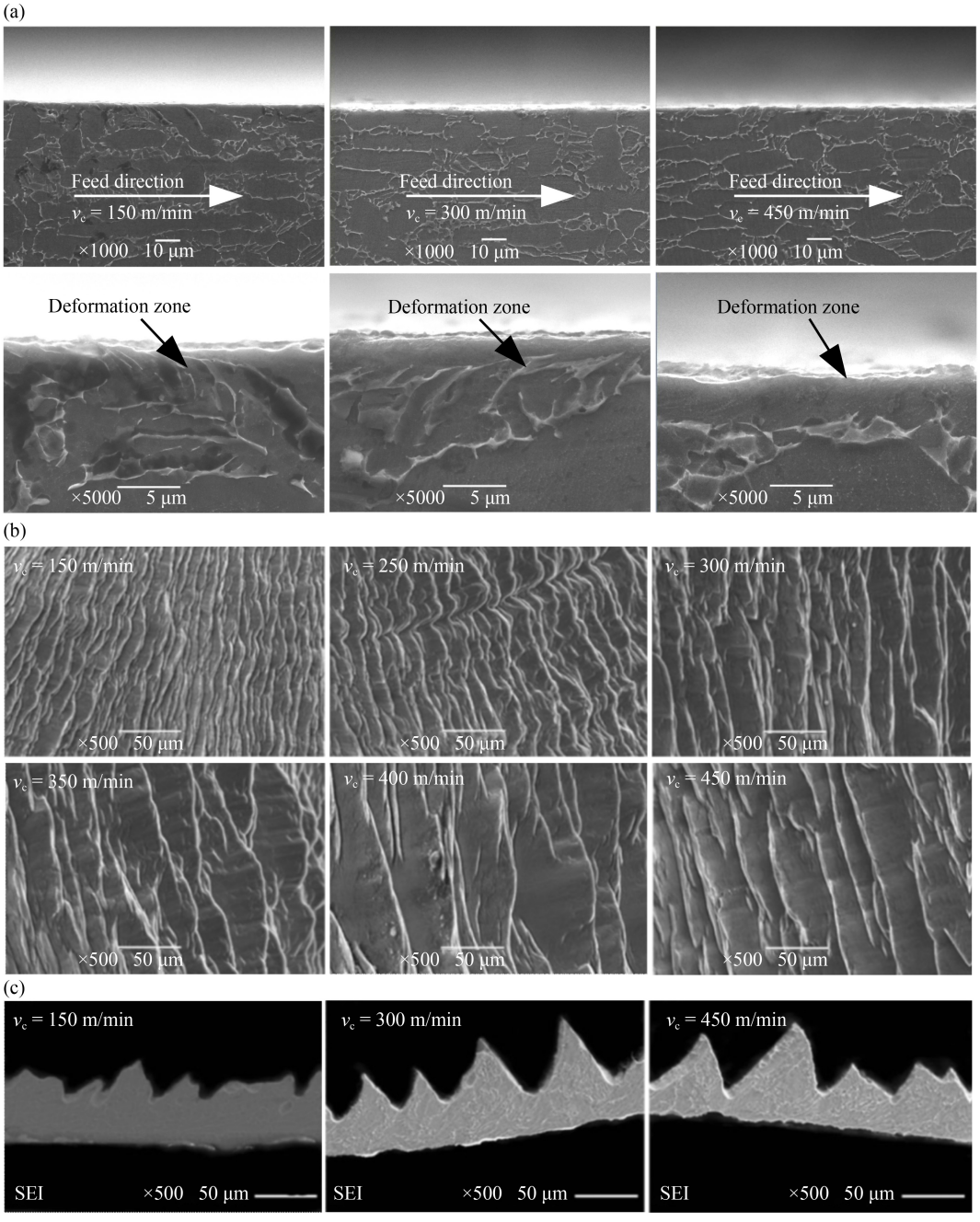

Fig. 4 Influence of cutting parameters on microstructure and chip morphology: (a) workpiece microstructure and deformation zone under different v_c [107], (b) effect of v_c on chip morphology [108], and (c) major section of chips at different v_c [108]. Reproduced with permissions from Refs. [107,108] from Trans Tech Publications Ltd. and Springer Nature.

findings indicate that CVD-coated tools could show great cutting effects with suitable v_c values, the authors did not study the milling of TC4 with PVD-coated tools.

Even when using coated tools, the cutting parameters of HSDM should be reasonably selected. Safari et al. [109] tested the surface roughness and microhardness of a workpiece surface under different cutting conditions with a PVD-coated tool (TiAlN/TiN) when v_c ranged from 100 to 300 m/min and f_z from 0.03 to 0.06 mm/z. As v_c increased from 100 to 300 m/min, the surface roughness decreased by 55%. The surface roughness decreased by 40% at a v_c value of 100 m/min as f_z increased from 0.03 to 0.06 mm/z. Tool wear and work-hardening problems were also observed when v_c and f_z increased simultaneously [109]. Furthermore, the researchers used the same PVD tool for the HSDM processing of TC4-ELI. The results showed that the machined surface improved as v_c increased from 200 to 300 m/min. When f_z was small, the cutting force in the HSDM process was lower than that in the CM process. Compared to the uncoated tool, the PVD-coated tool did not significantly improve the surface roughness because of the adverse effect of the large v_c value [110]. The results indicated that, even if the coated tool was selected, it was difficult to improve the machining effect if the selection of cutting parameters was not suitable.

The above studies did not compare the cutting effects of CVD-coated and PVD-coated tools under the same conditions. Niu et al. [111] used PVD coating (TiN/TiAlN) and CVD coating (TiN/Al_2O_3/TiCN) as tools for HSDM processing of TC6 titanium alloy. Relevant research on the HSDM of TC6 regarding the cutting force and surface roughness was summarized, and the difference between the PVD and CVD tool coating performance was demonstrated from the aspects of the tool wear evolution and failure mechanism. The milling force and surface roughness of TC6 were high when the v_c value was higher than 80 m/min. This indicated that the two coated tools were not suitable for the HSDM processing of the TC6 titanium alloy. However, it is apparent that the tool wear resistance of PVD-coated tools is much better than that of CVD-coated tools because the thermal conductivity of Al_2O_3 decreased and that of TiAlN increased with increasing cutting temperature [111]. Considering the influence of tool coating on HSDM processing, Liu et al. [112] assumed that the regressive development of tool coating was the main factor restricting the promotion and application of HSDM in the industry. Based on this, they reported the influence of AlTiN-coated tools and TiAlSiN-coated tools on HSDM processing of TC4. The XRD (X-ray diffraction) diffraction patterns of the two differently coated tools, shown in Fig. 5(a) [112], were compared. Compared to the AlTiN tool, the tool life of the TiAlSiN-

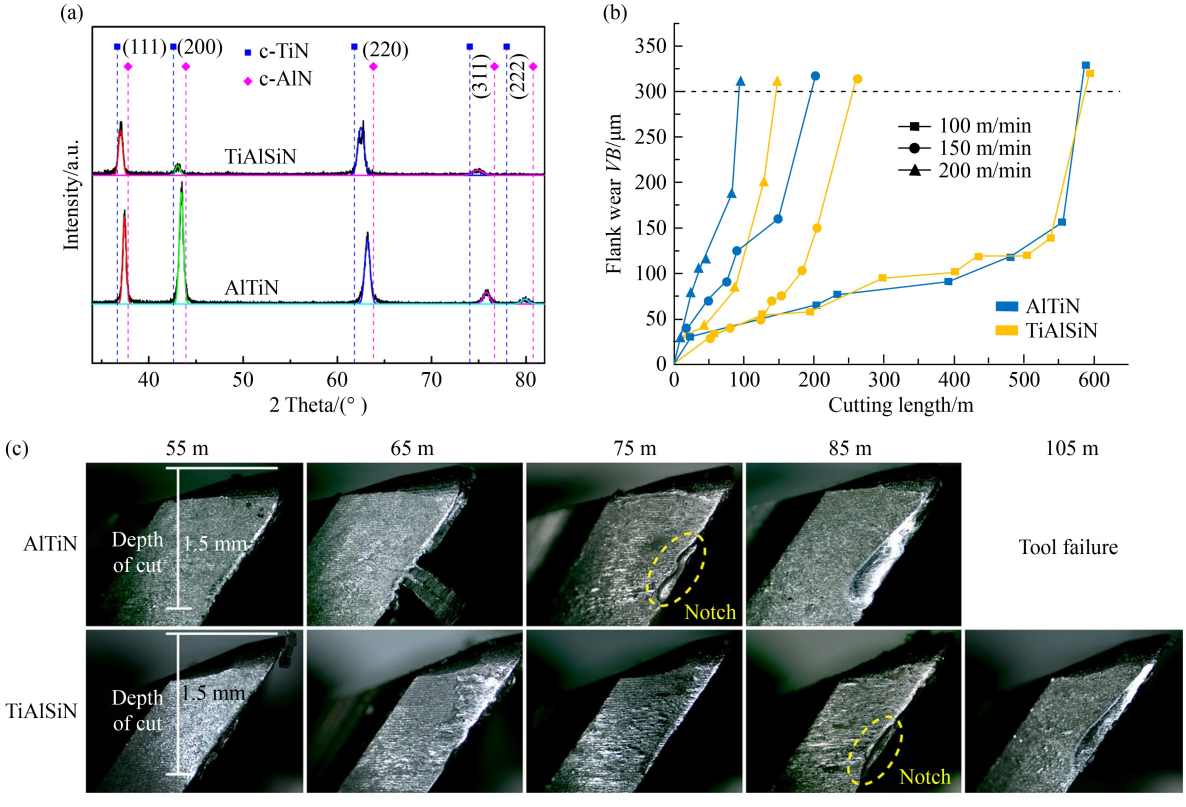

Fig. 5 XRD, flank wear and tool wear images of AlTiN- and TiAlSiN-coated tools: (a) XRD diffraction patterns, (b) flank wear of cutting length under different v_c, and (c) tool flank wear images under different cutting lengths [112]. Reproduced with permission from Ref. [112] from Springer Nature.

coated tool increased by 32% and 66% at v_c values of 150 and 200 m/min, respectively, as shown in Fig. 5(b) [112]. The tool-wear image in Fig. 5(c) [112] reveals that the TiAlSiN coating can significantly prolong the tool life of the cutting edge. Furthermore, the TiAlSiN-coated tool exhibits better oxidation resistance and more uniform chips [112].

2.2 HSDM of high-strength steel

The wear resistance of the workpieces determines their service performance. Huang et al. [114] focused on the influence of HSDM of AISI D2 (when milling high-strength steel, the high-speed cutting range is reached at a v_c of 300 m/min [113]) on the surface integrity and wear resistance. After the HSDM, the wear resistance of the machined surface was evaluated through friction and wear tests without lubrication. The results showed that the surface morphology, microhardness, and yield strength of the workpiece exhibited anisotropic characteristics after friction and wear experiments. Because of anisotropy, the wear resistance of the workpiece surface mainly depends on the sliding direction. Furthermore, the surface of the workpiece hardens. During the initial phase of wear (the first 10 min), the surface wear of HSDM was 62% less than that of CM milling [114].

The surface quality indices include the surface roughness, hardness, and residual stress. Zheng et al. [115] used a CVD-coated tool (Al_2O_3 + TiC) for the HSDM of AISI 4340 steel. The relationships between cutting parameters, cutting force, and surface roughness were discovered, and the effects of tool wear on the cutting force and surface roughness were studied. It was found that the cutting force was most influenced by α_p, whereas f_z had the greatest effect on the surface roughness. Based on the empirical model, optimal cutting parameters for small cutting force and surface roughness were obtained when α_p ranged from 0.2 to 0.4 mm, f_z ranged from 0.03 to 0.06 mm/z, v_c was selected between 350–450 m/min, and α_e ranged from 3 to 4 mm. Based on the SEM results, the wear rate of the coated tool was low. By observing the effects of friction and wear, it was found that the increase in the cutting force and surface roughness was small in the initial and stable wear stages. However, when the wear value exceeded 0.25 mm, the increase in cutting force suddenly increased significantly. The experimental results also indicated that the wear of coated tools was mainly caused by adhesion, oxidation, and diffusion, accompanied by a small amount of spalling and chipping [115]. In addition, the authors studied the influence of tool coating (TiAlN + TiN, AlTiN, and TiN/TiCN/TiAlN) and cutting parameters on the cutting force and surface roughness. Among these three coated tools, the TiN/TiCN/TiAlN-coated tools were the most suitable for the HSDM processing of AISI 4340. Owing to the resultant force, the flank wear width and surface roughness values were minimal. As the optimal cutting parameters, values for α_p of 0.4 mm, f_z of 0.02 mm/z, α_e of 2 mm, and v_c in the range from 280–440 m/min were obtained [116]. In addition to the above investigations, researchers used a TiCN-NbC composite coating tool for HSDM of AISI 4340 steel and found that when the cutting parameters were within HSDM conditions, the surface roughness value changed from 0.25 to 0.45 μm, and the surface roughness was minimal at a v_c of 350 m/min. Furthermore, applying the TiCN-NbC composite coating tool resulted in work hardening of the workpiece surface. The results showed that the hardness value after processing was 1.1–1.2 times that of the workpiece body material, and the hardening layer depth was 60 to 80 μm, as shown in Fig. 6(a) [117]. The residual stresses in the cutting direction ranged from –490 to –320 MPa, whereas the residual stresses in the feed direction ranged from −600 to –370 MPa, as shown in Fig. 6(b) [117]. Furthermore, higher f_z, v_c, and α_e and smaller α_p values can provide a workpiece with high residual compressive stress [117].

2.3 HSDM of nickel-based alloy

The cutting parameters can significantly affect the cutting force and generate tool wear. Li et al. [118] conducted HSDM experiments on Inconel 718 workpieces with an (Al, Ti)N-coated milling cutter (for nickel-based alloy cutting, the high-speed cutting range was reached at a v_c of 100 m/min) [119]. The change in cutting forces was investigated as α_p, v_c, and f_z values increased from 0.5 to 2 mm, from 140 to 240 m/min, and from 0.1 to 0.18 mm/z, respectively. According to the results, the radial, tangential, and axial forces increased with an increase in f_z. With increasing v_c, the axial force fluctuated significantly and then decreased, but the change in v_c had little effect on radial and tangential forces. With the increase in α_p, irrespective of the changes in f_z and v_c, the values of the radial, tangential, and axial forces always increased [118]. The above investigations demonstrate that only an increase in v_c can appropriately reduce the cutting force. However, the effects of cutting parameters on tool wear have not been studied. The tool wear under different v_c is shown in Fig. 7 [120,121]. Kamdani et al. [120] used PVD-coated tools (TiN/TiAlN) to study the influence of v_c and α_e (radial cut width) on the tool wear of Inconel 718 processed by HSDM and observed that when v_c was in the range of 80–120 m/min, the tool wear increased with an increase in α_e and reached its maximum when v_c increased to 120 m/min. According to Fig. 7(a) [120], tool wear was more severe with an increase in v_c and α_e.

As the above studies did not simultaneously consider both the cutting force and tool wear mechanism in the HSDM processing of nickel-based alloys, Zhang et al. [122] applied PCBN tools to the HSDM of GH4169 and

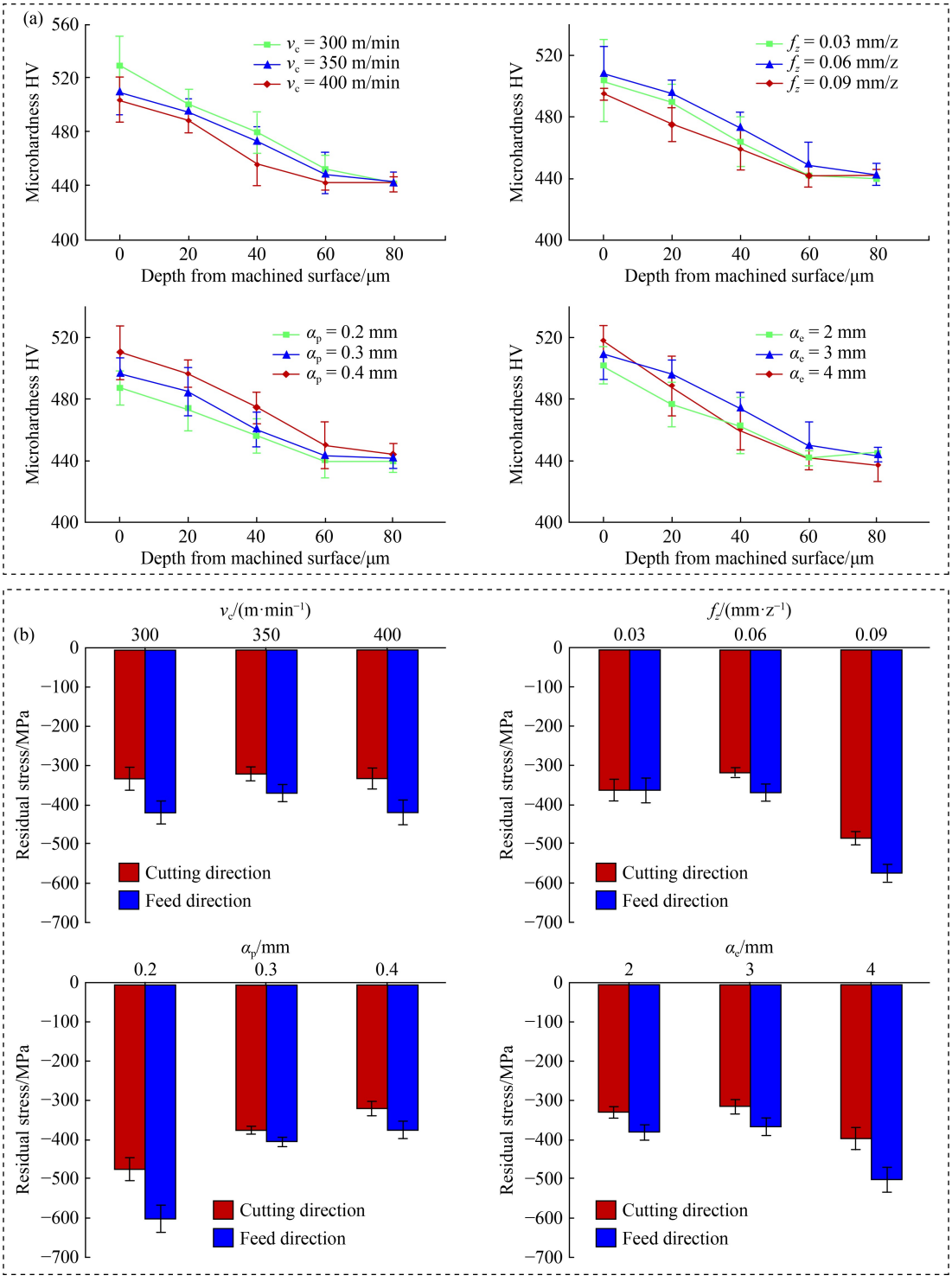

Fig. 6 Microhardness and residual stress under different cutting parameters: (a) microhardness of depth from the machined surface under different cutting parameters and (b) variation of machining surface residual stress with cutting parameters [117]. Reproduced with permission from Ref. [117] from Elsevier.

observed the influence of v_c, f_z, and α_p on cutting force and tool wear. The cutting force increased with an increase in α_p, whereas it decreased with an increase in v_c. Furthermore, with an increase in v_c and f_z or a decrease in α_p, flank wear gradually decreased. When v_c, f_z, and α_p were 1065 m/min, 0.12 mm/z, and 0.5 mm, respectively, the corresponding cutting parameters were optimal. The tool-wear values of the rake and flank surfaces became more uniform when v_c was 1065 m/min. Because Ti, Al, and O elements were concentrated on the bond layer at

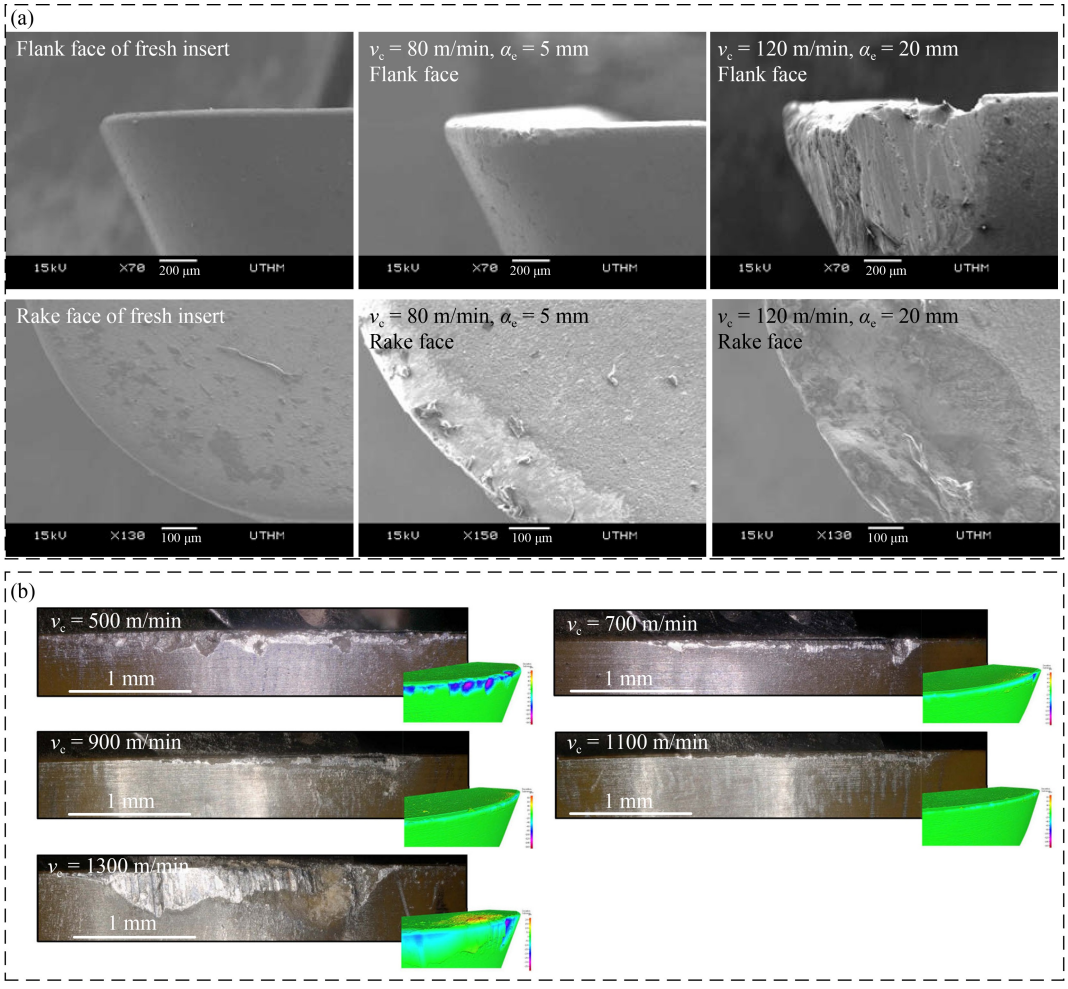

Fig. 7 Tool wear under different v_c: (a) tool wear under different machining conditions [120] and (b) experiment after cutting 21.75 cm^3 and flank wear of finite element method [121]. Reproduced with permissions from Refs. [120,121] from Malaysian Tribology Society and Springer Nature.

the cutting edge, the main wear mechanism was adhesive wear [122].

The above studies demonstrated the influence of milling parameters on the cutting force and tool wear during HSDM. However, the influence of the cutting parameters on the surface roughness of coated tools has not been studied. Therefore, Qiao et al. [123] used a PVD-coated (TiAlN/TiN) tool to conduct HSDM of nickel-based FGH97 alloy. The surface roughness of the workpiece surface was explored within the specified limits when α_p changed from 0.1 to 0.3 mm, v_c from 30 to 210 m/min, and f_z from 0.08 to 0.12 mm/z. The results showed that the surface roughness increased with an increase in α_p and f_z, but with increasing v_c, the surface roughness first increased and then decreased. The minimum surface roughness was obtained for v_c values in the range of 170–190 m/min [123].

The cutting parameters not only affect the surface roughness but also influence the tool wear and cutting temperature. In addition to the cutting parameters, the coating type also affects the surface roughness. Molaiekiya et al. [124] studied the cutting performance of a SiAlON ceramic tool in the HSDM of Inconel 718 and measured the tool life, tool wear, and cutting force during machining. When the same volume of material was removed, tool wear first decreased and then increased with an increase in v_c. When v_c remained in the range of 900–1100 m/min, the tool life was the longest, as shown in Fig. 7(b) [121]. The change rule of the tool surface temperature gradient was also explored using the FEM under different v_c conditions. During HSDM, a large amount of cutting heat was generated on the contact surface of the tool and chip, and the temperature was mainly concentrated in the narrow strip of the second deformation zone, as shown in Fig. 8(a) [121]. This is because of the extremely low thermal conductivity of the SiAlON ceramic tool and the short cutting time within the set range of v_c. Furthermore, when v_c was 900 m/min, the thermal softening effect was prominent, leading to a relatively low cutting force. Based on the experimental data for the cutting force, cutting heat, and tool wear, the optimal v_c value was 900 m/min. By analyzing the tool

wear under different cutting parameters of FEM, it was found that at the same tool wear rate, compared with ordinary cemented carbide tools, the SiAlON ceramic tool could improve the material removal rate four to five times, as shown in Fig. 8(b) [121]. In addition, the authors used a SiAlON ceramic tool and a PVD-coated (WC-Co) tool for HSDM processing. Compared with the PVD-coated tool, the SiAlON ceramic tool exhibited a better surface roughness, as shown in Fig. 9 [124]. However, the ceramic tool formed a very hard white layer with depths ranging from 1 to 2 μm on the surface of the workpiece during HSDM. After corrosion, it remained white under a metallographic microscope. The maximum residual tensile stress in HSDM processed with the PVD-

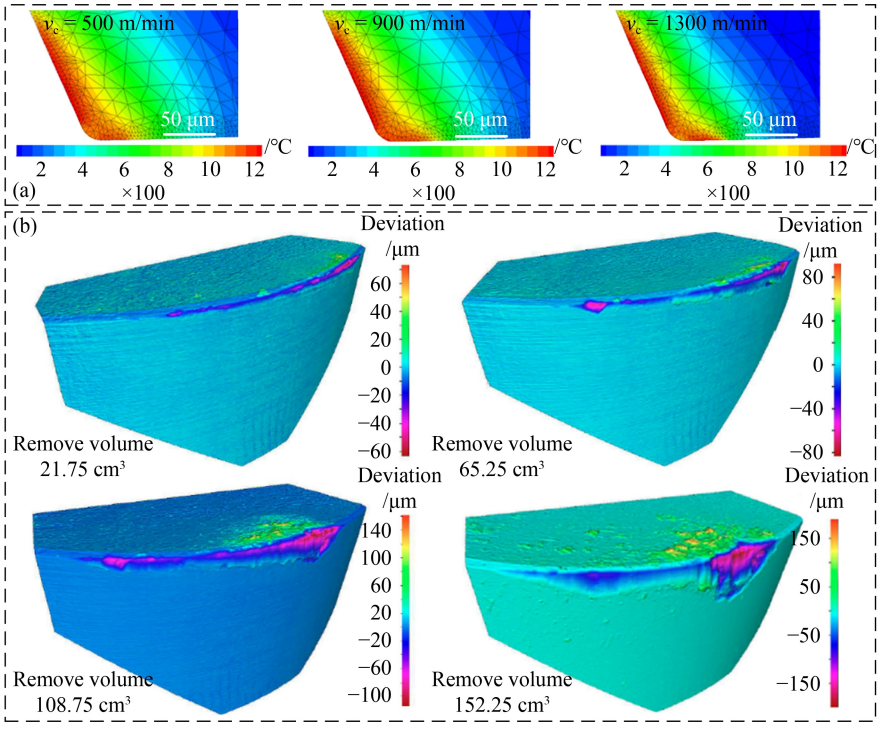

Fig. 8 Cutting temperature and tool wear under different cutting conditions: (a) temperature distribution under different v_c conditions and (b) tool wear with different cutting volumes [121]. Reproduced with permission from Ref. [121] from Springer Nature.

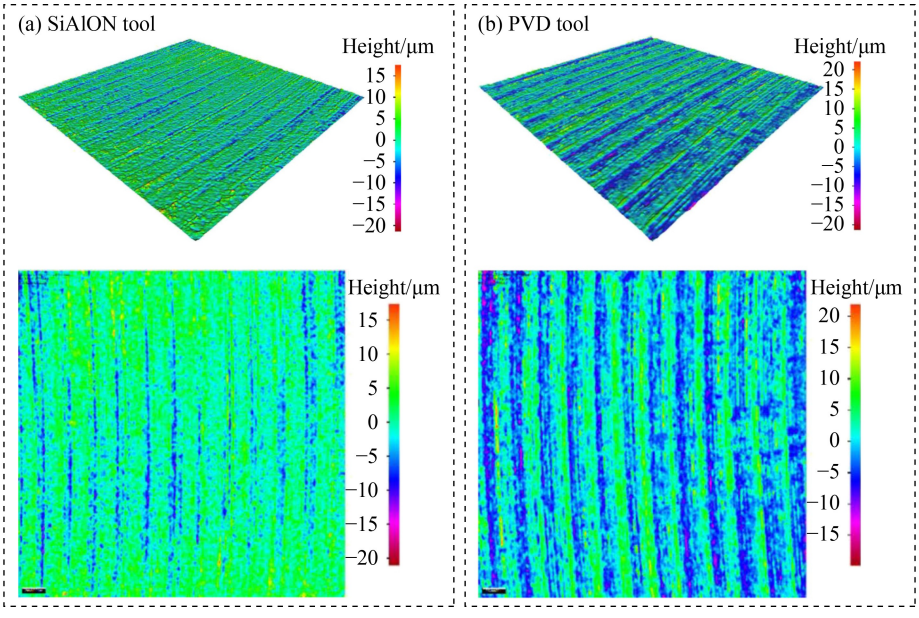

Fig. 9 Surface roughness corresponding to different coated tools: (a) SiAlON tool and (b) physical vapor deposition tool [124]. PVD: physical vapor deposition. Reproduced with permission from Ref. [124] from Springer Nature.

coated tool was 2.5 times higher than that obtained with CM pouring cutting, which was caused by rapid cooling at high temperatures. Therefore, CMQL technology is necessary to reduce the thermal damage caused by tool or workpiece surfaces during HSDM processing [124].

Although Molaiekiya et al. [124] systematically studied the HSDM process of SiAlON ceramic tools, the hardness of the hard white layer and cutting forces were not explored under HSDM and CM conditions. To determine the change in hardness, Şirin et al. [125] used HSDM and SiAlON ceramic tools to process nickel-based X-750 alloys. The surface roughness, cutting temperature, cutting force, and microhardness of the workpiece were measured in the v_c range of 500–700 m/min, and the v_f range of 0.025–0.075 mm/r. It was found that the surface roughness increased with increasing v_c and v_f. Under all cutting conditions, the surface roughness corresponding to HSDM was relatively large. The cutting force and temperature were 565.7 N and 450 °C, respectively. The tool wear was small because the tool coating provided anti-wear properties during processing. Compared with CM pouring cutting, HSDM can increase the hardness of the workpiece by 16.94% [125].

The above studies systematically revealed the cutting effect of the HSDM of nickel-based alloys with SiAlON ceramic tools, but a formula for the cutting force and cutting temperature in the cutting process has not been established. Thus, Zha et al. [126] investigated the HSDM process of Inconel 718 with a SiAlON ceramic tool based on FEM and derived formulas for the cutting force and cutting temperature. Subsequently, an HSDM experiment was performed using the specific cutting temperature to verify the cutting force formula. When α_p, α_e, f_z, and v_c reached 0.3 mm, 6 mm, 0.03 mm/z, and 527.52 m/min, respectively, the cutting force began to decrease, indicating that the cutting temperature exceeded the softening temperature of Inconel 718. The experiments showed that when v_c was higher than 527.52 m/min, the HSDM process for Inconel 718 was easier. The accuracy of the formula for the cutting force and temperature was verified based on experimental results [126].

2.4 Summary of HSDM of difficult-to-machine metal materials

Based on the above investigations, the cutting speed ranges of difficult-to-machine metal materials are different in the HSDM process owing to the different properties of these materials. The suitable cutting speed range is 100–300 m/min for titanium alloy, 300–450 m/min for high-strength steel, and 500–1100 m/min for nickel-based alloys. Titanium alloys are commonly used for aircraft fuselages, while nickel-based alloys are primarily used for aircraft engines. However, the engine service life is typically shorter than that of the fuselage. To increase the cutting speed of nickel-based alloys, it is necessary to introduce high-performance SiAlON ceramic tools. In terms of the entire aircraft, the content of titanium alloy is much higher in structural parts than in high-strength steel landing gears. This means that increasing the cutting speed of titanium alloy has a greater impact than increasing the cutting speed of high-strength steel. Based on Fig. 10 and the above research results, the cutting force and surface roughness in the HSDM process are difficult to reduce with uncoated and ordinary coated tools (TiN/TiAlN, TiN/Al_2O_3/TiCN, and AlTiN), and the tool wear is also severe. High-performance tools (SiAlON ceramic tools) and composite-coated tools (TiN/TiCN/TiAlN, TiCN-NbC) can reduce the cutting force, temperature, and surface roughness and minimize tool wear during the machining process. However, compared with CM pouring cutting, the depth of the surface-hardening layer and the residual stress of HSDM machining are higher, which limits the application and promotion of the HSDM machining process. Considering that the deficiency of HSDM processing can be eliminated by LAM, UVAM, and CMQL technologies, which have been sufficiently researched, the subsequent work of HSDM mainly focuses on energy field-assisted milling technology.

3 LAM of difficult-to-machine metal materials

LAM is a new auxiliary processing mode for the local softening of workpieces using a laser heat source before processing. Because LAM technology can reduce energy consumption by reducing the cutting force, it is a typical green and low-carbon processing technology [127]. This principle is shown in Fig. 11(a) [128]. The incident angle of the laser beam (feeding simultaneously with the milling cutter) is set to ensure that the heat source radiated into the shear zone of the workpiece surface. Subsequently, the optimal laser parameters (P_L, d_L, etc.) and milling parameters (v_c, α_p, etc.) are combined to reduce the strength and hardness of difficult-to-cut materials. Therefore, LAM can reduce the cutting force, prolong the tool life, improve the material removal rate, reduce the cutting energy consumption, reduce the manufacturing cost, and optimize the workpiece surface quality [128]. The LAM of difficult-to-machine metal materials is divided into three classes according to the LAM preheating temperature range, and the logical structure is shown in Fig. 11(b).

For studies on LAM of high-strength steel, first, the laser parameters and cutting parameters were changed to reduce the cutting force and improve tool rigidity. Second, the influence of the laser preheating temperature on the cutting force and specific cutting energy was

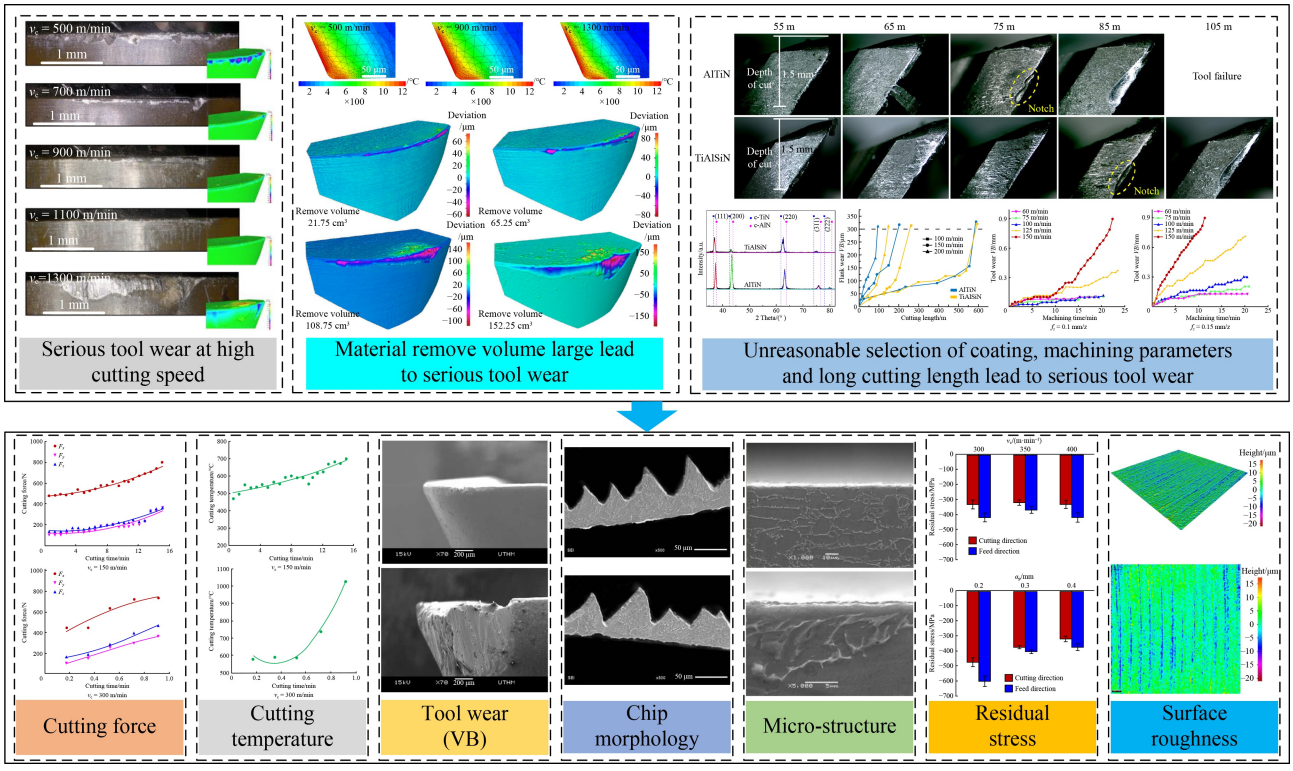

Fig. 10 Summary of high-speed dry milling machinability.

studied. Third, it was verified that LAM could reduce the cutting force with the help of FEM. Combining the FEM method and experiments, the researchers found that LAM could reduce the cutting force and surface roughness and that the most influential parameter on the surface roughness was the cutting speed. A comparison of the tool wear under high and low feed conditions revealed that LAM can significantly improve material removal under high feed conditions. Subsequently, after the optimization of the laser and cutting parameters, it was verified based on slot milling experiments that LAM could greatly reduce surface roughness and tool wear. To reduce the experimental workload, a physical-based LAM cutting force model is proposed, and the accuracy of the model is verified. Furthermore, to attain an optimal laser preheating effect, a two-stage LAM process was proposed to match the laser softening depth with the cutting manufacturing depth. Finally, to effectively control the range of the heat-affected zone (HAZ), the influence of the laser preheating parameters on the HAZ size was explored in detail.

To study the LAM of titanium alloys, the preheating temperature was first set to 618 °C to explore the influence of cutting parameters on the cutting force and microstructure of the planar workpiece. Second, the optimal laser power for surface machining was determined by combining FEM with the tool inclination angle, and its accuracy was experimentally verified. Third, a laser-assisted fillet milling strategy was developed, and it was found that the cutting force, specific energy, and surface roughness could be reduced at a preheating temperature of 600 °C. Furthermore, the surface LAM strategy of the tool inclination and fillet was integrated to reduce the cutting force and cutting specific energy. Subsequently, the cost of single-piece manufacturing under LAM conditions can be reduced by adjusting the laser parameters to obtain a preheating temperature of 500 °C. Finally, the laser and milling parameters were adjusted simultaneously to reduce the annual production costs of the enterprise.

When investigating the LAM of nickel-based alloys, the preheating temperature was first set to 800 °C using external laser-assisted equipment, and the effects of increasing the LAM plane of the workpiece on the cutting force, surface roughness, and tool wear were compared. Second, the influence of the laser power parameters on the tool wear in plane milling was studied. Third, the influence of simultaneous changes in the laser and cutting parameters on the cutting force and surface roughness in plane milling was explored. It was found that adjusting only the laser and cutting parameters led to an increase in the surface roughness. Subsequently, a new laser-assisted reciprocating preheating process was proposed, and LAM back and forth (B&F) preheating was found to reduce the surface roughness value during plane milling. Subsequently, contour LAM and slope LAM were proposed based on the results of the parameter optimization and a new process of plane milling. When comparing the cutting

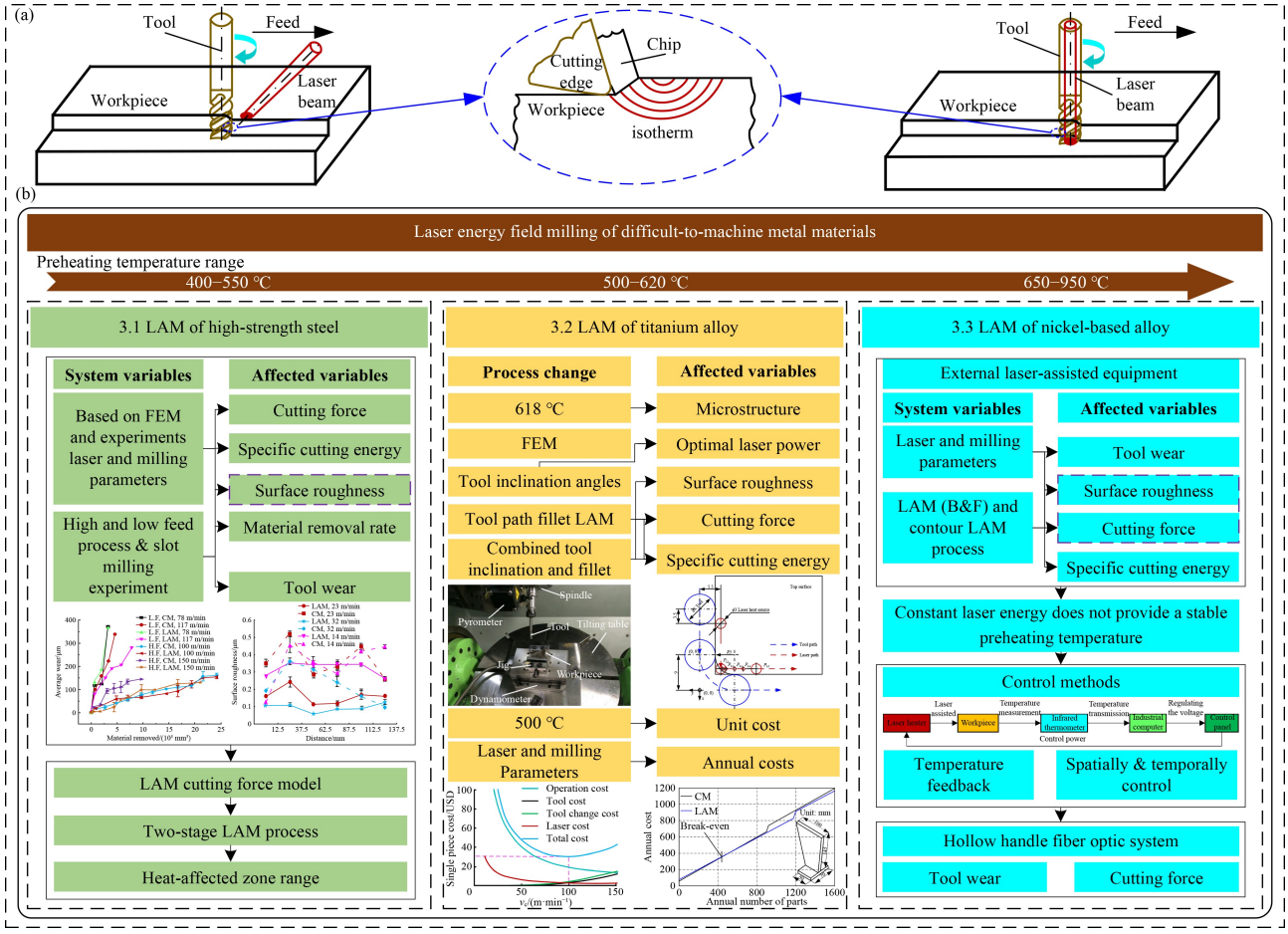

Fig. 11 Laser-assisted milling (LAM) principle and logic: (a) LAM schematic diagram [128] and (b) logical structure of LAM difficult-to-machine metal materials. FEM: finite element method; B&F: back and forth. Reproduced with permission from Ref. [128] from Springer Nature.

force, surface roughness, and specific cutting energy, the contour LAM had better effects than the slope LAM. In addition, the actual temperature of the workpiece surface significantly influences the LAM manufacturing process. The constant laser energy used in the experiment could not provide a stable preheating temperature. A temperature feedback control method is proposed to establish a tool life prediction model, and its accuracy is verified. Finally, it was established that the heating area was larger than the heat source size under actual working conditions, and a new space- and time-controlled laser-heating method was proposed. The chip morphologies and microstructures obtained by LAM, CM, and single laser scanning (LS) were compared in detail. Based on the hollow tool-holder fiber system, the effect of LAM on reducing the cutting force and tool wear was verified by changing the laser parameters.

3.1 LAM of high-strength steel

The laser parameters (P_L, laser position) and cutting parameters (v_c, α_p, and α_e) significantly affect the cutting force and dimensional accuracy of the workpiece. Singh and Melkote [129] conducted LAM experiments on H-13 steel using an ytterbium fiber laser (wavelength of 1064 nm) and a preheating temperature of 890 °C. The results showed that under the given cutting conditions, the laser parameters had a significant influence on the machining process. By properly controlling the P_L, d_L, and laser position, the strength of the workpiece material would be reduced, which can minimize the risk of tool failure, reduce the cutting force, and improve the rigidity of the tool. By observing the LAM hardness data, it was found that there was a measurable HAZ on the laser-heated surfaces. The HAZ area decreased with increasing V_L [129]. In addition, it was observed that α_p and P_L had a significant influence on the cutting force during the LAM process and that the surface roughness was affected by P_L [130]. Considering that P_L could affect the heating temperature, Jeon and Pfefferkorn [131] used a 200-W (continuous wave) Nd:YAG laser (wavelength of 1064 nm) for LAM processing experiments on 1018 steel with variable laser heating temperatures. When the laser-assisted temperature increased from 27 to 867 °C, the

average feed and cutting forces were reduced by 56% and 32%, respectively. The specific cutting energy decreased by 32% [131]. Because FEM can reduce the experimental cost and support the analysis of the temperature field distribution in the machining process, Özel and Pfefferkorn [132] conducted LAM research on AISI 4340 steel based on FEM and experiments. An Nd:YAG laser (wavelength of 1064 nm) was used in the heating process. The FEM results were analyzed using DEFORM-2D software. At high v_f, the cutting force of LAM (400 °C) was smaller than that of CM [132]. Cao et al. [133] found the best LAM process conditions for 13-8 stainless steel using a 1-kW HPDL laser (wavelength range of 940–980 nm) to obtain a surface temperature of 550 °C. First, the temperature field distribution of the laser-beam-preheated workpiece was determined based on the FEM method. Subsequently, the Taguchi experimental design was applied by changing v_c, v_f, and α_p. Finally, the optimal process parameters of LAM were established using variance analyses. Compared with the CM, the cutting force and surface roughness of the LAM were reduced by 20.1% and 34.4%, respectively. The results of variance analyses showed that under the appropriate LAM conditions, the cutting force was affected by α_p, whereas v_c had the greatest influence on the surface roughness [133].

The above studies showed that, in addition to the laser parameters, cutting parameters also have a significant influence on the LAM process. Bermingham et al. [134] used a 2.2-kW HPDL laser (wavelength range of 940–980 nm) and a preheating temperature of 300 °C and conducted comparative processing experiments with or without LAM of high-feed milling (H.F) or low-feed milling (L.F). Based on the above experimental variables in Fig. 12(a) [134], they established the relationship between the material removal volume and tool wear and observed no difference in tool wear between LAM and CM at 100 m/min H.F. However, under L.F conditions, the tool wear of LAM and CM was quite different. For the same tool wear, v_f was 117 and 150 m/min for LAM and CM, respectively, and the material removal by LAM was more than double that of CM. However, when v_f was 78 m/min, the removal rate of LAM was only 50% higher than that of CM. Based on the mechanism of adhesive wear and abrasive wear, it was proven that LAM technology could effectively prolong tool life. In addition, compared to CM, LAM can reduce the cutting force by 33% [134].

After optimizing the cutting parameters, it is necessary to design a variety of experiments (such as groove milling) to reduce surface roughness and tool wear. Meikote et al. [135] used an ytterbium fiber laser (wavelength of 1060 nm) to conduct laser-assisted groove milling experiments on A2 tool steel. They measured the dimensional accuracy, surface roughness, and tool wear of the equipment. The authors found that the dimensional precision of the workpiece groove of the LAM was closer to the drawing setting precision than that of the CM. As shown in Fig. 12(b) [135], the surface roughness of the LAM (7.5 W) was smaller than that of the CM at different cutting lengths, and the tool wear rate of the LAM was lower [135].

The cutting-force prediction model can reduce the workload of cutting experiments and accurately determine the cutting force in the LAM process. Kumar et al. [136] proposed a physical-based cutting force model to predict the cutting force during the LAM process, as shown in Fig. 13(a) [136]. The contents of the model included the thermal model of laser heating, thermal model of temperature rise caused by plastic deformation (shear) in the process of chip formation, material strength-related shear angle model, material flow strength model, milling model, and tool jump model. Based on the new model, the cutting force during LAM processing was

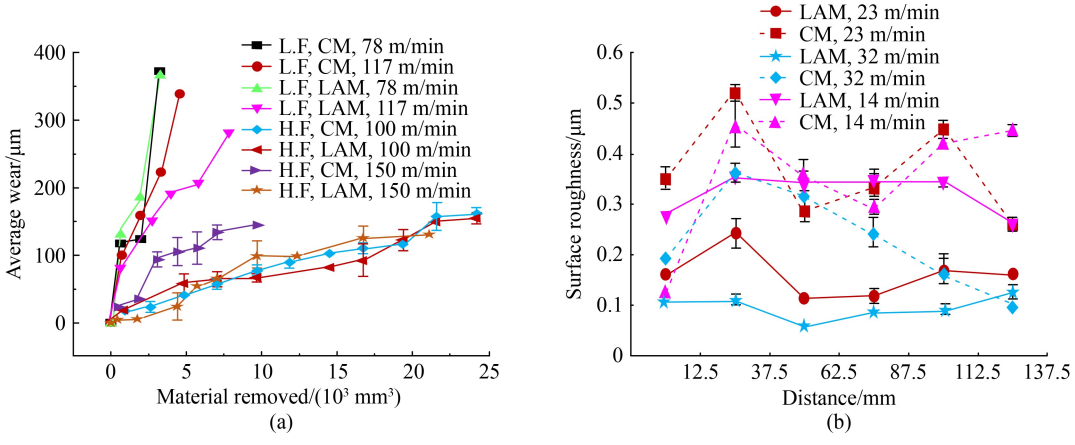

Fig. 12 Cutting forces and grain deformation distribution: (a) tool wear under different cutting conditions [134] and (b) surface roughness at different v_c [135]. CM: conventional milling; LAM: laser-assisted milling; H.F: high-feed milling; L.F: low-feed milling. Reproduced with permissions from Refs. [134,135] from Elsevier.

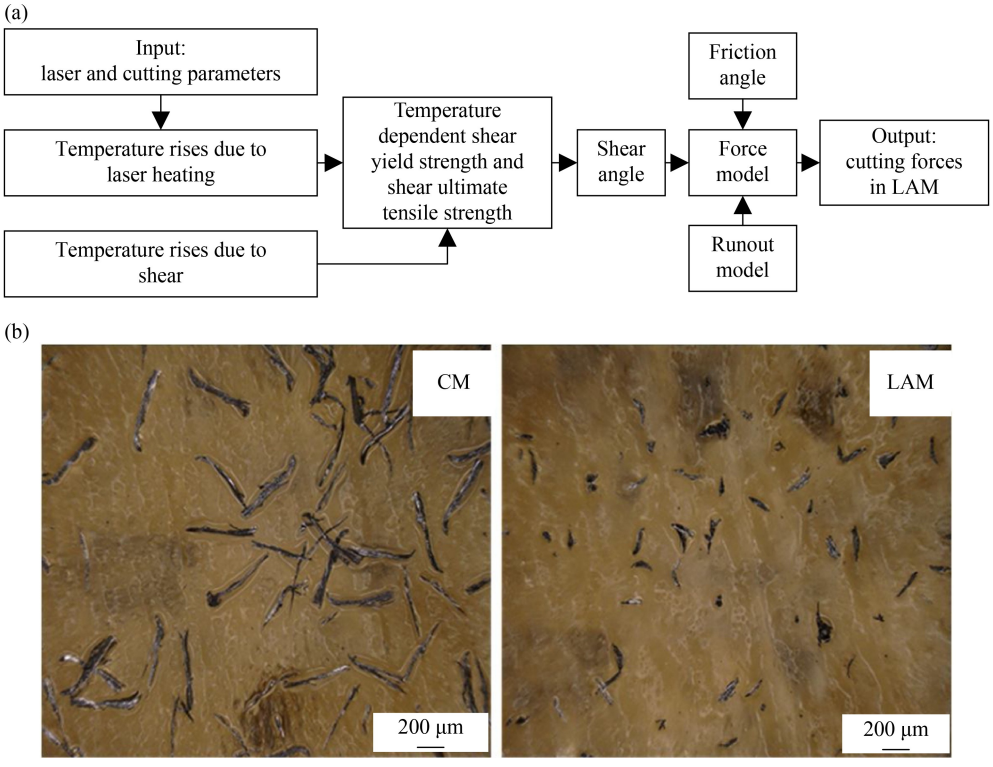

Fig. 13 Force prediction and cutting morphology: (a) laser-assisted milling (LAM) force prediction methodology [136] and (b) comparison of chip morphology [137]. CM: conventional milling. Reproduced with permissions from Refs. [136,137] from ASME and Elsevier.

predicted and verified. The P_L and V_L parameters of the 52100 bearing steel were changed using an ytterbium fiber laser (wavelength of 1060 nm). The experimental results showed that the cutting force of LAM (18 W) was smaller than that of CM. Both the material removal rate and tool life of LAM were higher [136].

The HAZ on the machined surface affects the dimensional accuracy and service performance of the workpiece after heating using the laser system. Kadivar et al. [137] proposed a two-stage LAM process to solve the problems in which a continuous wave or short-pulse laser may produce an HAZ that may be retained on the surface of the finished product, and the use of coolant would lead to a decrease in laser heating efficiency. The first stage is based on an ultrashort pulse laser to soften the shear zone on the workpiece surface. In the second stage, a micro-milling cutter is used to change the softened surface constructed in the first stage to the final size. The advantage of using an ultrashort pulse laser was that it achieved control of the HAZ range in real time. The workpiece could be machined to a certain softening size by controlling the laser parameters. The workpiece is then processed under different cutting conditions. Therefore, the processing parameters were independent of the laser parameters. However, the two-stage coordination can match the laser softening depth with the cutting manufacturing depth. The LAM of X5CrNi18-10 steel was conducted using a Yb:YAG picosecond laser. The laser heat parameters included P_L and the distance between the laser spot and tool. The cutting transformation parameters were v_c, f_z, and α_e. It was observed that the cutting force is affected by v_c. Compared with CM, LAM significantly reduced the axial and tangential forces by 70% and 50%, respectively. Regarding chip morphology, the LAM chip was small and thin, as shown in Fig. 13(b) [137], which also led to a smaller milling force for LAM. In addition, appropriate laser parameters are essential for achieving efficient LAM machining. Setting P_L to 10 W reduced the machining temperature by 50%. Therefore, for optimal LAM performance parameters, the laser power should be set to 10 W, and the distance between the spot and the tool should be 250 μm [137].

Controlling the HAZ is crucial for machining processes. Zeng et al. [138] found that LAM may induce a workpiece to produce a harmful HAZ. Accordingly, an HAZ analysis model was established to predict the HAZ generated by laser heating in the LAM of AerMet100 steel. A 1-kW HPDL laser (wavelength of 915 nm) was used to verify the proposed analysis model by transforming P_L and v_f. According to Fig. 14 [138], the HAZ size increased significantly with an increase in P_L (from 200 to 1000 W) and decreased with an increase in v_f. The temperature change in the HAZ ranged from 138.8 to 574.7 °C. The HAZ width increased with d_L, while the HAZ depth decreased because of the inverse correlation of the d_L energy concentration. Therefore,

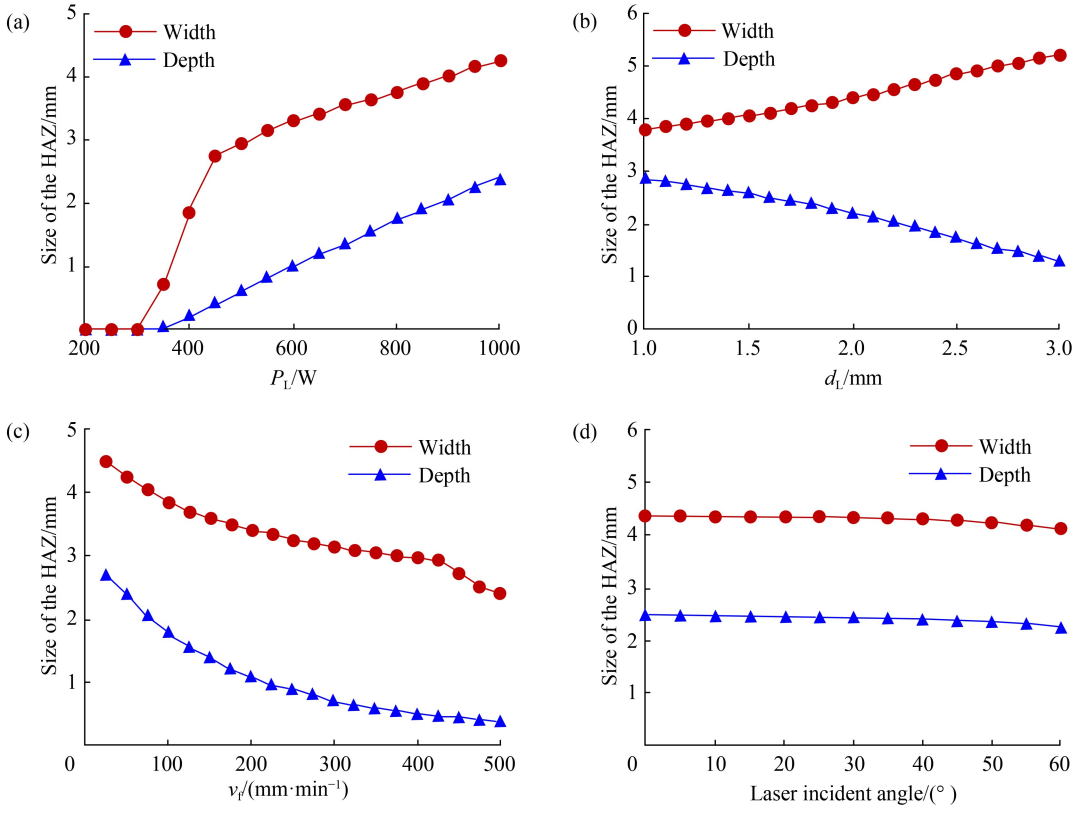

Fig. 14 Effect of different laser parameters on heat-affected zone: (a) P_L, (b) d_L, (c) v_f, and (d) laser incident angle [138]. HAZ: heat-affected zone. Reproduced with permission from Ref. [138] from Springer Nature.

considering that the side milling a_e value was small and the a_p value was large, it was recommended to use a laser with a smaller d_L value, whereas the opposite applies to face milling, for which a laser with a larger d_L value should be utilized. Compared with the other laser parameters, the influence of the laser incident angle on the HAZ was small. Furthermore, as shown in Fig. 14(a) [138], the HAZ could be caused by a critical P_L value because the P_L value was less than the critical P_L value. The absorption temperature of the workpiece did not reach the austenite transformation temperature of the material [138].

3.2 LAM of titanium alloy

LAM can aid in optimizing the cutting force and improving the microstructure of planar workpieces. Kim and Lee [139] used a 1-kW HPDL laser (wavelength range of 940–980 nm) and set the surface temperature of the LAM workpiece to 618 °C (laser power of 80 W) to perform comparative cutting experiments on TC4 workpieces with and without LAM processing. The purpose of this study was to assess the influence of v_c, f_z, and α_p on cutting force, tool wear, and surface roughness. The results showed that the cutting force of the LAM was reduced by 13%–46% compared with that of the CM. Adhesion of cracks and chips was not observed on the tool wear surface under the SEM conditions. In all experiments, the surface roughness and microstructure were improved, as shown in Fig. 15 [139].

In actual machining processes, titanium alloy parts mostly possess curved surfaces, such as compressor blades and casings of aeroengines. The optimal laser power for machining curved surfaces can be determined based on the tool-inclination angle. Sim and Lee [140] worked on the preheating and machining optimization of the tool-path inclination angle in the LAM process. First, FEM was applied for the thermal analysis of TC4. Based on this, the optimal P_L was determined according to the tool-path angle. TC4 milling experiments were then conducted using a 1-kW HPDL laser (wavelength range of 808–980 nm, laser power of 80 W). According to the results, the preheating temperature decreased with increasing tool-path inclination, as shown in Fig. 16(a) [140]. However, when the tool inclination angle exceeded 75°, the preheating temperature began to increase. The accuracy of the simulation process was verified by the experimental results. The experiments also revealed that the cutting force in the LAM process decreased with an increase in the tool-path inclination angle [140].

Considering the reduction in the stress concentration of fillets, the fillet can improve the service life of the workpiece, and the fillet strategy is widely utilized in actual tool path design. Therefore, it is necessary to create

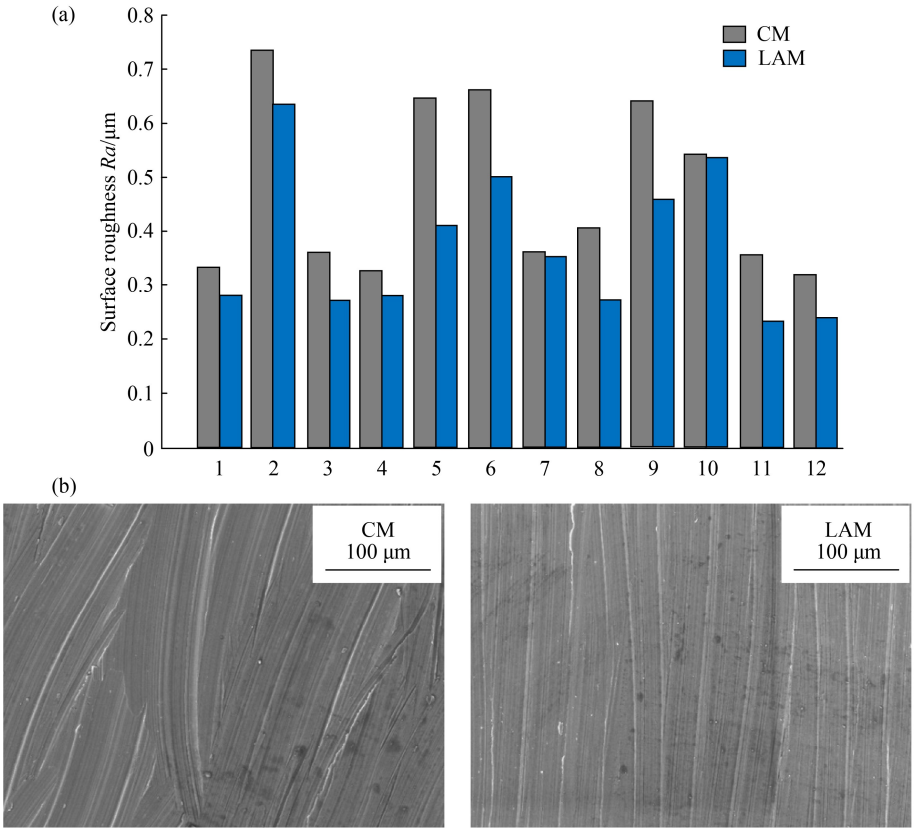

Fig. 15 Conventional milling and laser-assisted milling (LAM) machined surface: (a) surface roughness and (b) microstructure [139]. CM: conventional milling. Reproduced with permission from Ref. [139] from MDPI.

a detailed LAM strategy for the tool path of the fillets. Woo and Lee [141] proposed a laser energy field-assisted fillet milling strategy to solve the problem in which the laser beam could not continuously irradiate the top of the workpiece when laser energy field-assisted corner milling was conducted using an additional axis laser module. The laser-assisted fillet milling path and processing conditions based on the linear difference are shown in Fig. 16(b) [141]. The specific implementation scheme included the following: First, the milling origin (0, 0), the expected fillet radius (R), the number of coordinate points, and the tool radius angle (α_i) were determined to calculate the coordinate tool point (P_{ci}). The calculation formula for the tool coordinate point can be expressed as

$$x = r \times \cos(180 + \alpha) + r, \quad r = r_c + R, \tag{1}$$

$$y = r \times \sin(180 + \alpha) + r, \tag{2}$$

where r represents the radius of the cutting tool, and r_c represents the sum of the radius of the cutting tool.

Second, the distance (x_{cl}) between the tool center and the laser heat source center as well as the heat source radius were determined, and the distance (Δ_{xi}) between the initial coordinate point (P_{li}) of the heat source and the end coordinate point (P_{Li}) of the laser heat source was calculated. Finally, the calculated tool coordinates and laser heat source coordinates were transformed into G and M codes and were input into the machine tool.

After the fillet LAM strategy was completed, the effective cutting depth was obtained by thermal analysis, as shown in Fig. 17 [142]. The response surface method was used to design the experiments. Finally, the experiment was conducted using a 1-kW HPDL laser with wavelengths ranging from 940 to 980 nm and a preheating temperature of 600 °C. A cutting-force prediction model was established based on the regression analysis. Optimal manufacturing conditions for milling TC4 are provided. The results showed that, compared with CM, the feed force, axial force, cutting ratio, and surface roughness of LAM were reduced by 23.7%, 20.6%, 24.2%, and 47%, respectively [141,142].

The LAM of curved surfaces under real operating conditions can be determined by combining the tool-inclination angle with the fillet LAM strategy. Oh et al. [143] combined a curved surface milling method with LAM technology using a 1-kW HPDL laser (wavelength range of 940–980 nm) and determined that the preheating temperature for milling TC4 material was 980 °C. The cutting force and specific energy of conventional surface milling and curved-surface LAM technology under different processing conditions were assessed. Compared with conventional surface milling, the cutting force and

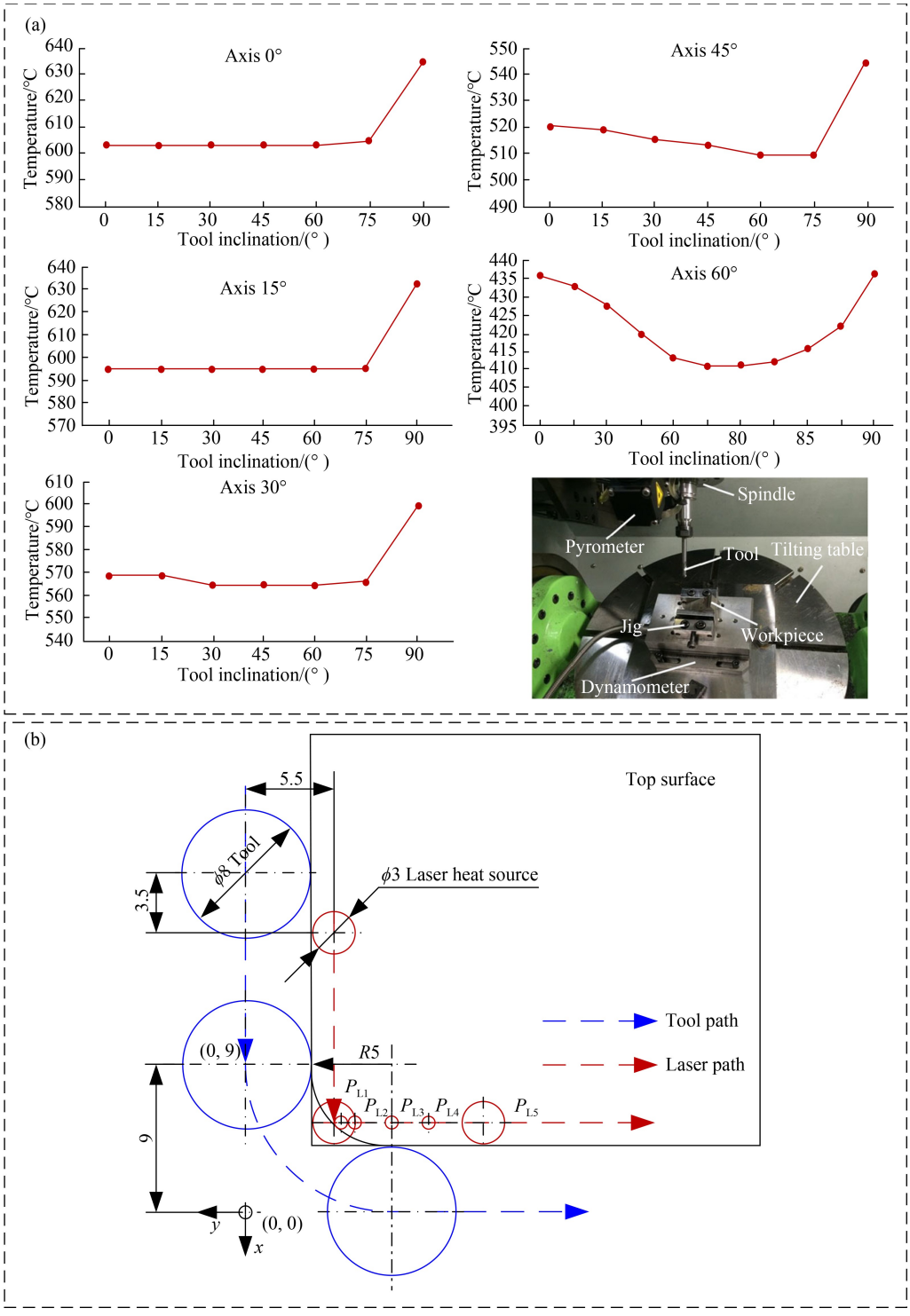

Fig. 16 Rotation angle and round angle of laser-assisted milling: (a) temperature distribution of rotation angle [140] and (b) round-angle laser-assisted milling path [141]. Reproduced with permission from Refs. [140,141] from Springer Nature.

specific cutting energy of curved surface LAM decreased by 33% and by 28% to 41%, respectively [143].

According to Taylor's tool-life equation, the single-piece manufacturing cost of LAM can be quickly obtained. Hedberg et al. [144] conducted LAM research on TC4 using a 1-kW IPG Photonics ytterbium fiber laser (wavelength of 1071 nm). Based on the heat transfer mechanism of TC4, a temperature distribution prediction model for LAM was established. The appropriate laser parameters were optimized using the prediction model. The surface quality, unit cost, and annual cost are presented in Fig. 18 [144,145]. To ensure the surface

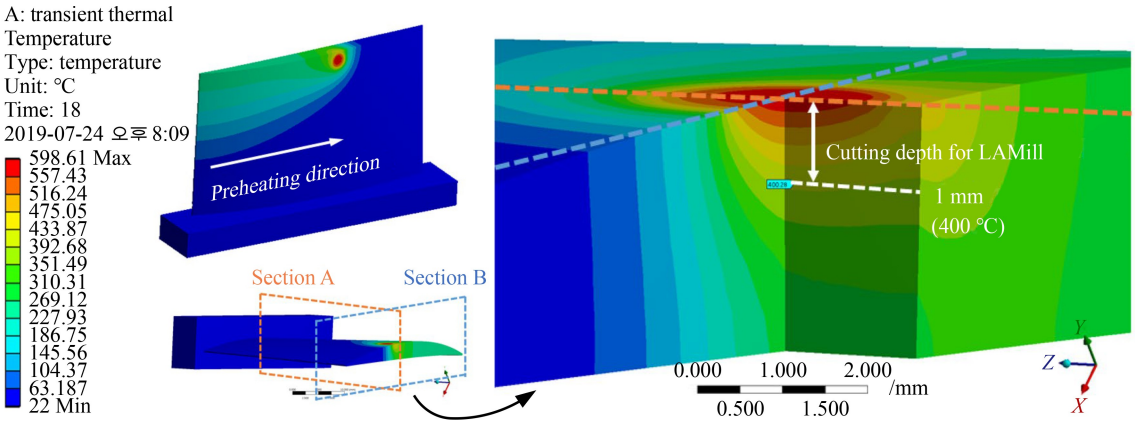

Fig. 17 Thermal analysis of laser-assisted milling [142]. Reproduced with permission from Ref. [142] from Springer Nature.

integrity and service performance of the workpiece manufactured by LAM, the cutting force, tool wear, microstructure (Fig. 18(a) [144]), XRD structure, surface hardness, residual stress (Fig. 18(b) [144]), and economy of LAM technology were determined. According to Taylor's tool life equation obtained from the results of the hypothesis and experimental tests, the total costs of a single piece manufactured by CM and LAM technology under different v_c values were calculated, and the results are shown in Fig. 18(c) [144]. Compared to CM, the cutting force, residual stress, and manufacturing cost of LAM (preheating temperature of 500 °C) were reduced by 20%, 10%, and 33%, respectively. In addition, LAM extended the tool life by 64% and improved the material removal rate by 35% [144,146].

After optimizing the LAM parameters, the annual production cost of the enterprise can be significantly reduced. Wiedenmann et al. [147] applied LAM technology to conduct experiments on TC4 titanium alloys. The experiment was set up based on the central composite design (CCD) method using a 4-kW Nd:YAG laser (wavelength of 1064 nm) as an experimental auxiliary tool and P_L, d_L, x_L, α_p, α_e, and f_z as the parameter variables. After studying the influence of simultaneous changes in the laser and milling parameters on the cutting force, the authors found that among the selected parameters, P_L had the greatest influence on the cutting force in all directions, with an overall decreasing trend in the cutting force with increasing P_L. The determined theoretical optimal value of d_L was 2.65 mm [147]. Furthermore, compared with CM, LAM technology could reduce the cutting force, improve the material removal rate by 33%, and prolong the tool life by 19% when the preheating temperature was 800 °C [145]. As shown in Fig. 18(d) [145], taking the milling of titanium turbine blades as an example, the highest economic potential of LAM is the production of 1200 parts per year, which could save up to 10.5% of the manufacturing cost of all products.

3.3 LAM of nickel-based alloys

External laser auxiliary equipment is widely used owing to its convenient installation. Kong et al. [148] used an Nd:YAG laser (wavelength of 1064 nm) and a preheating temperature of 800 °C to conduct LAM of a planar workpiece made of K24 nickel-based alloy. The effectiveness of the LAM was explored by measuring the cutting force, surface roughness, and tool wear at different material removal temperatures, which could reduce the surface roughness and cutting force. From the experimental results, they discovered that the cutting force was reduced by 30%–70%, and the life of the coated tools was extended by 46%. By comparing different coated tools, the authors found that the main wear mechanisms of the tools in the LAM process were adhesive wear and abrasive wear, as shown in Fig. 19(a) [148]. The TiAlN-coated tools had the highest wear resistance at a cutting speed of 30 m/min, whereas the TiCN coating had the poorest performance. Notches can be observed after processing for a certain time, as shown in Fig. 19(b) [148]. Because the tool damage was caused by the high temperature in the machining process, Tian et al. [149] proposed a transient three-dimensional thermal model for LAM to accurately obtain the temperature distribution. The accuracy of the model was verified by measuring the surface temperature using an infrared thermal imager and thermocouple. The LAM experiment on a planar workpiece made of Inconel 718 was conducted using a 4-kW HPDL laser (wavelength of 808 nm). Tool wear was observed by SEM, indicating that with increasing P_L, abrasive wear became more uniform. Excessive P_L leads to an increase in the tool wear, as shown in Fig. 19(c) [149]. Therefore, the following experimental conclusion was obtained. The verification model could provide the transient temperature distribution of the workpiece when its geometrical shape changed during the machining process. After adjusting P_L, the laser temperature was set to 520 °C. Under this condition, compared with CM, LAM can

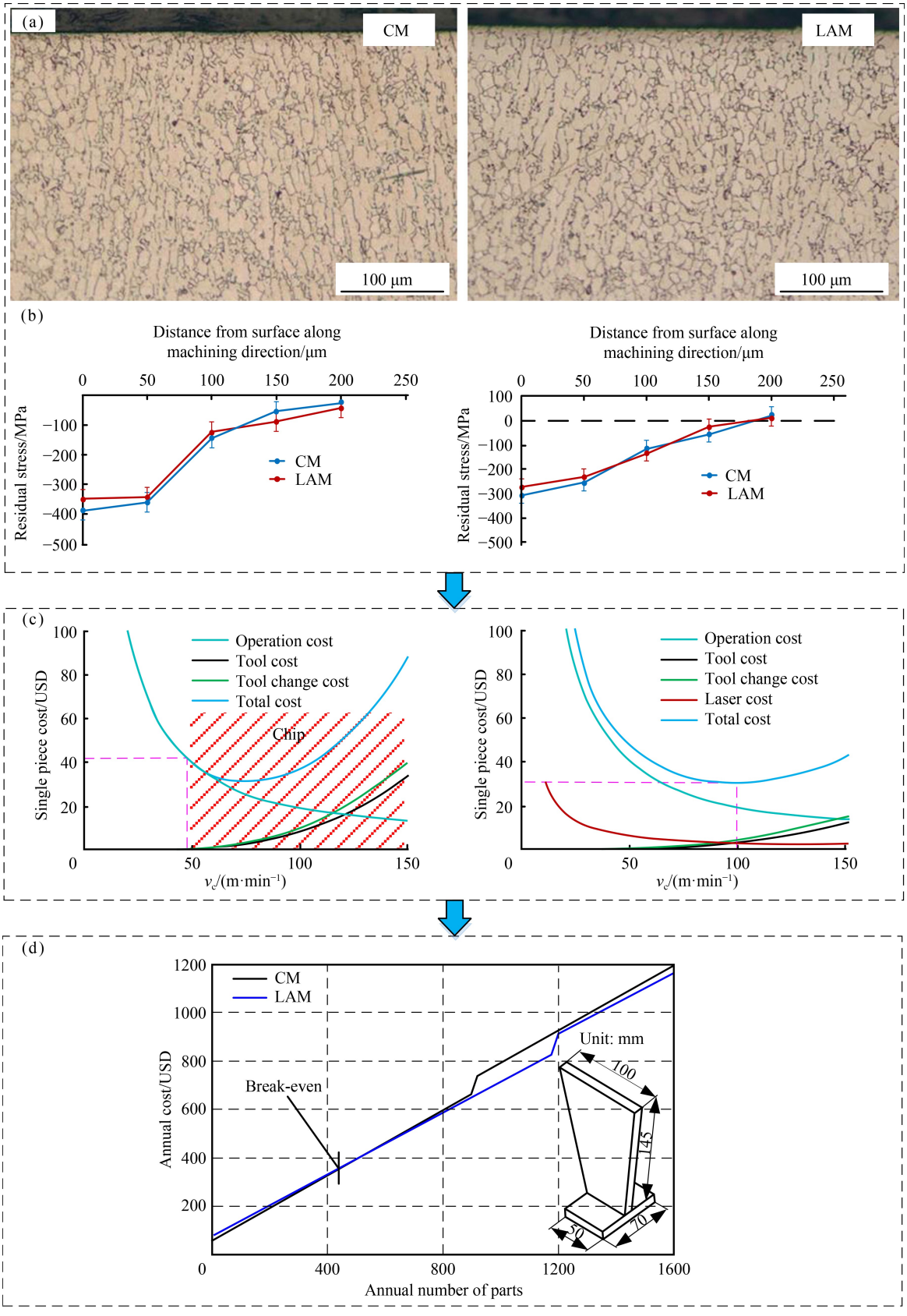

Fig. 18 Surface quality, unit cost and annual cost: (a) microstructure, (b) residual stress, (c) cost of the unit under different v_c [144], and (d) annual costs of produced parts [145]. CM: conventional milling; LAM: laser-assisted milling. Reproduced with permissions from Refs. [144,145] from Springer Nature and Elsevier.

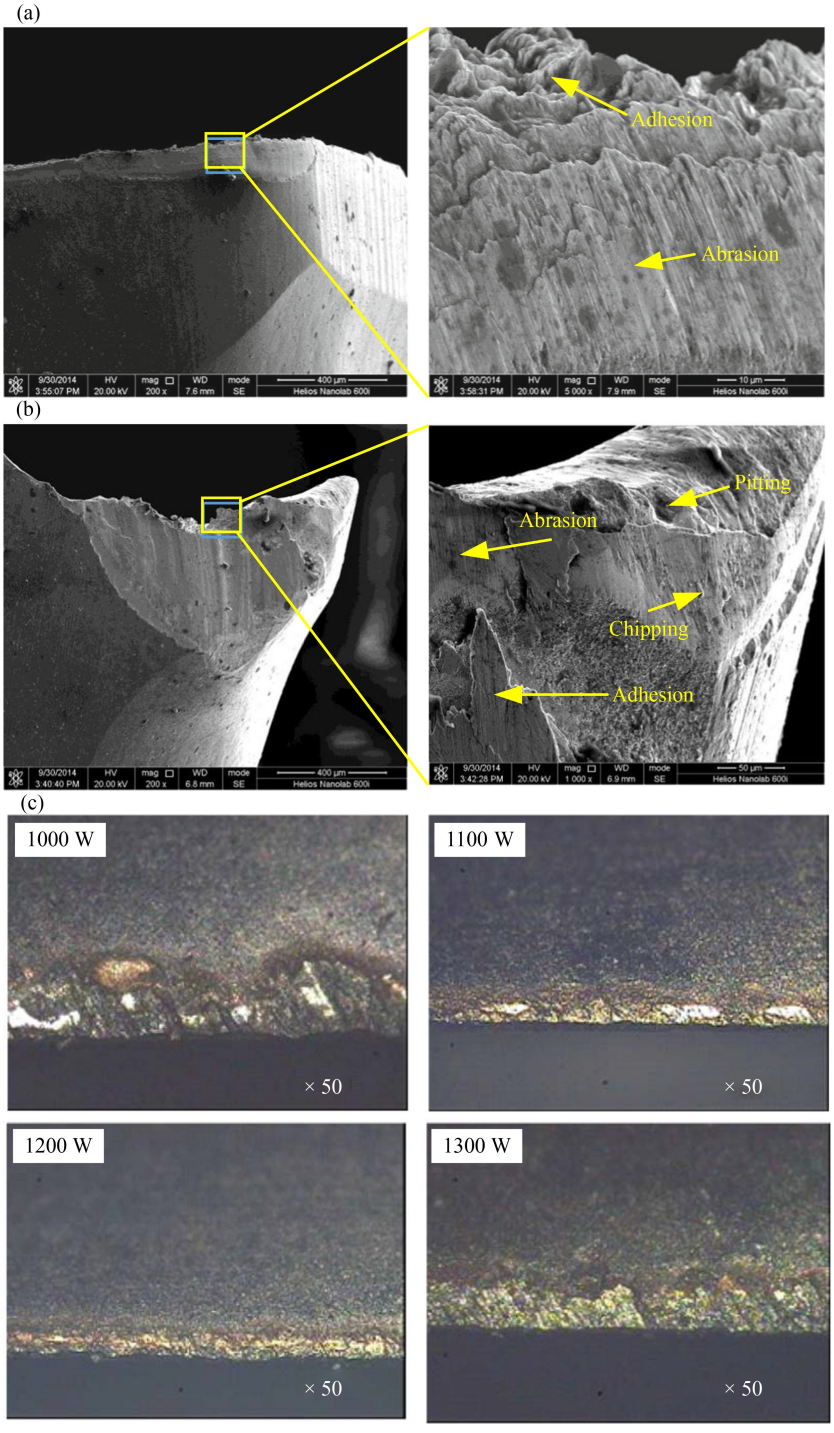

Fig. 19 Flank face wear at different milling conditions: (a) scanning electron microscope of coated tool at 10s with laser-assisted milling, (b) scanning electron microscope of coated tool at 16.6 min with laser-assisted milling [148], and (c) scanning electron microscope of the coated tool at 20 mm with laser-assisted milling under different P_L [149]. Reproduced with permissions from Refs. [148,149] from Springer Nature and ASME.

reduce the cutting force, number of chips, and surface roughness by 40% to 50%, 50%, and 50%, respectively [149].

A systematic understanding of the comprehensive mechanism of the processing technology and choice of laser parameters is crucial for a detailed understanding of the LAM process. Kin and Lee [150] performed an LAM experiment on a planar workpiece made of Inconel 718 with a 1-kW HPDL laser (wavelength range of 940–980 nm). First, material properties (thermal conductivity and specific heat) were obtained. The appropriate P_L and range of the predicted temperature were determined based

on the FEM. Subsequently, LAM experiments were conducted with different P_L and α_p. According to the results, the cutting force decreased with increasing P_L irrespective of the change in α_p. Compared to CM, the cutting force of LAM decreased by 55% when the preheating temperature was set to 900 °C (180 W), but the surface roughness increased by 70% [150]. Second, to eliminate the observed negative effect of the increase in surface roughness, a new technology, B&F, was proposed with a preheating temperature of 900 °C. In the experiments, different workpiece inclination angles were applied. The results showed that the cutting force decreased with increasing workpiece inclination. The levels of tool damage and surface quality were improved, as shown in Fig. 20 [151]. Finally, the cutting force of LAM (B&F) was smaller than that of LAM and CM. Compared with CM, the surface roughness of LAM (B&F) and LAM decreased by 34.2% and 56.8%, respectively [151]. Based on the parameter optimization for planar LAM and the new technology, the LAM experiments on contour and slope non-uniform rational B-spline (NURBS) three-dimensional surfaces outperformed at a set preheating temperature of 940 °C. The cutting forces of contour LAM and slope LAM decreased by 39.6% and 33.7%, respectively, compared with those of CM. The surface roughness and cutting ratio were reduced by 38.59% and 49.91%, respectively. It was demonstrated that contour LAM was better than slope LAM [152].

The temperature of the workpiece surface significantly influences the LAM process. Wu et al. [153,154] found that the laser preheating temperature was the most important parameter affecting the laser heating effect. However, a constant laser energy could not provide a stable preheating temperature during the cutting process. The temperature feedback and cutting temperature are shown in Fig. 21 [153,154]. A temperature feedback control method for the LAM process was proposed based on the results shown in Fig. 21(a) [153]. The authors established a composite simulation model including a preheating temperature model, temperature feedback model, temperature difference prediction model, and cutting process model. Furthermore, the cutting temperature field and cutting process were simulated to determine differences in temperature. Subsequently, the laser-heating temperature can be controlled by monitoring and adjusting. The simulation and experimental results showed that P_L was the main factor affecting the difference between the preheating, shear zone, and monitoring temperatures, as shown in Figs. 21(b) [154] and 21(c) [154]. The LAM of Inconel 718 was performed using a 1-kW HPDL laser (wavelength of 808 nm). Compared with CM, the main cutting forces corresponding to preheating temperatures of 400 and 700 °C were reduced by 23% and 45%, respectively [154]. Comparing the tool life of the CVD-coated tools and PVD-coated tools, it was found that the CVD coating was more suitable for the LAM process. The error of the tool life prediction model was less than 15% according to the experimental results, which verified the accuracy of the model [153].

An optimized process can effectively heat a region whose area is wider than d_L and ensure the uniformity of the temperature distribution in the heating region. Shang et al. [155] proposed a new spatially and temporally controlled (S&T) laser heating method, which was characterized by laser points with oscillations along specific trajectories and the generation of HAZs. In contrast to the oscillating heating method proposed by Bermingham et al. [134], the S&T method not only provides information about the configuration of laser heating (such as P_L, V_L, and the laser scanning path) but also shows the heating effect. In their study, the correctness of the laser configuration was mainly proven

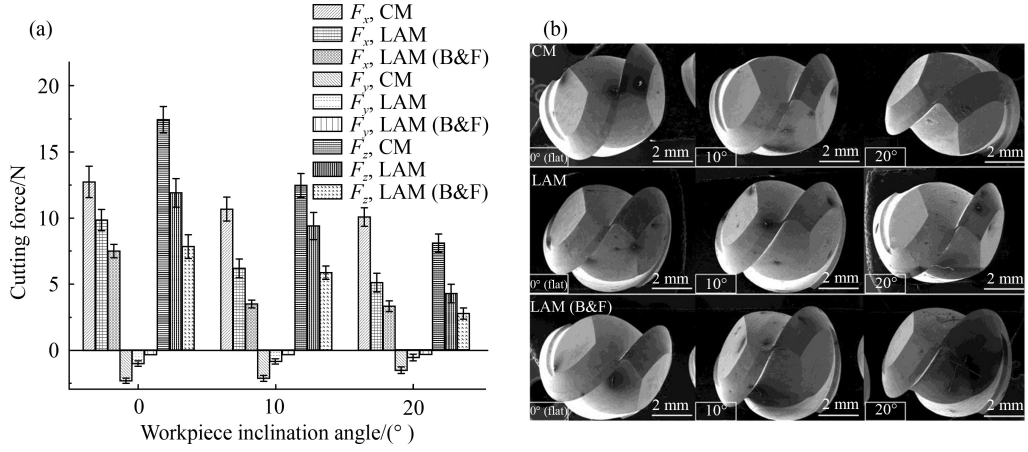

Fig. 20 The influence of workpiece inclination angles on cutting force and tool damage: (a) workpiece inclination and cutting force and (b) workpiece inclination and tool damage [151]. CM: conventional milling; LAM: laser-assisted milling. Reproduced with permission from Ref. [151] from Springer Nature.

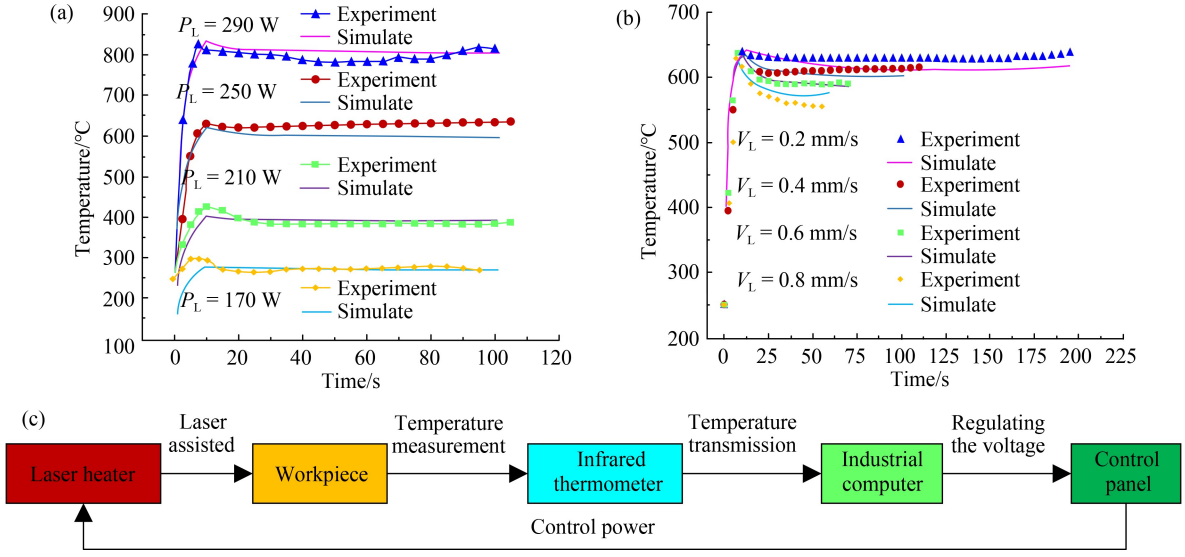

Fig. 21 Temperature feedback and cutting temperature: (a) effect of P_L on cutting temperature, (b) effect of V_L on cutting temperature [154], and (c) schematic diagram of the temperature feedback system [153]. Reproduced with permission from Refs. [153,154] from Springer Nature.

by forward and inverse heat conduction. Forward heat conduction can determine the temperature distribution in the workpiece with a given laser beam configuration. Reverse heat conduction was used to determine the optimal laser system parameters. The LAM of Inconel 718 was conducted using a 10-kW HPDL laser at a preheating temperature of 800 °C. The average value and peak of the cutting force in the LAM process were calculated based on the measured cutting force shown in Fig. 22(a) [155]. The peak and average values of the main cutting force were reduced by 55% and 47.8%, respectively, after the proposed S&T controlled laser heating method was applied. The peak and average feed forces decreased by 26.3% and 26.1%, respectively, which reduced the cutting power by 35.4%. In addition, compared with dry milling, LAM with the laser heating method controlled by S&T reduced the surface roughness by 14% [155]. The authors also conducted a comprehensive study on the residual stresses and microstructure of a workpiece processed by LAM technology (laser power in the range of 1300–1500 W) and further studied the chip morphology and microstructure formation. By comparing LAM, CM, and LS, a melting layer was observed on the free surface of the chips generated by LAM by comparing LAM, CM, and single laser scanning. The bending phenomenon of the LS workpiece was also compared. This bending effect was not eliminated after removal of the softening layer by the LAM process. These results indicate that LAM technology is more suitable for the machining of cylindrical parts. In addition, to further understand the plastic strain during processing, it is necessary to measure the intragranular local misorientation (LMO) in the chip crystal, namely, the dislocation accumulated in the crystal during grain deformation, as shown in Fig. 22(b) [156]. Among the images, a slip band composed of several slip planes is present in the LAM chip. However, the CM image showed a more obvious directional dislocation, and the LS image showed no obvious dislocation. The results indicated that LAM combines the advantages of reducing the cutting force and improving the material removal rates [156].

Built-in laser auxiliary equipment is difficult to install, and its large-scale implementation has high costs. Brecher et al. [157] developed a 2.3-kW (wavelength of 1070 nm) fiber laser system moved by an Hohl Shaft Kegel (HSK) hollow shank based on Fraunhofer Institute for Production Technology (Fraunhofer IPT), which preheated the surface of the shear zone of an Inconel 718 workpiece before machining to 800 °C. During the experiment, it was necessary to change P_L and measure the cutting force. Compared with the CM, the cutting force, axial force, feed force, and tool wear of the LAM were reduced by 60%, 60%, 40%, and 57.14%, respectively. Finally, it was observed that the tool wear was the smallest when the P_L value was 1.54 kW [157].

3.4 Summary of LAM of difficult-to-machine metal materials

Based on the above investigations, the preheating temperature ranges during LAM of difficult-to-machine metal materials are different because of their inconsistent basic properties. The tensile strength of high-strength steel decreases when the preheating temperature exceeds 400 °C. Because material oxidation can easily occur at temperatures above 600 °C, the preheating temperature of high-strength steel for effective processing ranges from 400 to 550 °C [132,133,138]. The tensile strength of

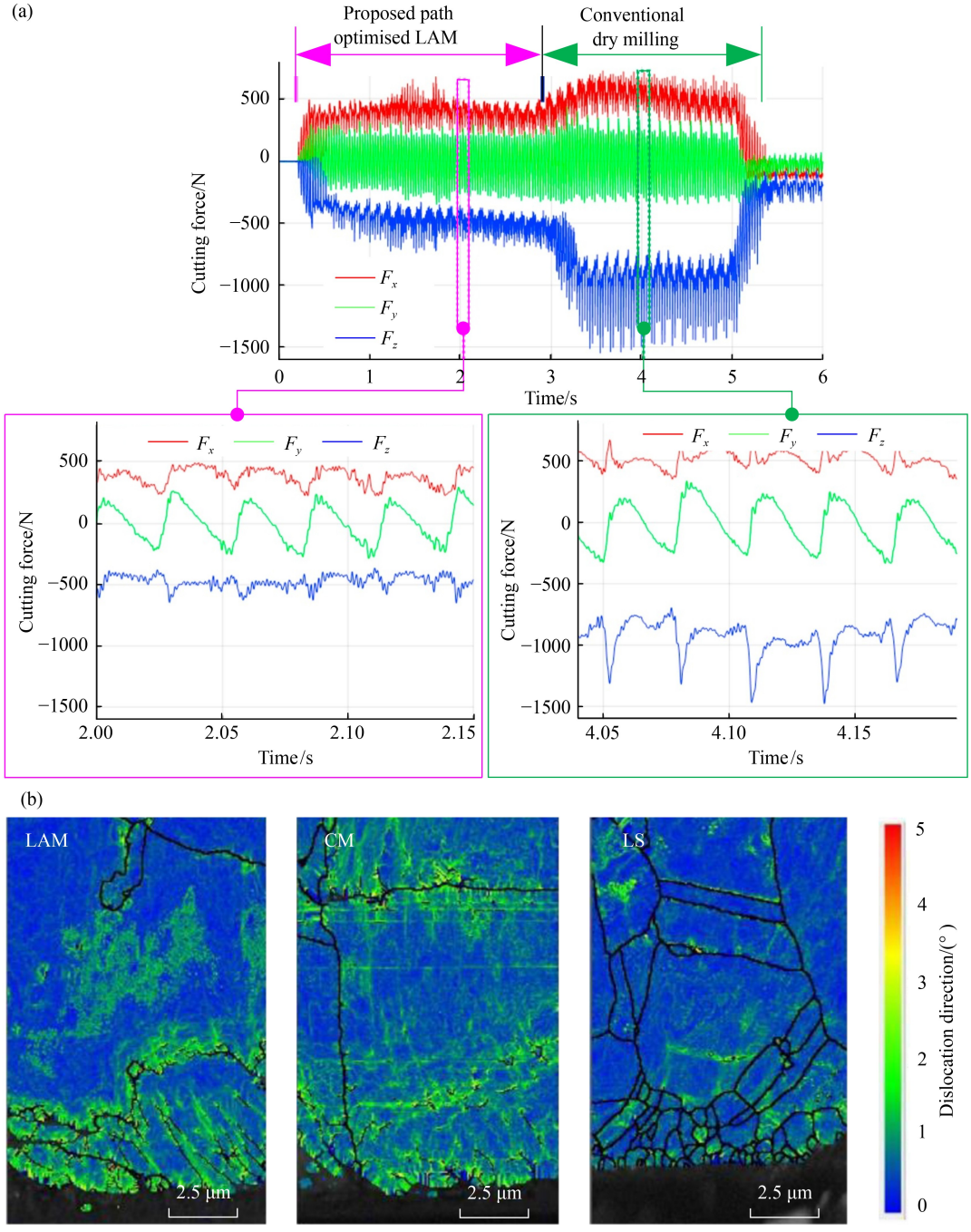

Fig. 22 Cutting forces and grain deformation distribution: (a) cutting forces of path-optimized laser-assisted milling (LAM) [155] and (b) grain deformation distribution in different machining processes [156]. CM: conventional milling; LS: single laser scanning. Reproduced with permissions from Refs. [155,156] from Elsevier.

titanium alloys is significantly reduced at temperatures above 600 °C, and the preheating temperature range of titanium alloys is between 500 and 620 °C for effective processing [139,141,142]. The yield strength of nickel-based alloys decreases sharply when the temperature exceeds 650 °C, and the preheating temperature of nickel-based alloys for effective processing ranges from 650 to 950 °C [148,150,151]. Compared with CM, although the preheating temperature range of difficult-to-machine metal materials for effective processing is different, LAM of high-strength steel, titanium alloy, and nickel-based alloy has advantages, such as a small cutting force, high material removal rate, long tool life, low specific cutting energy, low manufacturing cost, small chip size, and high surface quality, as shown in Fig. 23. However, the superiority of LAM for various difficult-to-machine metal materials has been verified experimentally. The research mainly focuses on the influence of the laser parameters

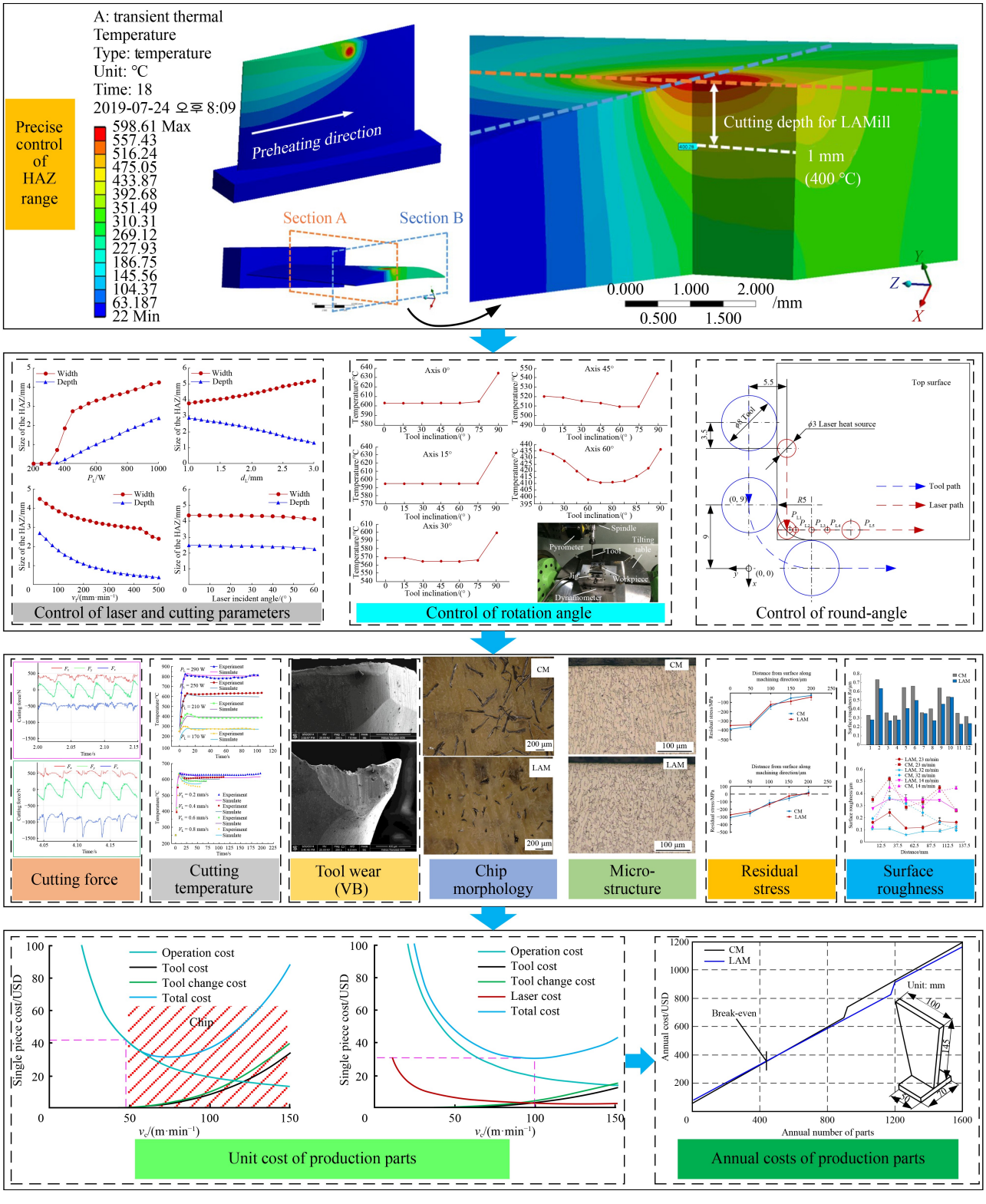

Fig. 23 Summary of laser-assisted milling machinability. HAZ: heat-affected zone.

(P_L, V_L, d_L, laser incident angle, and laser position) and cutting parameters (v_c, v_f, α_p, and α_e) on the effect of machining processes and the results of the experiments. However, some research aspects of LAM machining processes, including real-time temperature control and HAZ, are still worth studying. LAM processing technologies include laser-assisted cavity milling, spiral milling, and cycloid milling. Real-time temperature control is critical in LAM, and it involves various algorithms, such as fuzzy control, proportional−integral−

derivative (PID) control, and generalized predictive control. To avoid producing HAZ during LAM, researchers use finite element transient thermal analysis and consider emissivity and absorptivity in the HAZ model to determine the laser parameters. Further research in LAM should focus on the theory and mechanism of material removal and chip breaking using FEM and temperature field control technology. It is essential to monitor the temperature and phase transition of the shear zone under different processing conditions to understand the variation law of LAM of difficult-to-machine metal materials. A real-time sensing model of temperature change and microstructure transformation in the shear zone can help optimize the process parameters. To prevent HAZ from remaining on the workpiece surface, LAM processes should be optimized using FEM chip breaking simulation models and HAZ range. This optimization includes laser scanning path, laser incident angle, and temperature control times. Moreover, by considering the effects of laser and cutting parameters on various factors like cutting force, material removal rate, tool life, cutting specific energy, manufacturing cost, chip morphology, and surface quality, prediction models can be developed using various intelligent algorithms. These models can help promote the industrialization and application of LAM technology.

4 Ultrasonic energy field-assisted milling of difficult-to-machine metal materials

UVAM is a typical intermittent cutting process that can periodically open a cutting area [158]. By applying a micron-level ultrasonic frequency vibration to the workpiece or tool, f, and controlling the vibration direction, A, the high-frequency periodic separation of the workpiece and tool in the cutting process is realized, and the milling vibration is effectively reduced, thereby improving the machinability of difficult-to-machine metal materials. The basic principle and device of UVAM are shown in Fig. 24(a) [159,160]. Compared with CM, UVAM can reduce the cutting force and temperature, prolong the tool life, and optimize the quality of the workpiece surface. Periodic separation of the workpiece and tool produces a cutting process with variable thickness, which plays an effective role in chip breaking [161,162]. The UVAM of difficult-to-machine metal materials can be divided into three classes according to the applied vibration amplitude ranges; the logical structure is shown in Fig. 24(b).

For studies on UVAM of nickel-based alloys, first, the one-dimensional axial workpiece vibration method was used to analyze the influence of cutting parameters on cutting force, tool wear, and surface roughness. Second, the one-dimensional feed workpiece vibration method was used to analyze the influence of cutting parameter changes on the surface roughness and the suppression effect of A values on burrs. Finally, the effects of UVAM on the microstructure, hardness, fatigue life, and surface roughness of the workpiece were analyzed using the one-dimensional axial tool vibration method.

Regarding the research on UVAM of titanium alloy cut by a one-dimensional tool with axial longitudinal vibration, first, the influence of cutting parameters on cutting force and surface roughness was analyzed, and the effect of UVAM on surface roughness was compared. Second, the influence of A value on the cutting force, cutting temperature, and surface roughness was assessed by increasing the vibration amplitude. Third, the influence of cutting parameters on the cutting force, cutting temperature, residual stress, and surface roughness was analyzed based on one-dimensional tool axial longitudinal vibration. Working at the longitudinal vibration of a one-dimensional workpiece feed, first, the influence of A values on the surface scale structure and the surface roughness of the workpieces was analyzed based on the formation mechanism of the surface microstructure and the theoretical model of the formation process of the surface microstructure. Second, by combining the FEM with the tool tip trajectory, the influence of A values on the cutting force and surface roughness was assessed. Based on research on two-dimensional ultrasonic vibration, a cutting edge geometry model of a ball-end milling cutter considering two-dimensional longitudinal torsional tool vibration and axial position angle was established to analyze the change in the UVAM cutting force and build a model of cutting force under different flank wear. Second, the influence of the A value on the cutting force, tool wear, and surface roughness was analyzed. Because the tool change in the ultrasonic vibration machining process would lead to burrs in the connection area during the actual production process, a non-tool change machining method based on UVAM of a flat surface and a free curved surface connection area was developed to reduce the cutting force and surface roughness.

For studies on UVAM of high-strength steel, considering one-dimensional tool axial longitudinal vibration, the effects of UVAM on the cutting force, chip morphology, and surface quality were compared. Second, the influences of f, A, and the tool angle on tool wear and surface roughness were analyzed. Third, the influence of f on the surface roughness and residual stress was studied. To identify how one-dimensional workpiece axial vibration and one-dimensional workpiece feed vibration influence the machining process, the influence of UVAM cutting parameters on surface roughness was first studied. Second, a UVAM cutting force model was established, and a new method for determining the relationship between the critical cutting speed and undeformed chip thickness was proposed. Third, the effects of cutting parameters and milling methods on the cutting force,

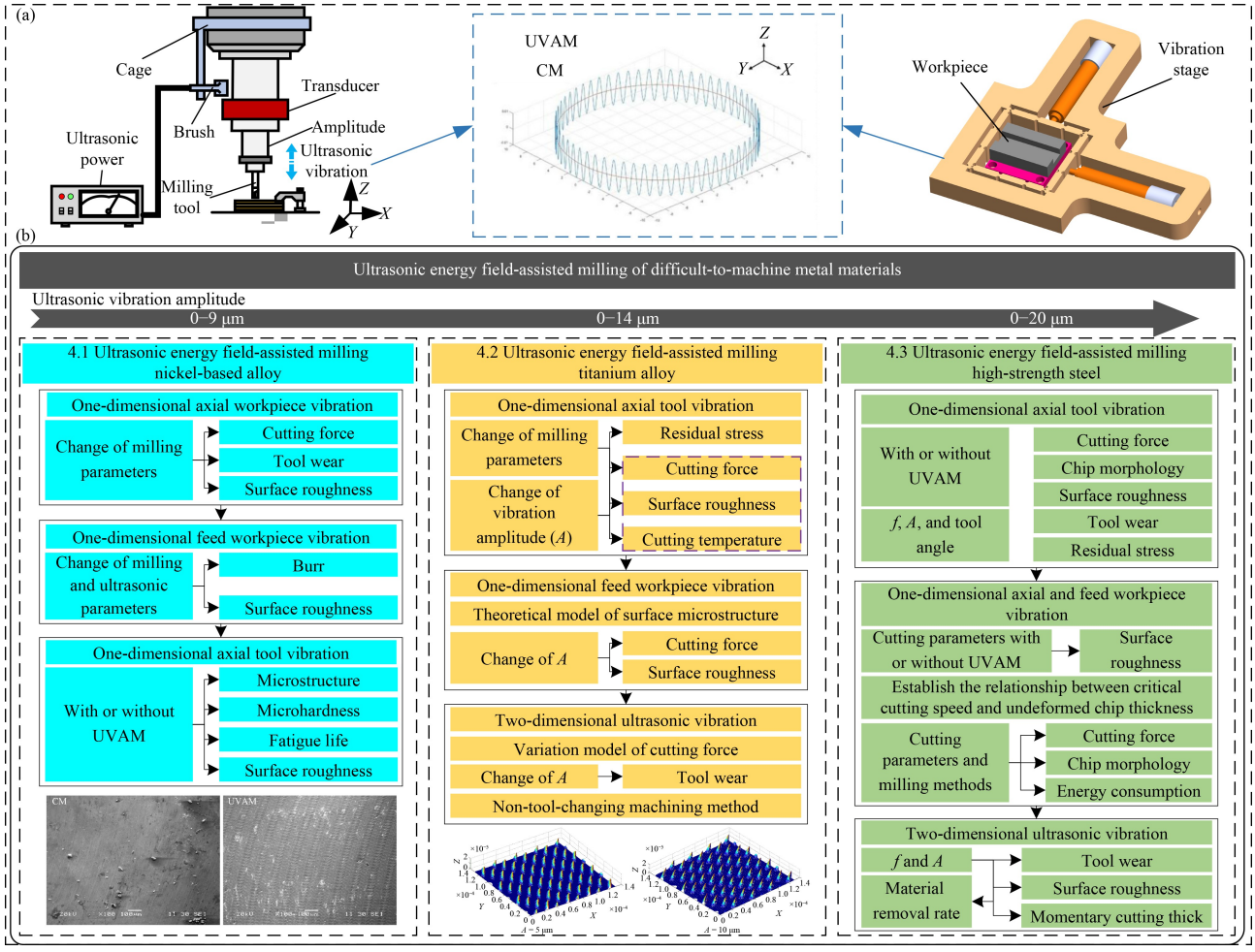

Fig. 24 Ultrasonic vibration-assisted milling (UVAM) principle and logic: (a) UVAM principle and device [159,160] and (b) logical structure of laser-assisted milling difficult-to-machine metal materials. CM: conventional milling. Reproduced with permissions from Refs. [159,160] from Elsevier.

surface roughness, and chip morphology were investigated. Finally, based on the helical milling (HM) process, the effects of UVAM on cutting force, machining energy consumption, and surface roughness were compared. Based on two-dimensional plane vibration, the effects of f and A on the tool wear, surface roughness, instantaneous cutting thickness, and material removal rate were analyzed.

4.1 Ultrasonic energy field-assisted milling of nickel-based alloy

The one-dimensional axial vibration method (workpiece vibration) can reduce milling temperature and tool wear and improve surface quality. Hsu et al. [163] conducted a UVAM experiment on a nickel-based MAR-M247 alloy. Using Taguchi's experimental design, they studied the effects of different tool materials, workpiece temperatures, cutting parameters, and f on the machining characteristics. The results indicated that UVAM reduced the milling temperature. Minimizing α_p can improve the surface quality and reduce the processing temperature and flank wear [163].

By applying one-dimensional feed longitudinal vibration (workpiece vibration), the influence of cutting parameters on the surface roughness was studied, and the burr suppression effect by changing A was explored. Fang et al. [164] used an ultrasonic energy field with f = 32 kHz and A = 3 μm for milling Inconel 718. The influence of f_z (2–6 μm/z) on the surface quality and burr of the workpiece under CM and UVAM conditions was studied. The authors found that UVAM effectively improved the surface quality. The number of surface defects decreased significantly with increasing f_z. When f_z exceeded 5 μm/z, the influence of UVAM on the surface quality was small, as shown in Fig. 25(a) [164], whereas the CM of the workpiece resulted in a poor surface quality within the given range of parameters. It is well known that surface quality can generally be described by surface roughness, as shown in Fig. 25(b) [164]. As shown in Fig. 25(b) [164], the surface roughness values after UVAM were smaller than those after CM

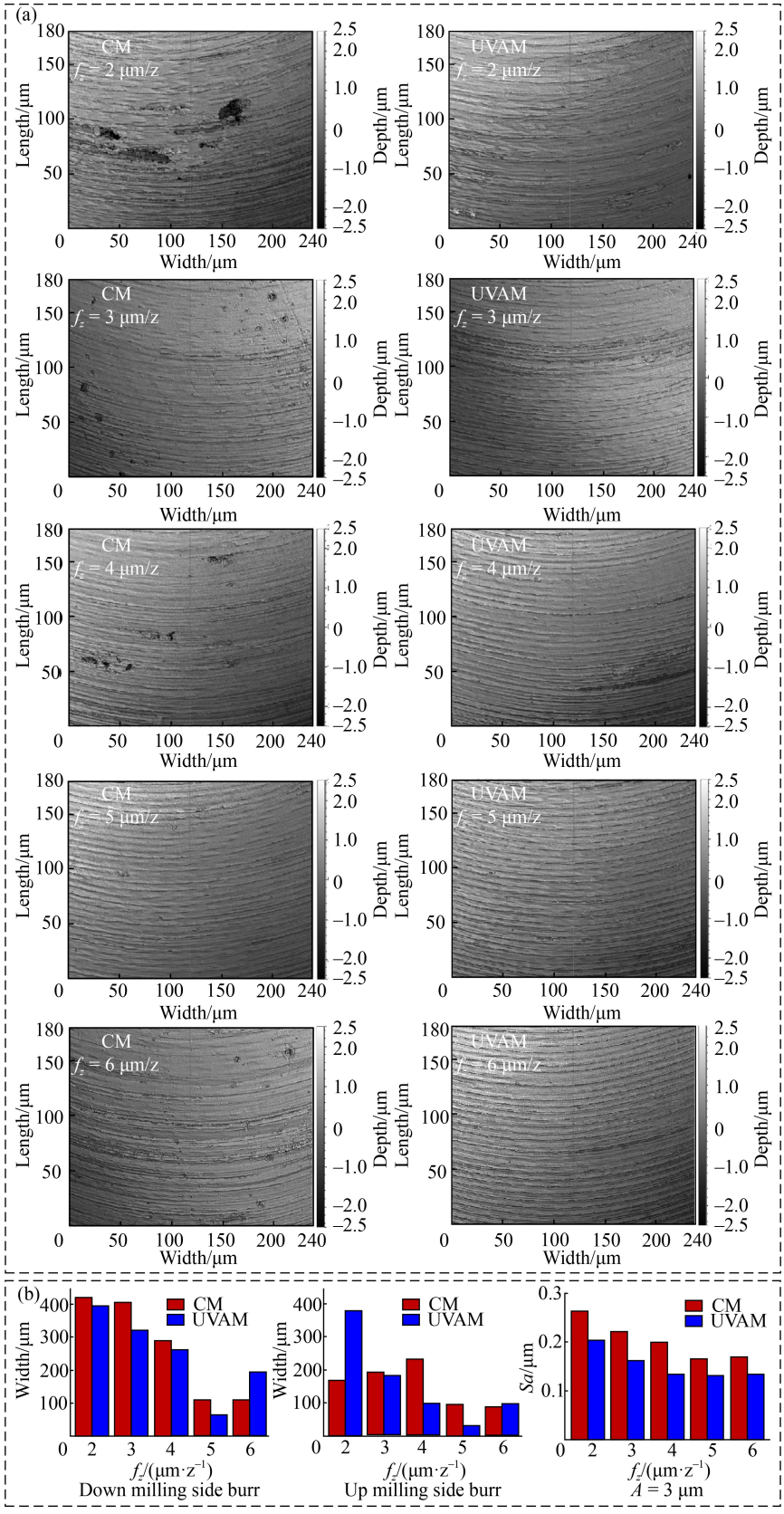

Fig. 25 Changes in surface morphology, burr size and surface roughness under different f_z: (a) bottom surface morphology and (b) burr width and surface roughness [164]. UVAM: ultrasonic vibration-assisted milling; CM: conventional milling. Reproduced with permission from Ref. [164] from Springer Nature.

processing. Furthermore, the surface roughness of the UVAM-processed workpiece decreased with an increase in f_z but increased slightly when f_z was 6 μm/z [164]. At the same f value, the team also studied the changes in Inconel 718 burrs at different v_c, f_z, and A, ranging from 18.84 to 75.36 m/min, 2 to 8 μm/z, and 0 to 9 μm, respectively. They observed that when the ratio of A to f_z was greater than 0.5, the chip breaking effect of UVAM changed the shape of the chips. Combining the FEM and experimental results, it was established that UVAM could effectively reduce the size of chips and burrs. With increasing A, the inhibitory impact of UVAM on burrs significantly increased, as shown in Fig. 25(b) [164]. Under conditions of small v_c, high f_z, and high A values, UVAM had the greatest inhibitory effect on burrs [165].

One-dimensional axial longitudinal vibration (tool vibration) is an auxiliary cutting method that can provide good machining surface quality. Suárez et al. [166,167] conducted UVAM of Ni alloy 718, setting f to 39.61 kHz and A to 1.5 μm. They focused on the influence of UVAM on surface integrity, fatigue resistance, tool wear, and cutting force. Compared to CM, UVAM reduced cutting force, improved surface microstructure (Fig. 26(a) [166]), and increased surface hardness and fatigue life of the workpiece by 3.79% and 14.74%, respectively. However, tool wear on the back surface increased by 10% [166]. After further study, the authors found that the roughness of the workpiece surface treated by UVAM decreased by 75% compared to that of CM, as shown in Fig. 26(b) [167].

4.2 Ultrasonic energy field-assisted milling of titanium alloy

Variations in cutting parameters and amplitude (A) can impact the cutting force, cutting temperature, and surface roughness of materials processed by UVAM with one-dimensional axial longitudinal vibration (tool vibration). Su and Li [168] investigated the cutting performance and mechanism of TC4 titanium alloy in a cutting experiment with f and A values of 30 kHz and 6 μm, respectively. Compared to CM, an increase in f_z and α_p reduced the corresponding cutting force of UVAM by 0.8%–42% and 5.3%–65%, respectively. The surface roughness also decreased by 10.82% to 37.97%. [168]. Based on this, the team also compared the surface roughness of selective laser melting (SLM) and conventional melting (CL) of TC4 with and without UVAM processing. Compared with CM, UVAM reduced the surface roughness values of the (SLM) TC4 and (CL) TC4 workpiece materials by 23.3% and 19.1%, respectively. Furthermore, it was observed that UVAM could effectively improve the surface morphology of (SLM) TC4 and (CL) TC4 [169], but the influence of UVAM on cutting temperature has not been studied. Gao et al. [170] studied the effect of A (from 0 to 6 μm) on the cutting force, cutting temperature, and surface roughness of TC4 workpiece material at an f value of 30 kHz, as shown in Fig. 27(a) [170]. In Fig. 27(b) [170], they observed that both the cutting force and cutting temperature decreased with increasing A but only slightly with increasing cutting temperature. When A

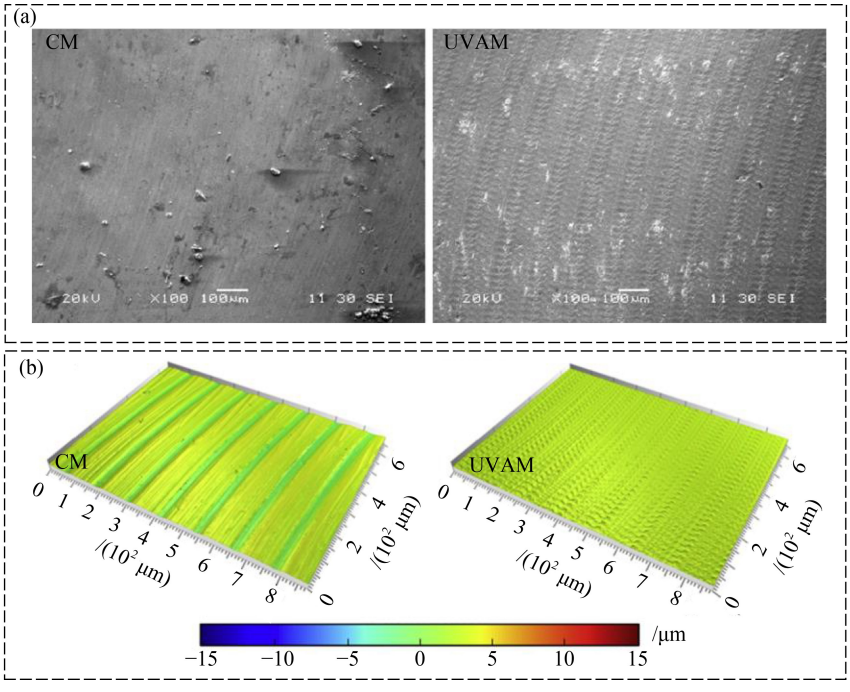

Fig. 26 Microstructure and surface roughness of conventional milling (CM) and ultrasonic vibration-assisted milling (UVAM): (a) microstructure of processed surface [166] and (b) three-dimensional surface roughness [167]. Reproduced with permissions from Refs. [166,167] from Springer Nature and Elsevier.

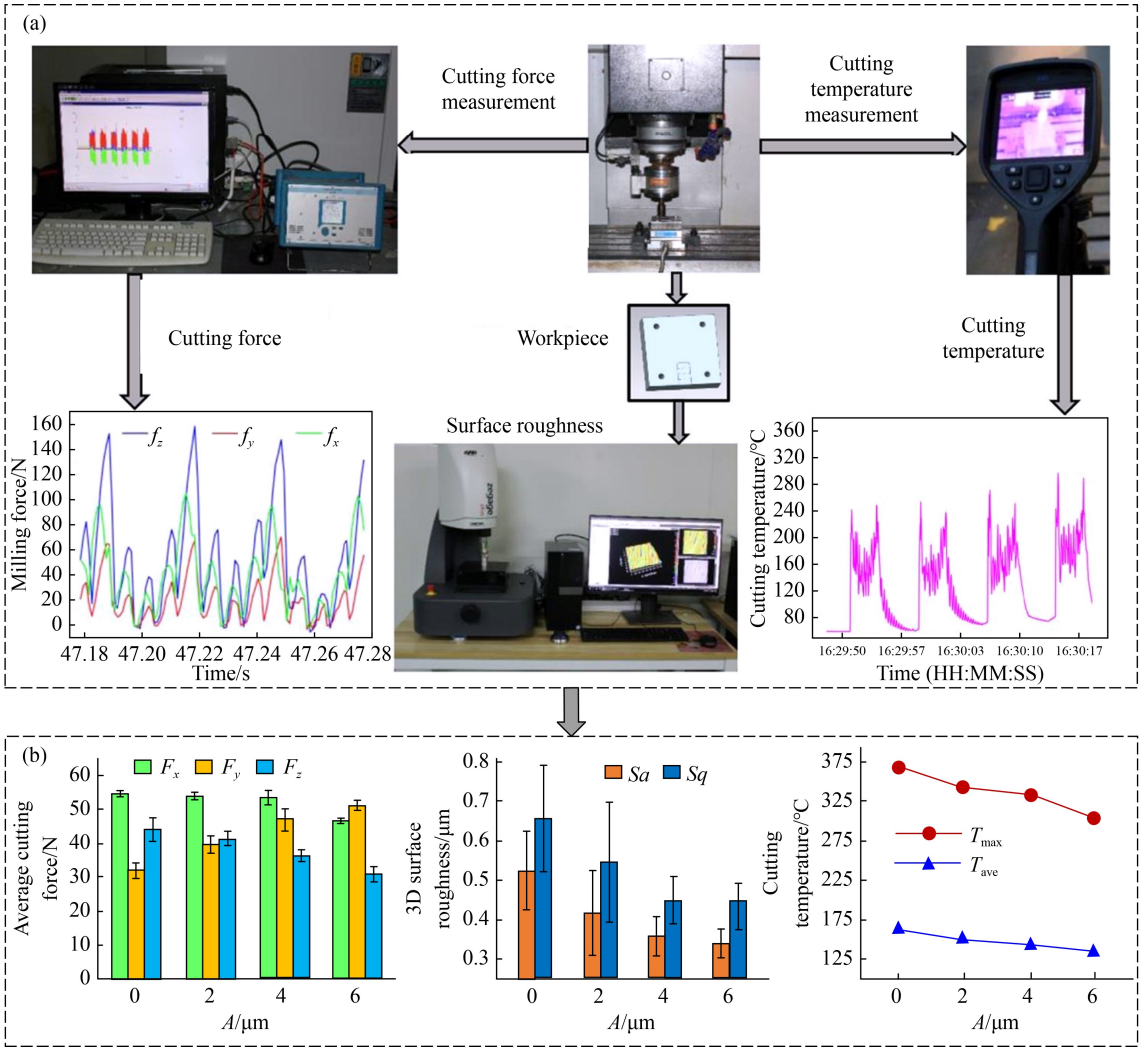

Fig. 27 Test parameter flow and data comparison: (a) ultrasonic vibration-assisted milling overall test parameter flow and (b) A impact on measurement data [170]. Reproduced with permission from Ref. [170] from Elsevier.

increased from 0 to 6 μm, the surface roughness *Sa* (average roughness) and *Sq* (surface root mean square roughness) decreased by 35.1% and 34.0%, respectively, and the surface morphology became more uniform, proving that the cutting performance and surface quality of TC4 could be significantly improved by UVAM [170].

The change in cutting parameters can also affect the formation mechanism of the residual stress and surface microstructure. Xie et al. [171] systematically studied the UVAM of TC18 and TC4 cells. First, based on the one-dimensional axial longitudinal vibration (tool vibration) when f was set to 33.9 kHz, the effects of A and v_c on the machining performance of the TC18 titanium alloy specimens were studied. The observation and analysis of these effects included the use of a dynamometer, thermometer, scanning electron microscope, X-ray diffractometer, and three-dimensional surface topography instrument. The authors found that v_c had significant effects on cutting force, surface morphology, cutting temperature, and residual stress. Compared with CM, the cutting force and cutting temperature of UVAM-processed workpieces decreased by 34.1% and 19.5%, respectively, whereas the residual stresses and surface roughness increased by 50.9% and 163.88%, respectively. Furthermore, the UVAM-processed workpiece surface exhibited a plastic deformation zone at a certain depth, and the deformation zone increased with increasing A [171]. Second, the basic formation mechanism of the surface microstructure during UVAM was analyzed using a theoretical kinematic model established by the authors, as shown in Fig. 28(a) [172]. According to Fig. 28(b) [172], a regular-scale microstructure was generated by UVAM along the feed direction. In addition, v_c, f_z, and A would affect the machining surface morphology and accuracy of the workpiece size. The single-factor UVAM experiment on TC4 titanium alloy with one-dimensional feed longitudinal vibration was performed at f of 22.7 kHz and various A values (0, 1, 2, 3, and 5 μm) to verify the accuracy of the theoretical model. The team also found that with an increase in A, the surface-scale

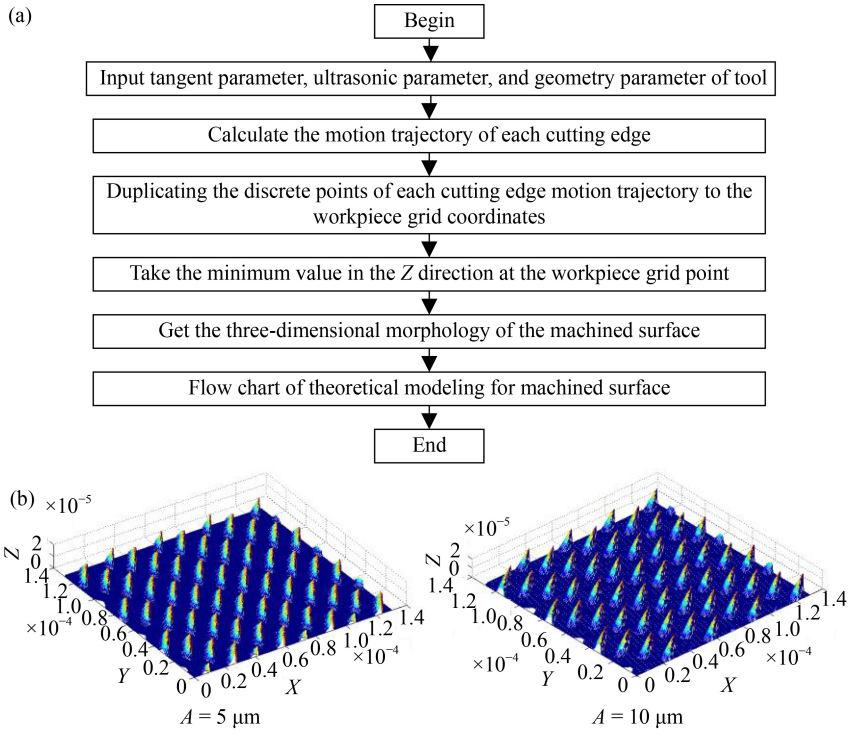

Fig. 28 Theoretical model and results: (a) theoretical model of the machined surface and (b) different A values of the machined surface [172]. Reproduced with permission from Ref. [172] from Journal of Vibroengineering.

structure gradually became uniform. The surface roughness value first decreased and then increased with increasing A. Friction and wear experiments revealed that the friction coefficient of the UVAM-processed workpiece surface was 60% lower than that obtained after CM [172].

The change in cutting parameters can also affect the dimensional accuracy of the workpiece and tip trajectory. Xu et al. [173] used the UVAM of TC4 with one-dimensional feed longitudinal vibration (workpiece vibration) when f was set to 19.832 kHz. They explored the influence of UVAM on the cutting force, surface quality, and workpiece size accuracy for different A and v_f. Compared to CM, UVAM reduced the cutting force by 17%. Therefore, the tool life is extended, and the dimensional accuracy of the workpiece is improved. Furthermore, according to the SEM observations of the surface morphology, UVAM can effectively reduce surface defects and machining tool marks. Thus, the surface quality is optimized after UVAM [173]. The tool tip trajectory also affected the machining effect. Zhu et al. [174] worked on the application of UVAM in the machining process of a workpiece. The vibration direction was along the feed direction, and the entire system was fixed to the workbench by the flange. To achieve an excellent vibration effect of the TC4 workpiece on the transducer, the resonant block was optimized using FEM, as shown in Fig. 29(a) [174].

Considering its direct effect on the texture and surface morphology of the workpiece, the tool path must be analyzed. The UVAM tool path is composed of tool rotation, table feed motion, and micron-scale ultrasonic vibration along the feed direction. In the Cartesian coordinate system of the workpiece, the tool tip trajectory equation is

$$\begin{cases} x = x_r + x_f + x_v, \\ y = y_r, \\ z = 0. \end{cases} \tag{3}$$

Because the ultrasonic generator can only output ultrasonic sine or sine signals, the ultrasonic vibration displacement function can be expressed as

$$x_v = A\sin(2\pi ft + \theta). \tag{4}$$

Based on Eqs. (3) and (4), the tool path equation for UVAM is obtained as

$$\begin{cases} x = R\cos\beta + v_f t + A\sin(2\pi ft + \theta), \\ y = R\sin\beta, \end{cases} \tag{5}$$

where x, y, and z represent the tip displacements, f and A are the ultrasonic frequency and amplitude, respectively, t is the cutting time, θ is the initial phase of the vibration signal, R is the radius of the end mill, β is the tool rotation angle, ω_r is the angular velocity of the spindle, v_f represents the feed rate of the workpiece, N_z is the number of tips, and z_i is the cutting edge number (i = 1, 2,…,N_z), $\beta = \omega_r t - 2\pi(z_i - 1)/N_z$, $x_r = R\cos\omega_r t$, $y_r = R\sin\omega_r t$, and $x_f = v_f t$.

According to Eq. (5), the tip trajectory in UVAM can

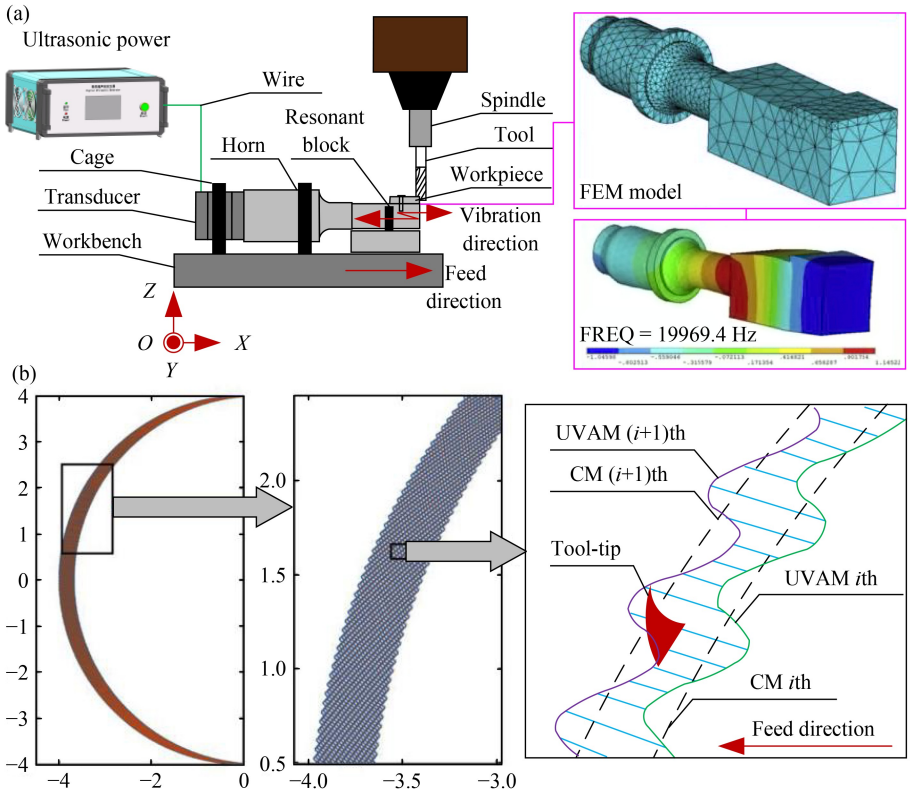

Fig. 29 Optimization of resonant block and analysis of tool tip trajectory: (a) finite element method (FEM) structure optimization of ultrasonic vibration-assisted milling (UVAM) system and resonant block and (b) tool-tip motion trajectory in UVAM and conventional milling (CM) process [174]. Unit: mm. Reproduced with permission from Ref. [174] from Elsevier.

be obtained, as shown in Fig. 29(b) [174]. In Fig. 29(b) [174], the trajectory and dynamic cutting thickness of the UVAM tip are clearly more complex than those of the CM process. In the local amplification diagram, the characteristics of UVAM are a wave-shaped trajectory and a phase difference. Based on the tool path analysis of UVAM, UVAM experiments with f = 19.8 kHz and A ranging from 8 to 14 μm were performed. The results showed that compared with CM, the milling force of UVAM and the associated surface roughness were reduced by 30% to 34.4% and 20% to 45%, respectively [174].

The mechanism of two-dimensional longitudinal-torsional ultrasonic vibration is very complicated. Therefore, a new technology for this vibration was proposed. The design of the geometric model of the cutting edge of the ball-end milling cutter with the axial position angle as the main parameter was presented. The authors derived the cutting force model of a ball-end milling cutter under the condition of longitudinal-torsional composite vibration. When f was 35.476 kHz and A was 10 μm, in the longitudinal-torsional UVAM experiment on TC4 titanium alloy, the radial, tangential, and axial forces of UVAM were reduced by 60%, 27.7%, and 33%, respectively, compared to CM [175]. Furthermore, under UVAM conditions, the relationship between the tool flank and cutting force was not established. Based on the above research, a new tool flank wear model that considers the chip flow angle and discretization of the cutting edge was developed. This model could predict the change trend of the cutting force at different flank wear values and optimize the processing parameters. The UVAM experiment on TC4 was performed with an f value of 35 kHz, A values in the range of 0–4 μm, and spiral angles between 35°–50°. According to the experimental results, when A was 2 or 3 μm, the tool wear became stable as the cutting length increased. Figure 30(a) [176] shows that the helix angle, unit cutting-edge length, friction time, and cutting temperature increased. The influence of the helix angle on tool flank wear changed in a similar manner; that is, when the helix angle was 35°, the increase in the wear value was more stable than at other helix angles, as shown in Fig. 30(b) [176]. The errors between the predicted model and experimental results in the feed (x) and normal (y) directions of the coordinate tool system (o-xyz) were 19.1% and 12.9%, respectively. Compared to CM, the feed and normal cutting forces of UVAM decreased by 21.7% and 5.4%, respectively. When the cutting length exceeded 67.5 m, the tool wear value of UVAM decreased by 38.7% [176]. The application of two-dimensional longitudinal torsional vibration can produce

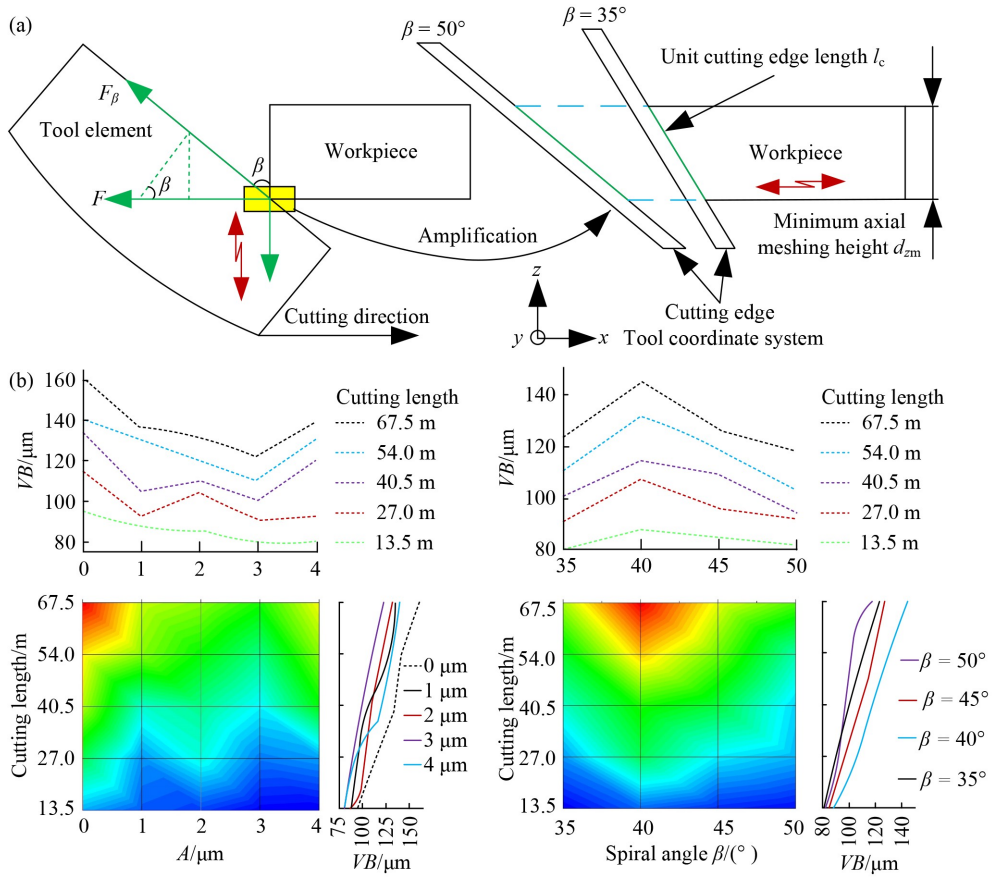

Fig. 30 Principle and test results: (a) influence principle of different helical angle tools on cutting edge length and (b) effect of A and helical angle on tool wear value of different cutting lengths [176]. Reproduced with permission from Ref. [176] from Elsevier.

better machining effects on the workpiece cutting force, tool wear, and surface roughness. Rinck et al. [177] studied the cutting force, tool life, and surface quality of TC4 titanium alloy by changing A (4, 6, 8, 10, and 12 μm) based on two-dimensional longitudinal-torsional vibration when f was 32 kHz. Compared with CM, the cutting force, tool wear, and surface roughness of UVAM were reduced by 57%, 20%, and 16.7%, respectively [177].

The tool change in the machining process of straight and free-curved surface cutting leads to burrs in the connection area during the actual production process. Ren et al. [178] proposed a machining method without tool change based on UVAM for straight and free-curved surface connection areas. At f = 25 kHz and A = 5.6 μm, the processing performance of UVAM and CM was assessed by changing parameters v_c, v_f, and α_p. Compared with CM, no obvious burrs were observed at the interface between the planar and free-curved surfaces after using UVAM, so there was no need to use a tilt spindle or transform tool. In addition, the milling force of UVAM decreased by 20%–40%, and the surface roughness decreased by 44.3%. As shown in Fig. 31 [178], when v_c was less than 157 m/min, UVAM led to an increase in surface roughness. However, when v_c was greater than 157 m/min, the surface roughness decreased [178].

4.3 Ultrasonic energy field-assisted milling of high-strength steel

One-dimensional axial longitudinal vibration of the cutting tool can affect the cutting force, chip morphology, and surface quality. Ahmed et al. [179] established an analysis model to calculate the cutting force during the machining process, and the results are shown in Fig. 32. An AISI H13 machining experiment was conducted at f = 40 kHz and A = 2 μm. The machining process was evaluated based on cutting force, chip morphology, wear rate, and surface integrity. The results showed that compared with CM, UVAM had a smaller cutting force and could produce more uniform, thin, and smooth chips. The surface quality of the UVAM workpiece also improved. By observing the friction and wear experimental data, it was found that the tool wear caused by CM or UVAM was similar. However, further studies showed that UVAM could prolong tool life by changing the vibration direction [179].

Considering one-dimensional axial longitudinal

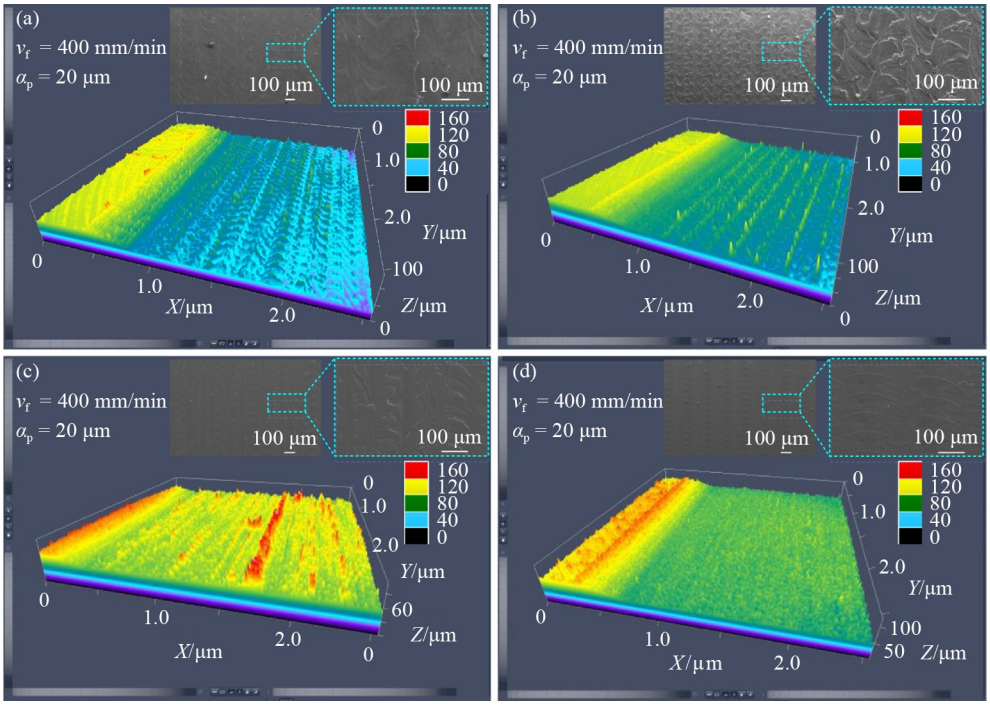

Fig. 31 Three-dimensional morphology of ultrasonic vibration-assisted milling (UVAM) and conventional milling (CM) machined surfaces: (a) CM at v_c = 125.6 m/min, (b) UVAM at v_c = 125.6 m/min, (c) CM at v_c = 157 m/min, and (d) UVAM at v_c = 157 m/min [178]. Reproduced with permission from Ref. [178] from Springer Nature.

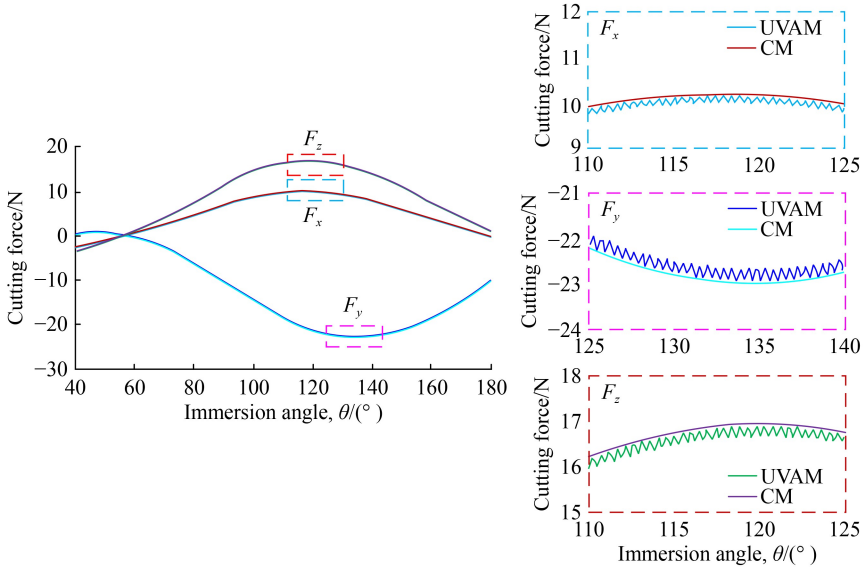

Fig. 32 Ultrasonic vibration-assisted milling (UVAM) and conventional milling (CM) analysis model of cutting force [179]. Reproduced with permission from Ref. [179] from Taylor & Francis.

vibration (tool vibration), the values of f, A, and the tool angle can affect tool wear and surface roughness. Tsai et al. [180] studied the effects of f (25 and 50 kHz), A (0, 2.2, and 3.68 μm), tool rake angles (6° and −6°), and tool helix angles (25°, 35°, and 45°) on tool wear and machined surface quality using AISI 420 processed by UVAM. The experimental results showed that compared with CM, the machined surface after UVAM processing was more uniform when f was 25 or 50 kHz. The machining tool mark became shallow with increasing f. With increasing A, the roughness of the machined surface first decreased and then increased. The surface roughness after UVAM was smallest when the tool rake angle was 6°. The surface quality was improved by increasing the

UVAM helix angle, as shown in Fig. 33(a) [180]. Maurotto and Wickramarachchi [181] conducted UVAM of AISI 316L while varying the value of f (0, 20, 40, and 60 kHz). They explored the influence of different f values on the surface roughness and residual stress. According to the results, the surface roughness increased slowly with increasing f, and the surface quality worsened. In addition, the residual stress was compressive when the parameters remained within a given range. The minimum compressive stress was obtained when f was 40 kHz, as shown in Fig. 33(b) [181].

Scholars have already considered the simultaneous influence of the axial vibration and feed vibration of workpieces during the machining process. Razfar et al. [182] studied the UVAM of high-strength steel. First, a UVAM experiment was conducted on AISI 1020 steel based on one-dimensional axial longitudinal vibration (workpiece vibration) when f was set to 20 kHz and the power was 250 W. Then, the effects of v_c, f_z, α_p, and ultrasonic treatment on the surface roughness were investigated, and the results showed that the surface roughness of CM and UVAM exhibited similar curves and increased with increasing f_z and v_c. Compared to CM, the average surface roughness after UVAM increased by 12.9% [182]. Second, based on the same vibration mode, a power of 220 W was used to conduct UVAM of AISI 304 steel. Subsequently, the influence of UVAM on the cutting force in three directions was tested. It was found that under UVAM conditions, the cutting forces were reduced in all three directions [183]. Finally, the cutting force in UVAM was described in a mathematical model. The authors proposed a new relationship between the critical cutting speed and thickness of the undeformed chips. According to the analytical relationship, the cutting force in the UVAM had different amplitudes. CM and UVAM experiments based on longitudinal vibration

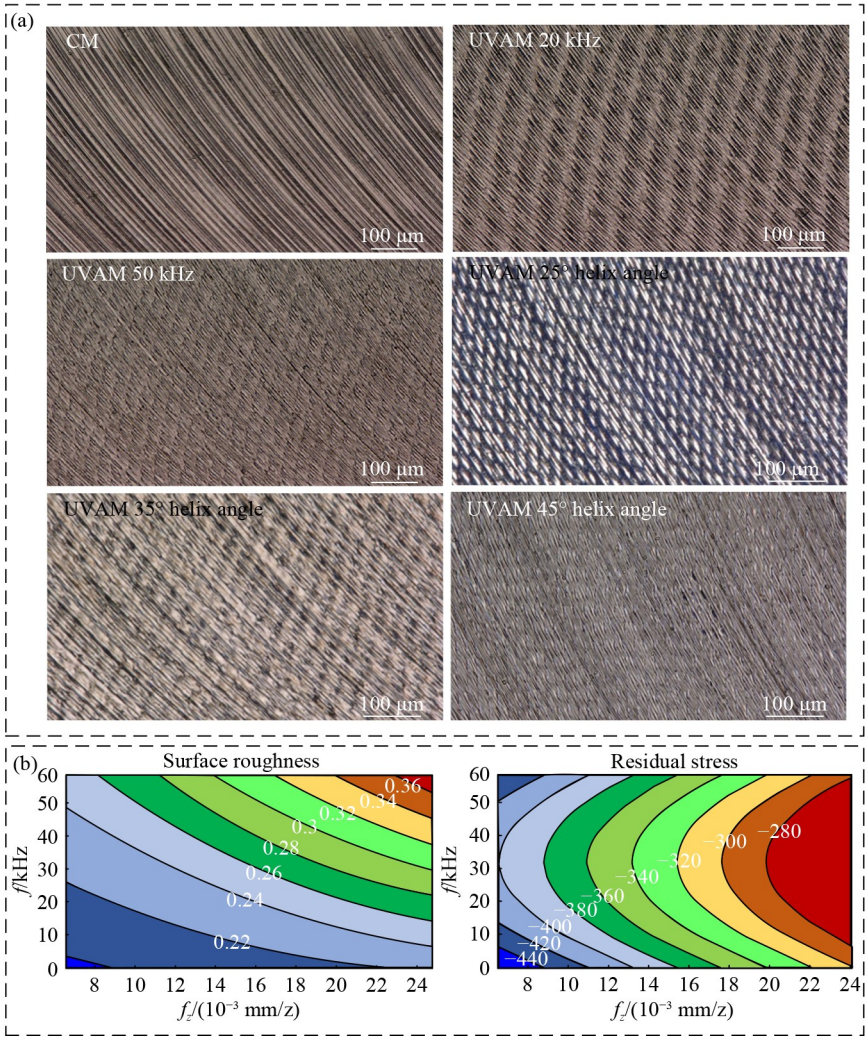

Fig. 33 Ultrasonic vibration-assisted milling (UVAM) and conventional milling (CM) surface quality: (a) influence of f and helix angle on the processed surface [180] and (b) effect of f_z and f on surface roughness and residual stress [181]. Reproduced with permissions from Refs. [180,181] from MDPI and Elsevier.

(workpiece vibration) in a one-dimensional feed direction were conducted at f = 23 kHz and A = 20 μm, and their cutting force and workpiece surface roughness were compared. UVAM of X20Cr13 stainless steel was first performed, and the effects of v_c, v_f, and milling methods on chip formation and workpiece surface quality were analyzed. The UVAM and CM chip morphologies and tool wear are shown in Fig. 34 [184,185]. The experimental results showed that UVAM could produce thinner and smaller chips, as shown in Fig. 34(a) [184], and the machined surface was smoother. Compared with CM, UVAM chips had larger curvatures and smaller sizes. With an increase in v_f, the chip curvature decreased [184]. Furthermore, side milling of AISI 420 stainless steel was performed. Subsequently, the effects of v_c, v_f, and milling methods on the cutting force and surface roughness were studied, indicating that the cutting force in UVAM was smaller than that in CM. Moreover, depending on the cutting conditions, the surface roughness of the workpiece in UVAM can be improved

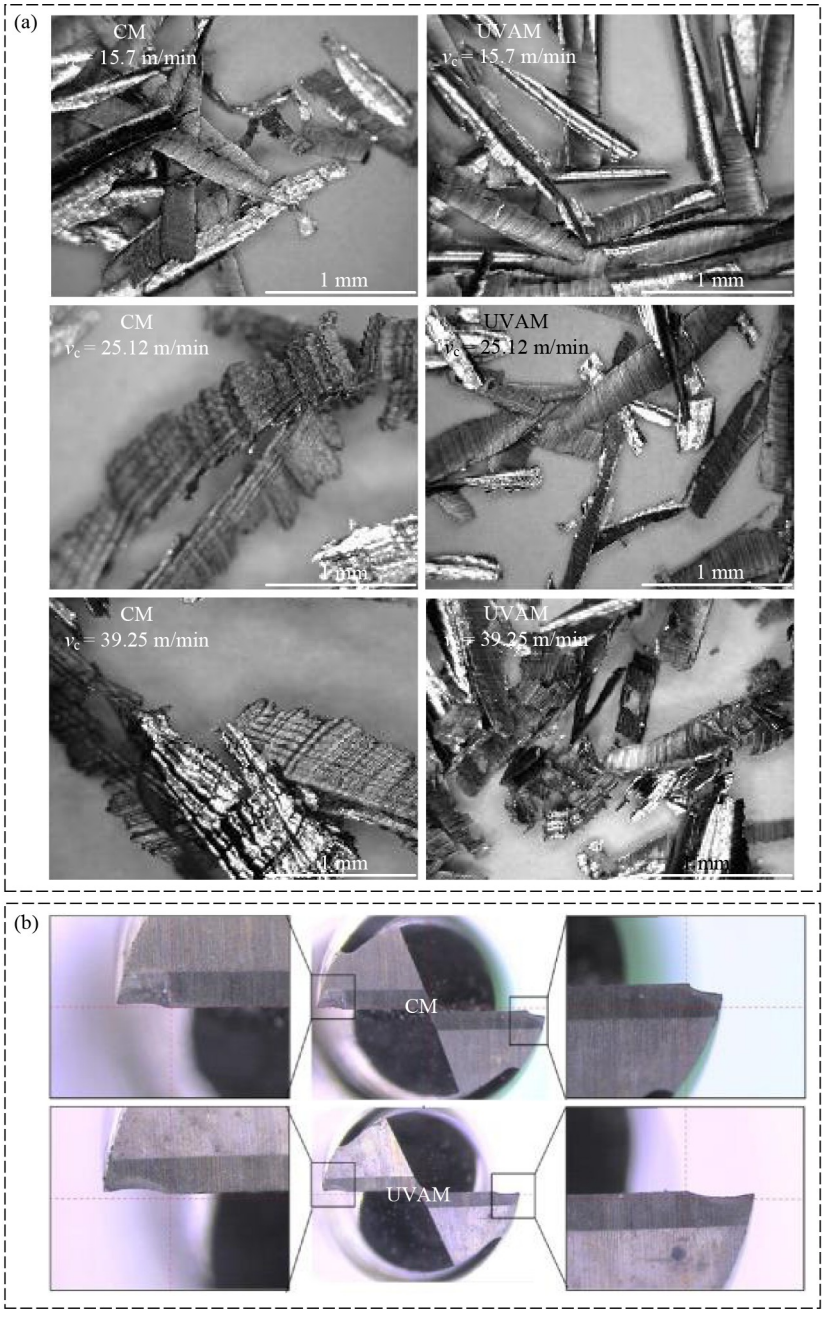

Fig. 34 Ultrasonic vibration-assisted milling (UVAM) and conventional milling (CM) chip morphology and tool wear: (a) chip morphology under different v_c [184] and (b) tool wear [185]. Reproduced with permissions from Refs. [184,185] from ASME and Elsevier.

compared with that obtained by CM. Further research showed that when v_f was small, the influence of UVAM reverse milling on the cutting force was more obvious. However, when v_f was large, the influence of UVAM forward milling was more pronounced. Under the conditions of low v_f, high v_c, and the reverse milling process, the effect of UVAM on the surface roughness was more evident [186].

The one-dimensional axial longitudinal vibration (workpiece vibration) based on the HM process can affect the cutting force, machining energy consumption, and surface roughness. Rao et al. [187] conducted UVAM of AISI 1020 steel using an f value of 20 kHz and an A value of 5 μm. HM was used to improve the energy efficiency. The energy consumption of the feed rate in three directions, that is, the chip-size prediction model, was theoretically established. It was found that UVAM had a significant intrinsic effect on chip morphology, cutting force, and machining energy consumption. Compared with the CM, the one-dimensional axial longitudinal vibration reduced the axial force, radial force, and cutting energy consumption by 47%, 14%, and 34%, respectively. Axial longitudinal vibrations can reduce manufacturing costs. The results of the prediction model were in good agreement with the experimental results, with average errors in cutting energy consumption, chip length, and chip width of 4.36%, 2.51%, and 3.92%, respectively [187]. This confirms the accuracy of the model. Considering the difference between two-dimensional plane vibration and one-dimensional axial longitudinal vibration, Ding et al. [185] performed UVAM of X46Cr13 stainless steel based on two-dimensional plane vibration under different ultrasonic f and A. Compared with CM, the surface roughness after UVAM decreased by 28.3%. The tool wear of UVAM decreased by 5%–20%, as shown in Fig. 34(b) [185]. The chip was thin and small, and the tool life was prolonged [185]. The authors also conducted an FEM analysis of the tool-tip trajectory using different vibration parameters and proposed a calculation model of the chip thickness. This model can accurately calculate the instantaneous chip thickness. Researchers verified the correctness of the model based on experimental process data [188] and improved the material removal rate.

4.4 Summary of ultrasonic energy field-assisted milling of difficult-to-machine metal materials

Based on the above investigations, the ranges of amplitude values applied in UVAM are different because of the inconsistent basic properties of difficult-to-machine metal materials. The amplitude ranges of the nickel-based alloy, titanium alloy, and high-strength steel are 0–9 μm, 0–14 μm, and 0–20 μm, respectively. The amplitude was consistent with the machinability of the three materials. Combining the above findings, the overall structure of the UVAM machinability is summarized in Fig. 35. By controlling the vibration direction of UVAM, f, A, and different processing parameters, the change rules of the cutting force, surface morphology, surface roughness, residual stress, chip morphology, and tool wear during the workpiece machining process were explored. Based on the experimental data, it is concluded that the advantages of UVAM and LAM for difficult-to-machine materials are similar. However, the trajectory of the UVAM tool tip and dynamic cutting thickness were different from those of the CM. Based on this, a calculation process for the UVAM wave trajectory is developed. Furthermore, considering the plastic deformation zone of UVAM, the microstructure theory and the FEM model of the machined surface were established. In addition, a new tool flank wear model was developed based on the tool angle to predict the surface roughness and tool wear of UVAM-processed workpieces. Compared to CM, the chip morphology and thickness of the UVAM-processed materials changed significantly. To accurately determine the instantaneous chip morphology after UVAM, a chip thickness model was developed using calculation and FEM. The accuracy of each model was verified experimentally. To improve the energy utilization rate, UVAM and HM processes were used to conduct cutting experiments on difficult-to-machine metal materials, which effectively reduced the manufacturing cost. Furthermore, based on ultrasonic and cutting parameters, a prediction model showing the influence of the instantaneous change in chip thickness on the cutting force, surface morphology, surface roughness, residual stress, chip morphology, and tool wear must be established to promote the development of UVAM technology.

5 CMQLAM of difficult-to-machine metal materials

CMQLAM is a new green machining technology that combines the application of a cold medium, micro-lubrication, and milling. In this process, a liquid/gaseous medium is sprayed into the shear zone in accordance with the jet form, which can replace the traditional cutting fluid to lubricate and cool the machining contact zone [77]. The workflow and functions of the CMQLAM system are shown in Fig. 36(a) [189]. The principle is to combine a cold medium with atomizing oil mist and water mist before reaching the nozzle, and then to cool the shear zone through the nozzle. The water mist vaporizes and absorbs heat, while the oil mist is present at the contact surface between the workpiece and the tool, reducing the friction coefficient and heat generation due to friction. The cold medium also reduces the viscosity of the chips, which can achieve an excellent effect when combined with micro-lubrication. Considering that

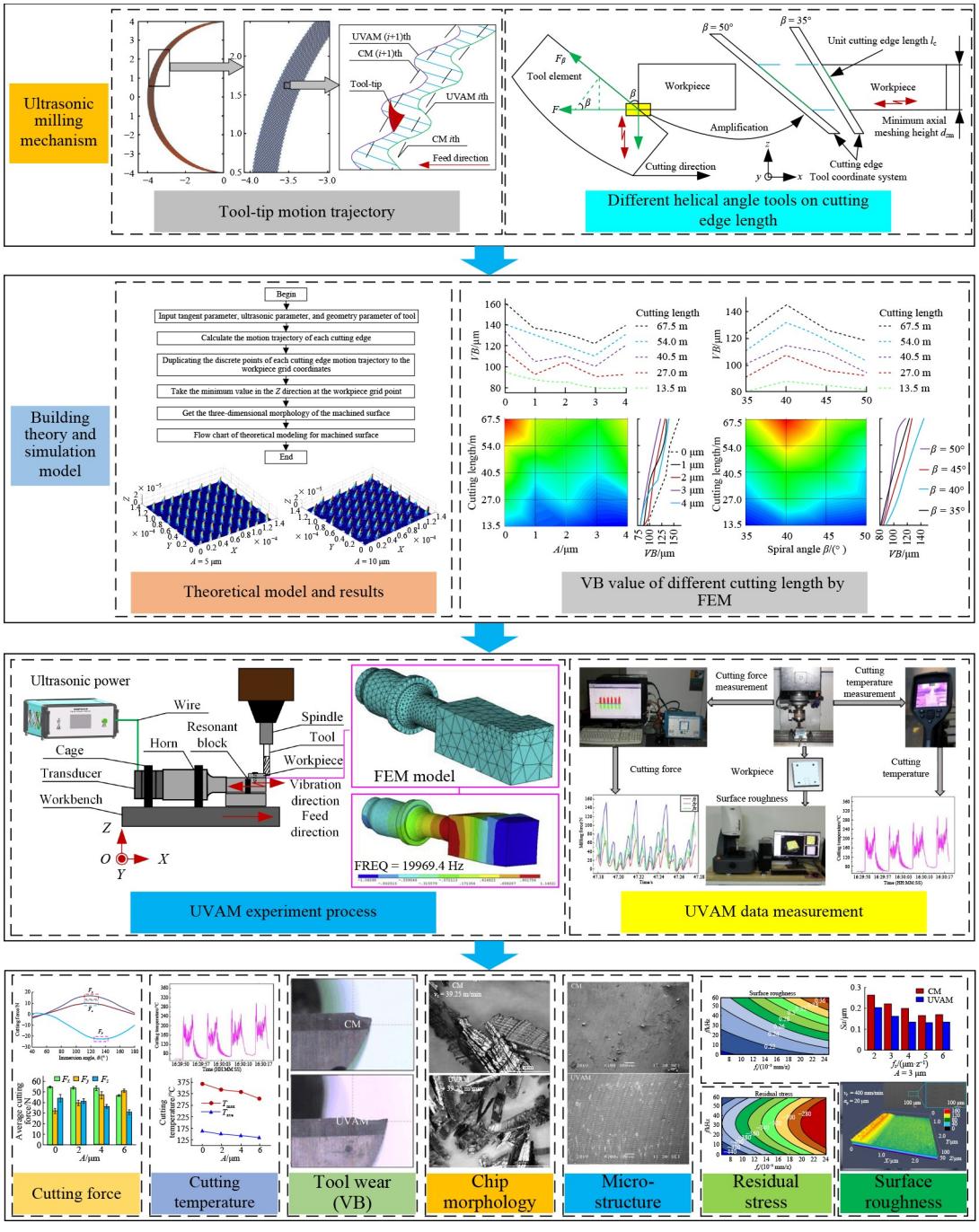

Fig. 35 Summary of ultrasonic vibration-assisted milling (UVAM) machinability. FEM: finite element method.

cutting oil is used in very small amounts in CMQLAM, an oil film boundary lubrication is established, as shown in Fig. 36(b) [189].

During nozzle operation, the amount of oil attached to the machined surface increases, and the film thickness gradually increases, as indicated by point *A* in Fig. 36(b) [189]. As CMQLAM continues, more lubricating oil is gradually added to the low-lying surface of the shear zone, as shown by point *B*. With increased amounts of nozzle oil and prolonged injection times, the surface film consists of peaks and valleys due to further adsorption of lubricating oil, as indicated by point *C*. When the oil amount does not exceed point *A*, the amount of oil is small and the oil film is thin, resulting in dry friction as the tool directly contacts the peak of the workpiece. When the oil amount is between points *A* and *C*, only the friction between the tool and the peak of the workpiece occurs, resulting in a constant friction coefficient. At this stage, the oil amount has little effect on the machined surface. When the oil film at the top of the peak is

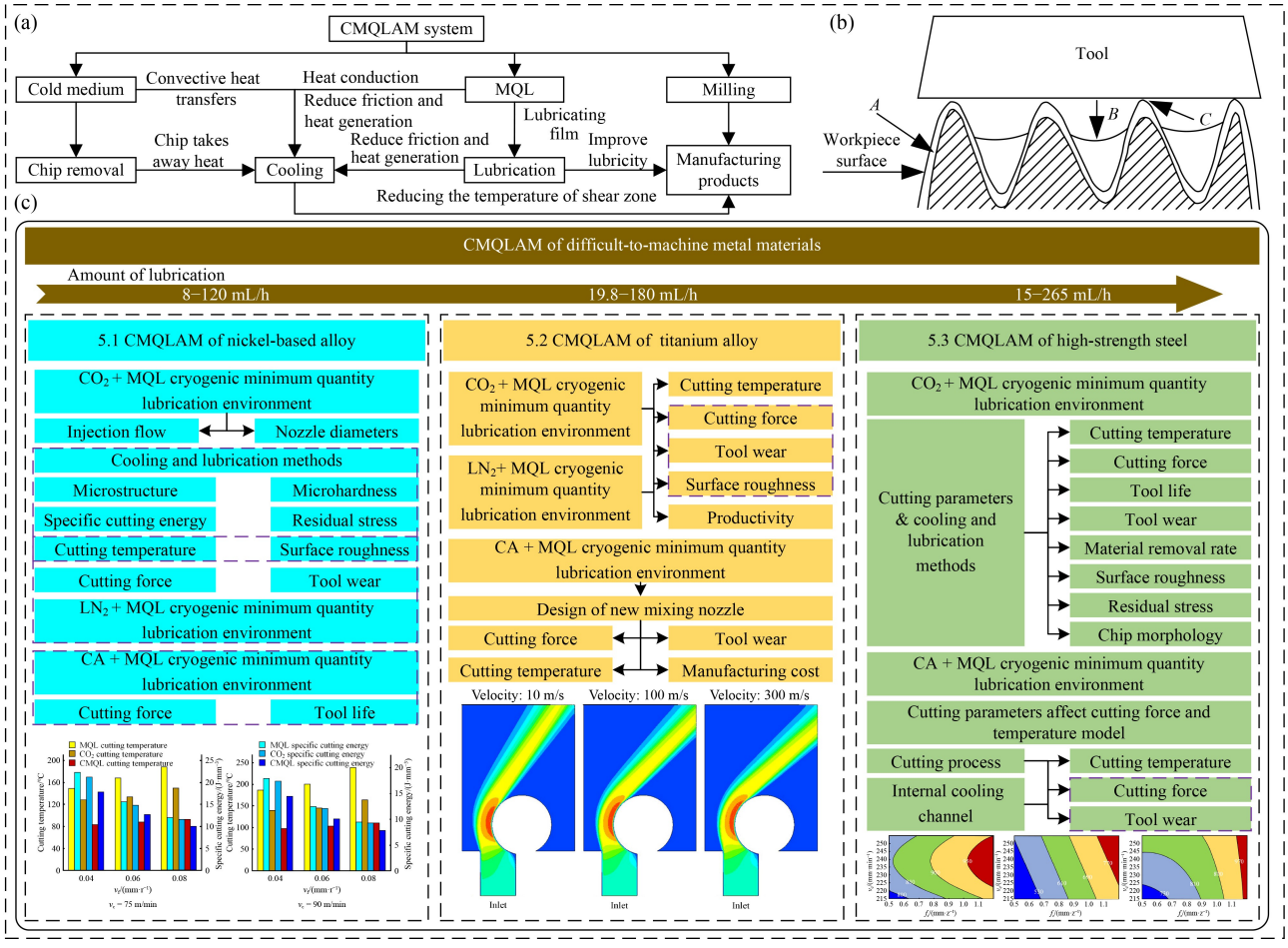

Fig. 36 Cryogenic minimum quantity lubrication energy field-assisted milling system (CMQLAM), lubrication mechanism and logic: (a) CMQLAM system, (b) workpiece surface boundary lubrication [189], and (c) logical structure of laser-assisted milling difficult-to-machine metal materials. CA: cold air; MQL: minimum quantity lubrication. Reproduced with permission from Ref. [189] from Mechanical Science and Technology for Aerospace Engineering.

damaged, the oil amount at point *B* can rapidly flow to the top of the peak with its own free energy to restore the original boundary lubrication state. However, when the oil content exceeds point *C*, the stability of the friction coefficient cannot be guaranteed [189]. Therefore, it is important to control the CMQLAM lubrication parameters carefully. CMQLAM of difficult-to-machine metal materials is divided into three classes according to the lubrication range of CMQLAM, as shown in Fig. 36(c).

Regarding the investigations on CMQLAM of nickel-based alloys, based on a CO_2 + MQL CMQL environment, first, different diameters of CO_2 outlets were compared, and numerical computational fluid dynamics (CFD) simulations were performed to obtain the best injection flow rate and nozzle diameter. Second, the effects of the five cooling and lubrication methods on the tool life were compared. Third, the effects of different cooling and lubrication methods on machining temperature, cutting specific energy, surface roughness, microhardness, and residual stress were assessed. Then, the effects of the five cooling and lubrication methods on the surface structure, surface morphology, and surface roughness were compared. Based on an LN_2 + MQL CMQL environment, the effects of the three cooling and lubrication methods on the surface roughness and tool wear were compared, and the effects of the tool coating and cooling lubrication conditions on the cutting force, tool wear, surface roughness, and cutting temperature were investigated. Based on a CA + MQL CMQL environment, the cutting force and tool life under dry and CMQL conditions were compared.

To study the CMQLAM of titanium alloys, the effects of five micro-lubrication technologies and cutting speed changes on tool wear, cutting temperature, cutting force, and surface roughness were analyzed based on a CO_2 + MQL CMQL environment. Under these conditions, the cutting force was the lowest, the surface roughness was the smallest, and optimal surface quality was obtained. The cutting parameters and four green conditions were varied to study their influence on cutting force, cutting temperature, surface morphology, and surface roughness. $SCCO_2$-OoWMQL had the best effect. Based on an

LN_2 + MQL CMQL environment, the cutting force and tool wear in a CMQLAM machining process were analyzed, and the effects of CMQLAM machining on tool life, surface roughness, cutting force, and productivity were studied. In the CA + MQL CMQL environment, CMQLAM significantly reduced flank wear. A new type of mixed nozzle capable of simultaneously injecting oil mist and cryogenic gas was designed. The Coanda effect under different inlet flow rates, friction heat, and tool wear using conventional and new nozzles were compared. The cutting force, tool wear, cutting temperature, and manufacturing costs under CMQLAM conditions were analyzed.

Regarding the studies on CMQLAM of high-strength steel, the effects of four cooling and lubrication methods on the cutting force, cutting temperature, and tool wear were compared in a CO_2 + MQL CMQL environment. Furthermore, the influence of the new CMQL methods on the cutting force, tool life, and surface roughness was analyzed. Subsequently, the effects of cutting parameters and cooling lubrication on tool life, material removal, surface roughness, and residual stress were assessed. Finally, the effects of the cutting speed and cooling lubrication on the surface roughness, chip morphology, flank wear, and cutting temperature were investigated. Based on a CA + MQL CMQL environment, the influence of cutting parameters on the cutting force and temperature was analyzed by simulation, and a prediction model was established. Experiments were conducted to verify the accuracy of the proposed model. Compared to dry milling, CMQL can reduce the cutting force and cutting temperature. The influence of cutting parameters on the white layer was also analyzed. The effect of three internal cooling channels on cutting force and tool wear was investigated with the result that the CMQLAM effect of a double straight channel (DSC) internal cooling tool was the best.

5.1 CMQLAM of nickel-based alloy

The optimal injection flow rate, nozzle diameter, and tool life can be obtained in a CO_2 + MQL CMQL environment. CMQLAM demonstrates good cooling and lubrication effects. Pereira et al. [190] conducted numerical and experimental analyses of the CO_2 + MQL CMQLAM. First, a CFD numerical simulation of CO_2 outlets with different diameters was conducted. Based on the CMQL energy field with a CO_2 pressure of 14 bar (1 bar = 10^5 Pa) and an MQL flow rate of 100 mL/h, Inconel 718 was processed via assisted milling, and the optimal CO_2 injection velocity and outlet diameter were 325 m/s and 1.5 mm, respectively. The team compared the effects of drying, pouring, CO_2, MQL, and CO_2 + MQL cooling and lubrication methods on cutting. Different nozzle diameters, cutting temperatures, and specific cutting energies are shown in Fig. 37 [190,191]. Compared with CM pouring machining, the tool life of dry milling was shortened by 53.3%. When only CO_2 or MQL was used to assist milling, the tool life increased by 67.7% and 84.2%, respectively. CMQLAM could increase the tool life to 93.5% and reduce the cutting oil by 90%, which proved that CMQLAM could be applied in practical engineering [190,192], as shown in Fig. 37(a) [190].

The effects of different cooling and lubrication methods on the machining temperature, specific cutting energy, surface roughness, microhardness, and residual stress were compared in a CO_2 + MQL CMQL environment. Ross et al. [191] found that MQL and cryogenic cooling can replace the CM cutting fluid; however, the cooling and lubrication characteristics of CO_2 + MQL CMQLAM were not explored under high-speed cutting conditions. They compared the processing effects of Nimonic 80A under CO_2, MQL, and CMQL conditions and conducted in-depth research on the processing temperature, energy consumption, surface, and subsurface. At a CO_2 pressure of 2.5 bar and MQL flow rate of 60 mL/h, the processing temperature and specific cutting energy under CMQL conditions ranged between 34%–53% and between 17%–19%, respectively, and were reduced compared with MQL, as shown in Fig. 37(b) [191]. In addition, CMQL decreased the grain size by reducing the friction at the cutting point, thereby increasing the surface fatigue strength of the workpiece and providing the best cooling effect during processing, which showed the superiority of CMQL, as shown in Fig. 38(a) [191]. The team also conducted a study to analyze the effects of CM pouring, MQL, CO_2, and CMQL on cutting temperature, surface roughness, tool wear, microhardness, and residual stress. The results showed that, compared to CM pouring, MQL, and CO_2, the processing temperature was reduced by 41%–53%, 29%–46%, and 17%–23%, respectively, under CMQL conditions. The surface roughness also decreased by 42%–54%, 34%–45%, and 19%–29%, respectively. The tool wear was reduced by 48%–71%, 42%–56%, and 22%–40%, respectively. Furthermore, the surface microhardness increased by 9.57%, 9.13%, and 4.87%, respectively. When compared to CM pouring, the residual compressive stress obtained by CMQL processing increased by 25.18%. It was verified that CMQL has the advantages of a low cutting temperature, high residual compressive stress, microhardness, and good surface quality, as shown in Fig. 38(b) [193].

The effects of five cooling and lubrication methods on the surface microstructure, morphology, and roughness were compared in a CO_2 + MQL CMQL environment. Milling of Inconel 718 was conducted by Sterle et al. [194] The effects of drying, CM pouring, LCO_2, LCO_2 + MQL (oil), and LCO_2 + MQL (MoS_2) cooling and lubrication methods on the surface smoothness, roughness, surface morphology, and microstructure were compared. The LCO_2 pressure and MQL flow rate were 12 kg/h and 120 mL/h, respectively. The experimental

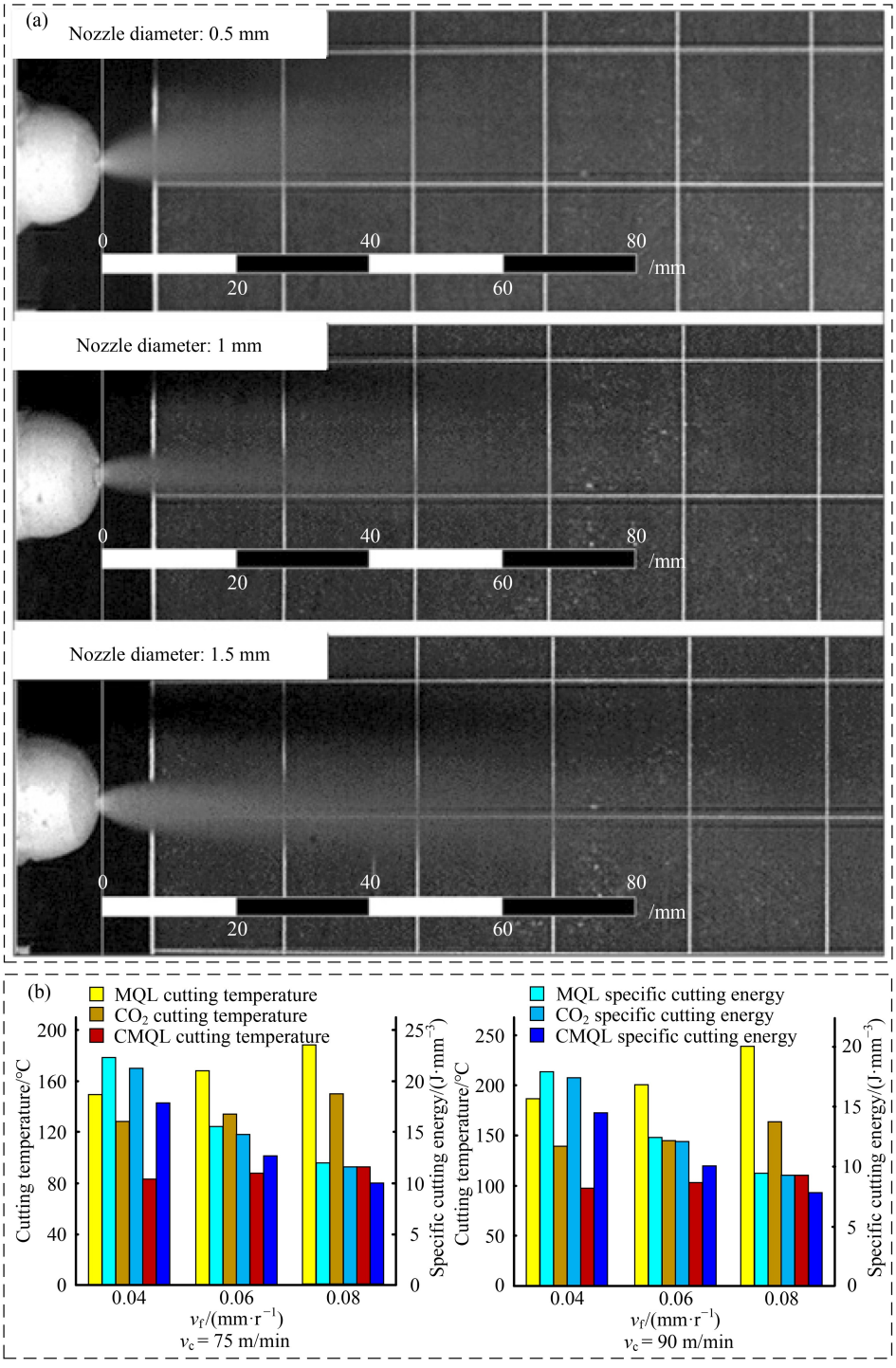

Fig. 37 Different nozzle diameters, cutting temperatures, and specific cutting energies: (a) experimental results of different nozzle diameter outlets [190], and (b) effects of green lubrication and cutting parameters on cutting temperature and specific cutting energy [191]. MQL: minimum quantity lubrication. Reproduced with permissions from Refs. [190,191] from Springer Nature and Elsevier.

results showed that the surface finish under LCO_2 treatment was close to that obtained with dry cutting. Compared with LCO_2 + MQL (oil), the surface smoothness obtained by LCO_2 + MQL (MoS_2) was improved, and the MoS_2 particles were easier to remove after milling. Compared with CM casting milling, the application of LCO_2 + MQL (MoS_2) resulted in lower surface roughness, better surface morphology, and a more uniform surface microstructure [194].

In addition to CO_2 + MQL, LN_2 + MQL also caused a reduction in tool wear and surface roughness. Shokrani et al. [195] found that MQL, LN_2, and CMQL processing were effective cooling lubrication technologies for improving the machinability of difficult-to-machine metal

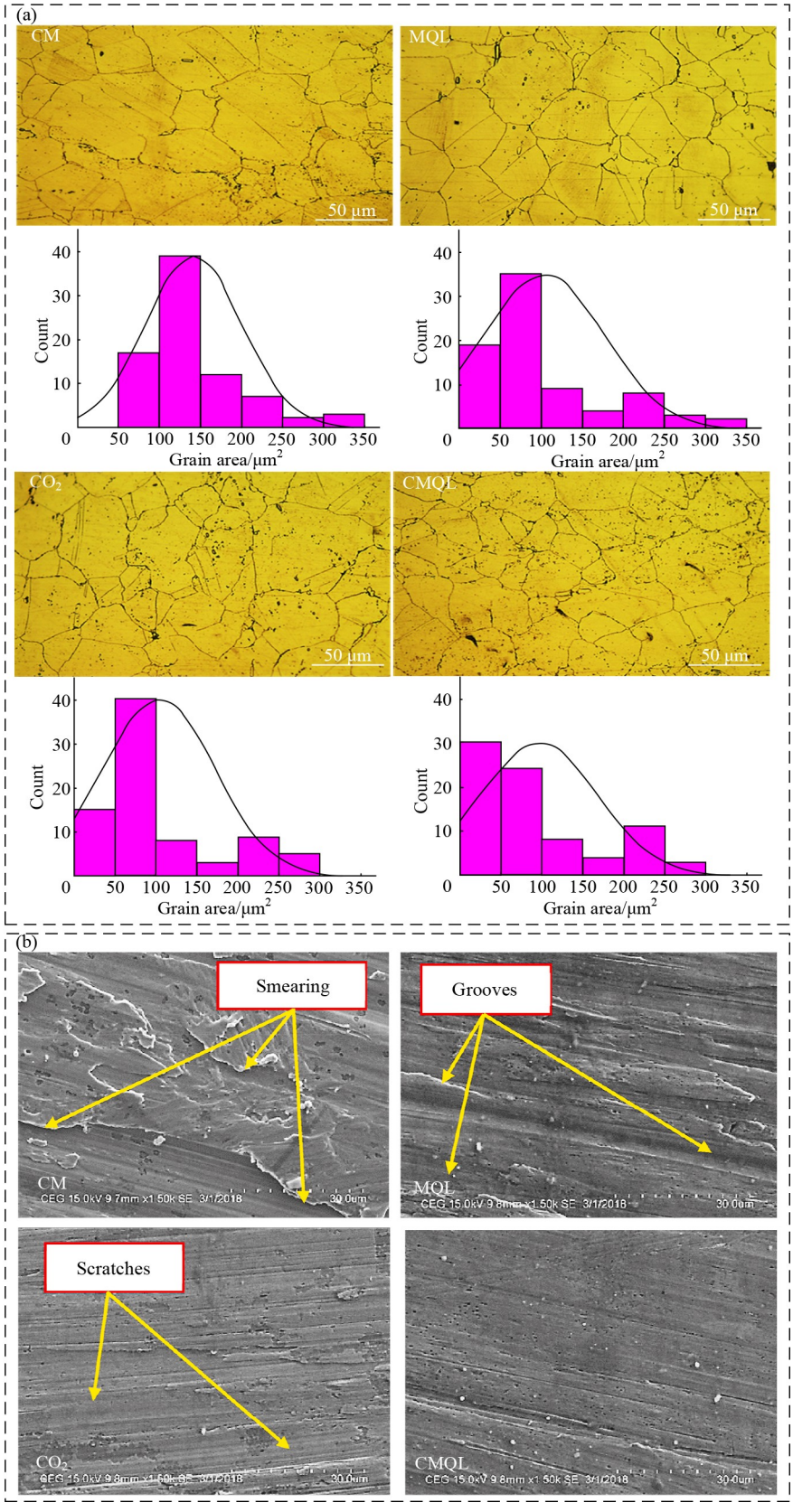

Fig. 38 Grain size distribution and scanning electron microscope: (a) effect of green lubrication on grain size distribution [191] and (b) scanning electron microscope images of different green lubricants [193]. CM: conventional milling; MQL: minimum quantity lubrication. Reproduced with permissions from Refs. [191,193] from Elsevier.

materials. Therefore, groove milling experiments were performed on Inconel 718 using the MQL, LN_2, and CMQL cooling and lubrication methods at an LN_2 pressure of 1.2 bar and an MQL flow rate of 60 mL/h. Compared with MQL, CMQL increased the tool life by 200% and reduced the surface roughness of the groove bottom surface by 18% and that of the groove side surface by 5% [195]. Based on the above experiments, the team changed the LN_2 pressure to 1 bar and the MQL flow rate to 70 mL/h and conducted comparative experiments under CM pouring cooling lubrication conditions. The results showed that compared with CM pouring cutting, CMQL could increase tool life by 77%. The surface roughness values of the side and bottom of the machined parts were less than 0.4 μm. By monitoring the energy consumption of the machine tool, it was found that the energy consumption increased with tool wear. These studies clearly demonstrate that the application of CMQLAM to Inconel 718 is feasible [196].

The combination of tool coating and green lubrication conditions will have a better effect on the machining process. Şirin et al. [197] conducted an experimental study on the Inconel X750 alloy and explored the effects of tool coating (no coating, low-temperature treatment, and TiAlN coating) and green lubrication conditions (LN_2, MQL, and CMQL) on tool wear, surface roughness, surface morphology, cutting force, and cutting temperature. Using an LN_2 pressure of 15 bar and an MQL flow rate of 50 mL/h, the authors showed that although the hardness of the tool increased by 7.36% after low-temperature treatment, the tool life decreased in the following order: TiAlN coating, low-temperature treatment, and no coating. Compared with the use of LN_2, the tool wear of the uncoated tool was lower when applying MQL and CMQL; for the coated tool, the tool wear decreased by 63.8% and 70.1%, respectively. Compared with the uncoated tool, the surface roughness of the tool subjected to low-temperature treatment and the coated tool was reduced by 2.72% and 6.22%, respectively, while the cutting force decreased by 4.81% and 7.11%, as shown in Fig. 39 [197]. Compared to the application of LN_2, the surface roughness values obtained with MQL and CMQL decreased by 4.81% and 18.52%, respectively. Under green lubrication conditions, compared to LN_2, the cutting forces using MQL and CMQL were reduced by 7.1% and 10.76%, respectively, for the coated tool. Compared with the noncoated tools, the cutting temperature of the coated tools decreased by 5.75%.

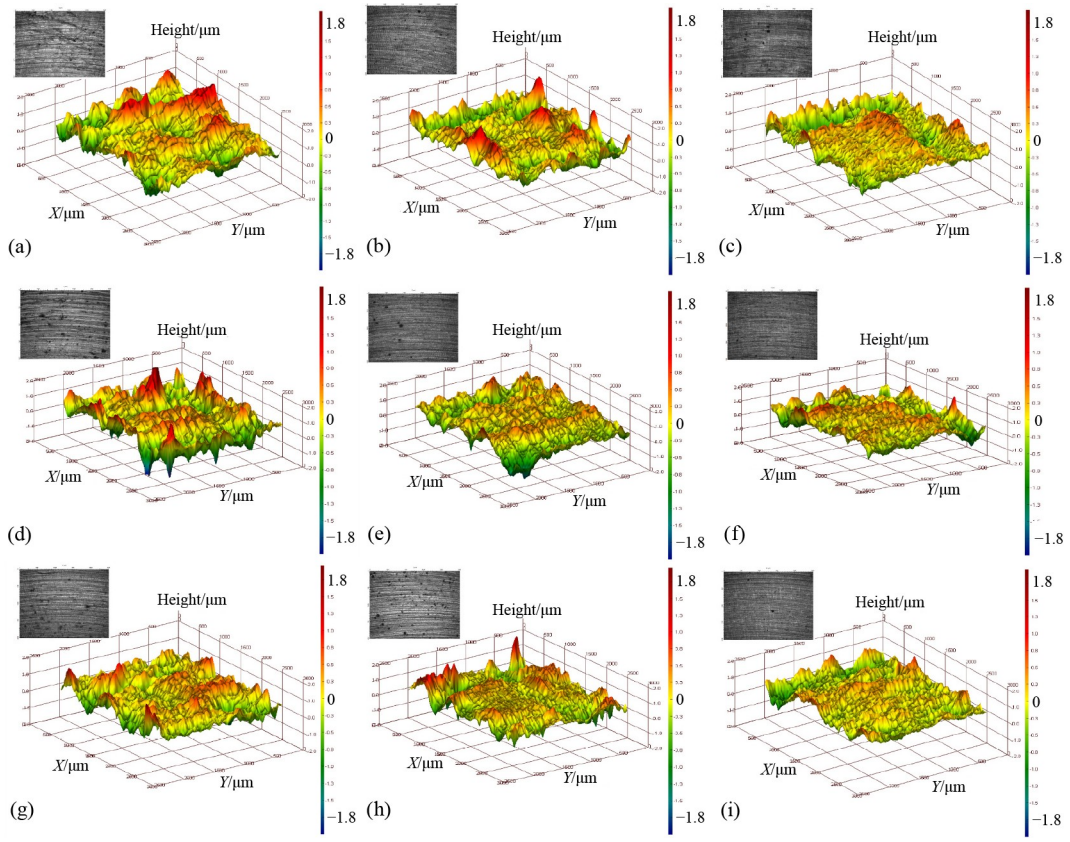

Fig. 39 Different green cooling lubrication and tool machining surfaces: (a) uncoated tool liquid nitrogen, (b) uncoated tool minimum quantity lubrication (MQL), (c) uncoated tool cryogenic MQL (CMQL), (d) low-temperature treatment tool LN_2, (e) low-temperature treatment tool MQL, (f) low-temperature treatment tool CMQL, (g) TiAlN-coated tool LN_2, (h) TiAlN-coated tool MQL, and (i) TiAlN-coated tool CMQL [197]. Reproduced with permission from Ref. [197] from Elsevier.

Compared to LN_2, the cutting temperature decreased by 30.31% under CMQL cooling and lubrication conditions [197].

CA + MQL can prolong the tool life and reduce the cutting force. Zhang et al. [198] studied the influence of different cutting conditions on tool life and cutting force changes during the machining of Inconel 718. In the CMQLAM process, the CA pressure was 1.5 bar, and the MQL flow rate was 8 mL/h. Under dry milling and CMQL conditions, flank wear and cutting edge fracture were found to be the main factors leading to tool failure. Compared with dry milling, CMQL reduced the cutting force, increased the tool life by a factor of 1.57, and significantly improved the machinability of Inconel 718 [198].

5.2 CMQLAM of titanium alloy

A minimal cutting force and surface roughness were observed in the CO_2 + MQL CMQLAM process. Bagherzadeh et al. [199] studied the effects of MQL, CO_2, LN_2, CO_2 + MQL, and LN_2 + MQL on tool wear, cutting temperature, cutting force, and surface roughness in the machining process of TC4 at different cutting speeds. The CO_2 and LN_2 pressures and MQL flow rates were set to 10.8 kg/h, 36, and 90 mL/h, respectively. When comparing the tool wear under different cooling lubrication conditions at v_c = 60 m/min, applying CO_2 + MQL resulted in a 31.8% lower tool wear than using CO_2 alone, while that under LN_2 + MQL conditions was 59.6% lower than when using only LN_2, and the minimum tool wear could be obtained when applying MQL only, as shown in Fig. 40(a) [199]. When v_c was 120 m/min, the tool wear obtained using CO_2, LN_2, CO_2 + MQL, and LN_2 + MQL decreased by 35.4%, 29.6%, 38.9%, and 53.6%, respectively. The minimum tool wear can be achieved under LN_2 + MQL conditions, as shown in Fig. 40(b) [199]. The cutting force at v_c = 120 m/min under cooling conditions (CO_2 or LN_2) alone was higher than that under MQL conditions, whereas both the cutting force and surface roughness were assumed to be the lowest values when applying CMQLAM (CO_2 + MQL) [199].

Optimal surface quality can be obtained in a CO_2 + MQL CMQL environment. Hanenkamp et al. [200] used a CMQL energy field (CO_2 + MQL) with a CO_2 pressure of 10 kg/h and an MQL flow rate of 60 mL/h for the assisted milling of TC4. The research showed that compared with CM gating cutting, the surface roughness values under CO_2 and MQL conditions increased by 11.0% and 82.5%, respectively. When applying CMQLAM, the surface roughness was the smallest, and the surface quality was improved [200].

The best results were obtained under $SCCO_2$-OoWMQL conditions. Cai et al. [201] studied the milling of TC4 in four green environments: dry cutting, $SCCO_2$, $SCCO_2$-WMQL, and $SCCO_2$-OoWMQL. They analyzed the effects of v_c, f_z, α_e, and green lubrication on the cutting force, temperature, surface morphology, and surface roughness. In the experiments, the $SCCO_2$ pressure and MQL flow rate were set to 7.5 bar and 50 mL/h, respectively. Irrespective of the green lubrication environment, when v_c increased from 20 to 60 m/min, the average cutting force increased by 273.6%. Under the $SCCO_2$-OoWMQL condition, owing to its excellent cooling lubrication, chip removal, and chip breaking performance, the friction coefficient of the contact surface between the tool and workpiece was reduced, resulting in a lower cutting force. Furthermore, owing to the forced convection heat transfer, vaporization heat absorption, and promotion of chip removal and lubrication of OoWMQL particles by $SCCO_2$, the cutting temperature and surface smoothness were optimal, as shown in Fig. 41(a) [201]. The cutting temperature increased with an increase in v_c, f_z, and α_e, whereas the surface roughness increased with increasing v_c and f_z, as shown in Fig. 41(b) [201]. Under the action of $SCCO_2$, owing to the increase in material strength and hardness, the friction at the tool and workpiece interface decreased, and the cutting force increased, ranging from 8% to 64%. This would result in poor processing performance [201].

In an LN_2 + MQL CMQL environment, the influence of cutting parameters on the cutting force, tool wear, surface roughness, and productivity was analyzed. Suhaimi et al. [202] applied assisted milling to TC4 with a CMQL energy field (LN_2 + MQL) using 2.5–3 bar air pressure and an MQL flow rate of 180 mL/h. Compared to CM pouring cutting, the cutting force and tool wear obtained by CMQLAM were reduced by 54% and 90%, respectively [202]. The team also explored the processing mechanism of CMQLAM and found that using only LN_2 for processing led to strong adhesive wear of the tool. Through the detection of the cutting force, it was determined that the point where the cutting force decreases to 0 N was the blade fracture point [203]. To explore the influence of multiple parameters on CMQLAM processing, Shokrani et al. [204], based on a full-factor experimental design, combined the CMQL energy field (LN_2 + MQL) with an LN_2 pressure of 1.5 bar and an MQL flow rate of 70 mL/h for assisted milling of TC4. It was found that compared with CM pouring, CMQLAM increased the tool life by a factor of 30. The effective cooling and lubrication characteristics of CMQLAM control tool wear and adhesion rates. When only LN_2 was used to cool the workpiece surface, the hardness of the material and the plastic deformation of the cutting edge increased, thereby promoting adhesive wear. When v_c was high, CMQLAM exhibited excellent cooling and lubrication performance, which reduced the friction force and tool wear, as shown in Fig. 42(a) [204], stabilized the surface roughness at 0.2 μm, and increased productivity by 50%. To study the tool life under

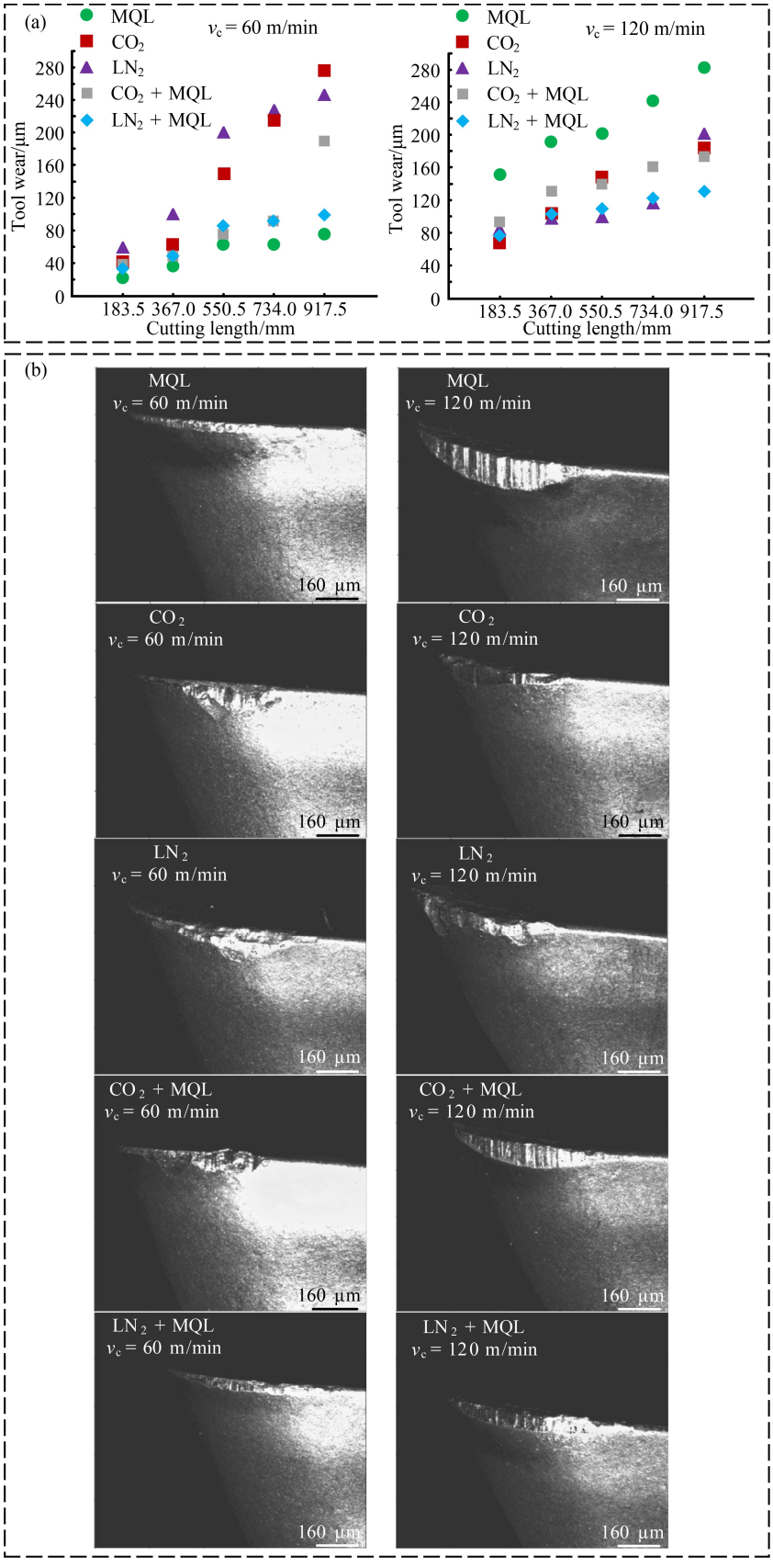

Fig. 40 Tool wear under different v_c and lubrication/cooling methods: (a) flank wear of all lubrication/cooling methods and (b) final tool wear of all lubrication/cooling methods [199]. Reproduced with permission from Ref. [199] from Elsevier.

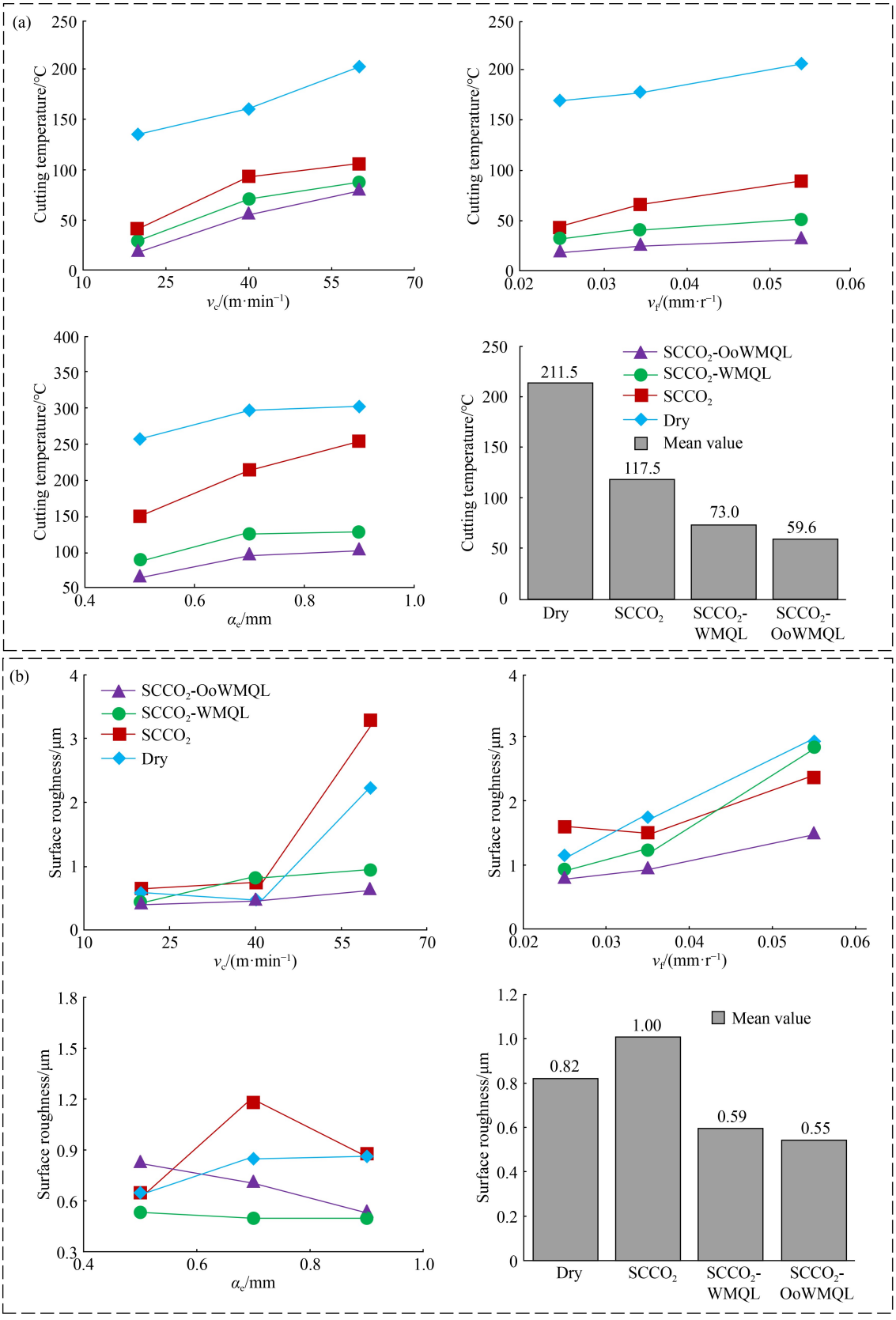

Fig. 41 Effect of green lubrication and cutting parameters on (a) cutting temperature and (b) surface roughness [201]. Reproduced with permission from Ref. [201] from Springer Nature.

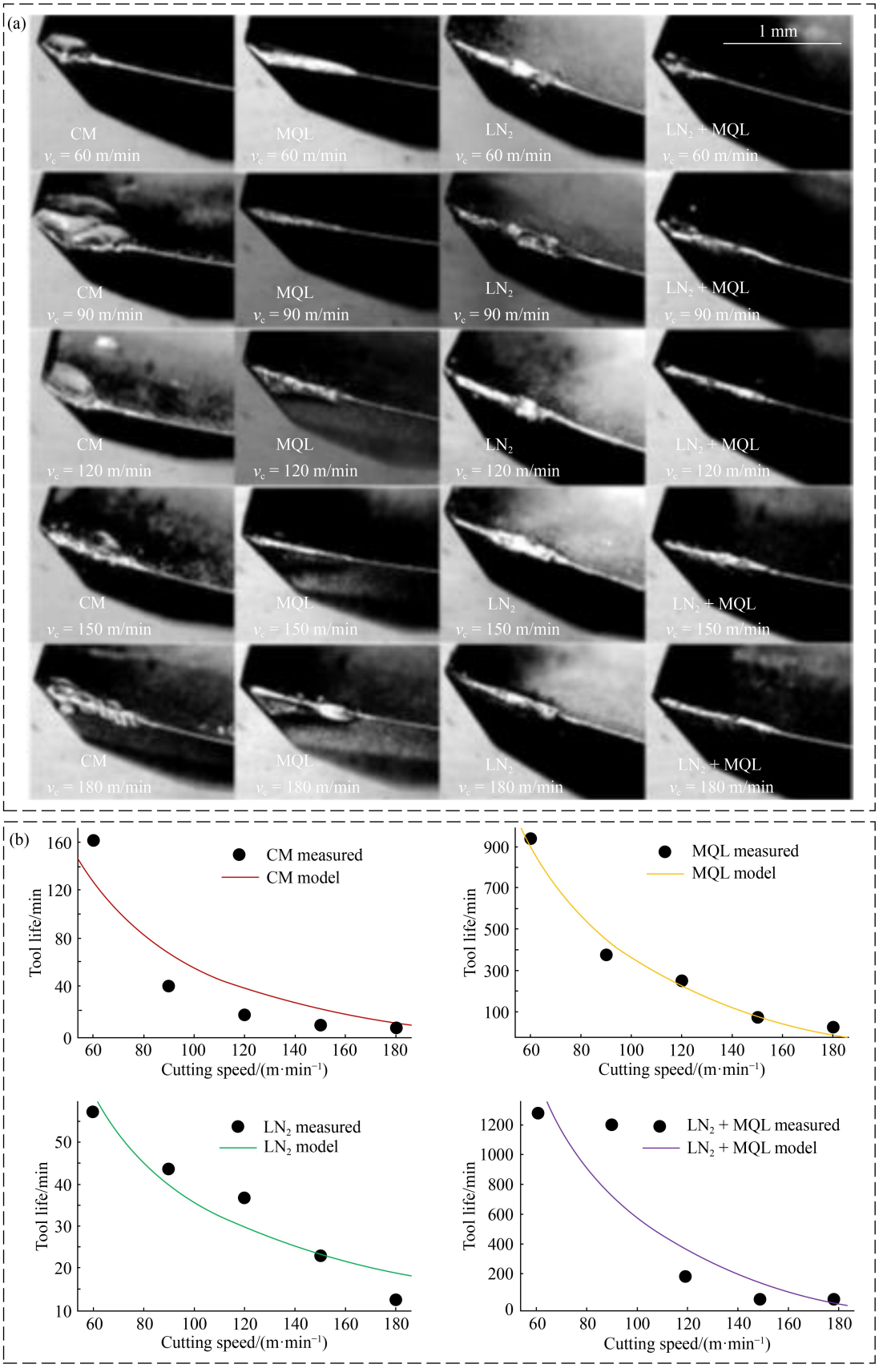

Fig. 42 Tool life and microscopic images under different cutting conditions: (a) microscopic images of the cutting edge at the end of tool life and (b) tool life measurement and prediction results [204]. Reproduced with permission from Ref. [204] from Elsevier.

different milling conditions, the tool life under multi-parameter conditions was modeled and predicted, as shown in Fig. 42(b) [204].

Compared with other cryogenic media, the use of CA is related to a higher economic value, and CA + MQL can significantly reduce flank wear. Therefore, Su et al. [205] employed TC4 in high-speed end milling experiments and compared the effects of dry, CA, and CMQL cooling and lubrication methods on the cutting temperature and tool wear. The CA pressure and MQL flow rate were set to 6 bar and 90 mL/h, respectively. It was found that the measured temperature values of the shear zone increased in the order of CMQL, CA, and dry milling. The flank wear when using CA was almost the same as that obtained with dry milling, whereas the flank wear observed when applying CMQL was significantly reduced [205].

After the CMQL and milling parameters were determined, the atomizing nozzle structure of CMQL had a direct impact on the machining process. Song et al. [206] found that when MQL and cryogenic gas were applied on both sides of the tool, the oil mist could not penetrate the shear zone owing to the low injection pressure of the cryogenic gas. Therefore, it is necessary to design a hybrid nozzle that can simultaneously inject oil mist and cryogenic gases. Based on the Coanda effect and CFD software analysis, the Coanda effect of the nozzle was tested at different inlet flow rates, as shown in Fig. 43(a) [206]. It can be observed by CFD that flow separation occurs earlier at lower flow velocities. Therefore, the flow parameters should be controlled to achieve ideal cooling and lubrication effects after nozzle design. To evaluate the performance of the nozzle, combined with CA (pressure of 5 bar) and CO_2 gas (pressure of 8 bar), TC4 was processed using the designed nozzle (MQL flow rate of 19.8 mL/h) and conventional nozzle (MQL flow rate of 54.9 mL/h). According to the results, low-temperature micro-lubrication energy field-assisted milling with the designed nozzle can reduce the friction heat in the processing area, tool wear, and the minimum

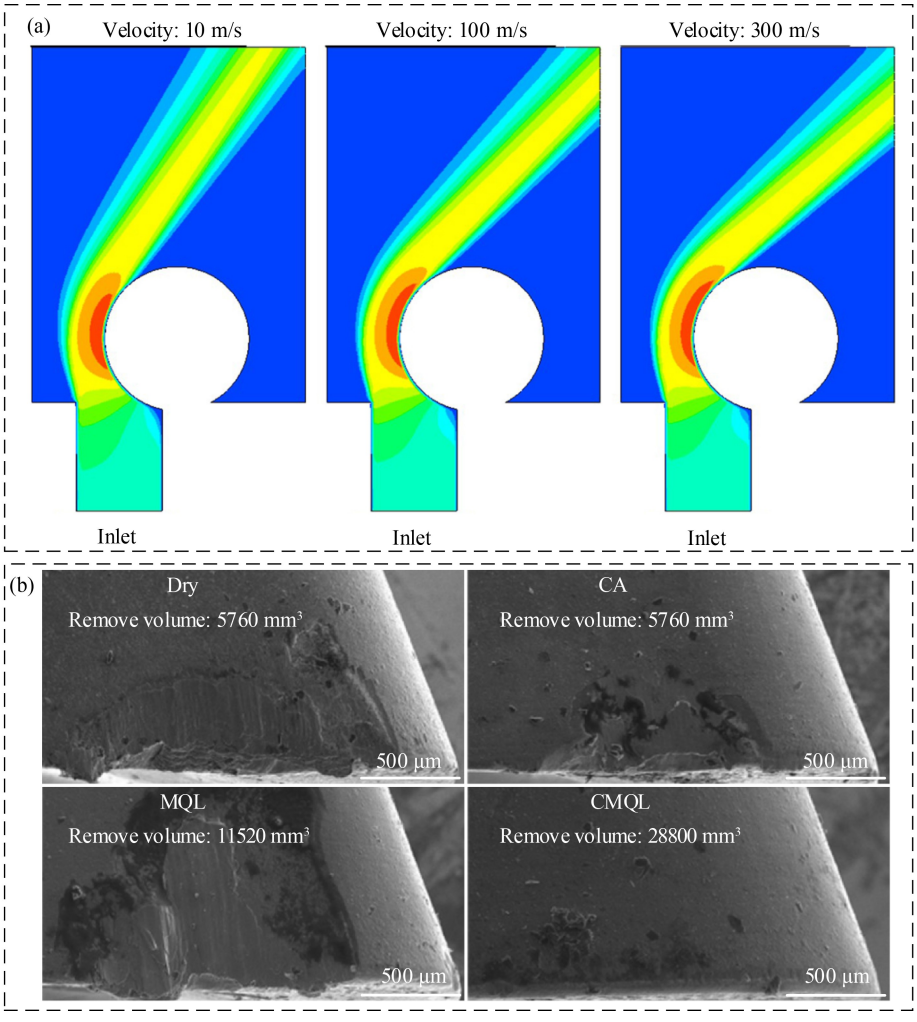

Fig. 43 Nozzle structure and tool wear: (a) nozzle Coanda effect [206] and (b) influence of green lubrication and cutting volume on tool wear [207]. Reproduced with permissions from Refs. [206,207] from Springer Nature.

temperature of the cutting zone to 310 °C [206]. For the milling of TC4, the team also compared the cooling lubrication performance of CMQL, dry conditions, CA, and MQL with a CO_2 pressure of 4 bar and an MQL flow rate of 19.8 mL/h. The results showed that under the same flow rate, CMQL reduced the cutting force, tool wear, and cutting temperature by 23%, as shown in Fig. 43(b) [207]. In addition, an economic analysis proved that CMQL is cheaper than conventional methods [207].

5.3 CMQLAM of high-strength steel

The new CMQL method can achieve better machining effects. Mulyana et al. [94] conducted a milling experiment on HTCS steel and studied the effects of dry milling, MQL, $SCCO_2$ and CMQL ($SCCO_2$ + MQL) conditions on the cutting force, temperature, and tool wear. The pressure of $SCCO_2$ was set to 4 bar, and the flow rate of the MQL was 160 mL/h. Compared to dry milling, the cutting force and cutting temperature under CMQL conditions were reduced by 60% and 55%, respectively. Compared with dry milling, MQL, and $SCCO_2$, the tool life increased by 150%, 87%, and 22%, respectively, when using CMQL. Overall, CMQL was the best choice for reducing tool wear and prolonging tool life, which could significantly improve the processing efficiency [94]. In addition to the common CMQL method ($SCCO_2$ + MQL), Yuan et al. [208] proposed a new CMQL ($SCCO_2$-OoW) cooling and lubrication system for milling 316L stainless steel. The effects of $SCCO_2$, OoW (oil-on-water), common CMQL, and new CMQL on the cutting force, tool life, and surface roughness were compared and analyzed. The $SCCO_2$ pressure and MQL flow rate were set to 0.12 kg/h and 20 mL/h, respectively. The experimental results showed that compared with common CMQL, $SCCO_2$, and OoW conditions, the application of the new CMQL method maintained a lower cutting force and stable cutting force variation throughout the cutting process. The tool life decreased in the order of the new CMQL process, OoW, ordinary CMQL, and $SCCO_2$. When v_c was 90 m/min, compared to $SCCO_2$ and OoW, the surface roughness of the new CMQL method decreased slightly. Compared with $SCCO_2$, the surface roughness of the workpieces processed under OoW and CMQL conditions decreased by 25% and 23%, respectively, when v_c was 120 m/min. At a v_c of 150 m/min, the surface roughness of OoW and CMQL was reduced by 39% and 32%, respectively, compared with $SCCO_2$, which proved that the new CMQL method had the best milling effect [208].

The green lubrication parameters and cutting parameters have a strong influence on machining. Wika et al. [209] applied CM pouring and the CMQL ($SCCO_2$ + MQL) cooling lubrication mode at different v_c and f_z in the milling of 304L stainless steel using an $SCCO_2$ pressure of 6 bar and an MQL flow rate of 60 mL/h. Compared with CM pouring cutting, the use of CMQL resulted in the longest tool life, with an increase of 324% when v_c and f_z were 215 m/min and 0.5 mm/z, respectively. The CMQL material removal increased by 158%. Although the surface roughness decreased with increasing f_z, it increased with increasing v_c. By using a high f_z and low v_c, the surface roughness can be reduced by 30%. Under the conditions of CM pouring and CMQL, tensile residual stress was produced on the workpiece surface. When combining experimental data, the authors found f_z to be the main factor affecting residual stress, as shown in Fig. 44 [209].

The above research shows that CMQLAM can effectively prolong tool life when the v_c value is high. Based on this, Manimaran and Nimel Sworna Ross [210] studied the influence of v_c in the range of 45–75 m/min on the cutting performance of AISI H13 steel at a constant α_p. The effects of dry milling, CM pouring, and CMQL conditions on the surface roughness, chip morphology, flank wear, and cutting temperature were tested. The CO_2 pressure was 2.5 bar, and the MQL flow rate was 60 mL/h. The results showed that under CMQL machining conditions, the cutting forces in the three directions were reduced by 12%–16%, 11%–14%, and 12%–13% compared to dry milling. When compared to the CM pouring process, the cutting forces were also reduced by 6%–8%, 5%–7.5%, and 6.5%–8%, respectively. Moreover, the application of CMQL reduced the cutting temperature by 52%–53% compared to dry milling, and by 38%–41% compared to CM pouring. Tool wear was also reduced by 50%–57% compared to dry milling, and by 14%–23% compared to CM pouring. The average surface roughness decreased by 65%–71% and 33%–41%, respectively. Additionally, the machining hardness of CMQL was 6% and 2% higher than those obtained by dry milling and CM pouring, respectively. Compared with dry conditions and CM pouring conditions, the use of CMQL resulted in a better chip-breaking performance, as shown in Fig. 45(a) [210].

The cutting force and temperature accompany the entire process. Zhang et al. [211] analyzed the influence of CMQL on the cutting force and temperature during the high-speed milling of 300M steel. First, the influence of cutting parameters on the cutting force and temperature was investigated. The model was established using a simulation and a prediction algorithm. Then, by single-factor experiments, with a CA pressure range of 6–10 bar and an MQL flow rate of 265 mL/h, the variations in cutting force and temperature with the cutting parameters v_c, f_z, α_p, and α_e were studied under dry milling and CMQL conditions, as shown in Fig. 45(b) [211]. Compared with dry milling, the CMQL method resulted in better lubrication and cooling effects, which could effectively reduce the cutting force and temperature in the shear zone. Based on this, the authors verified the accuracy of the prediction model and provided a

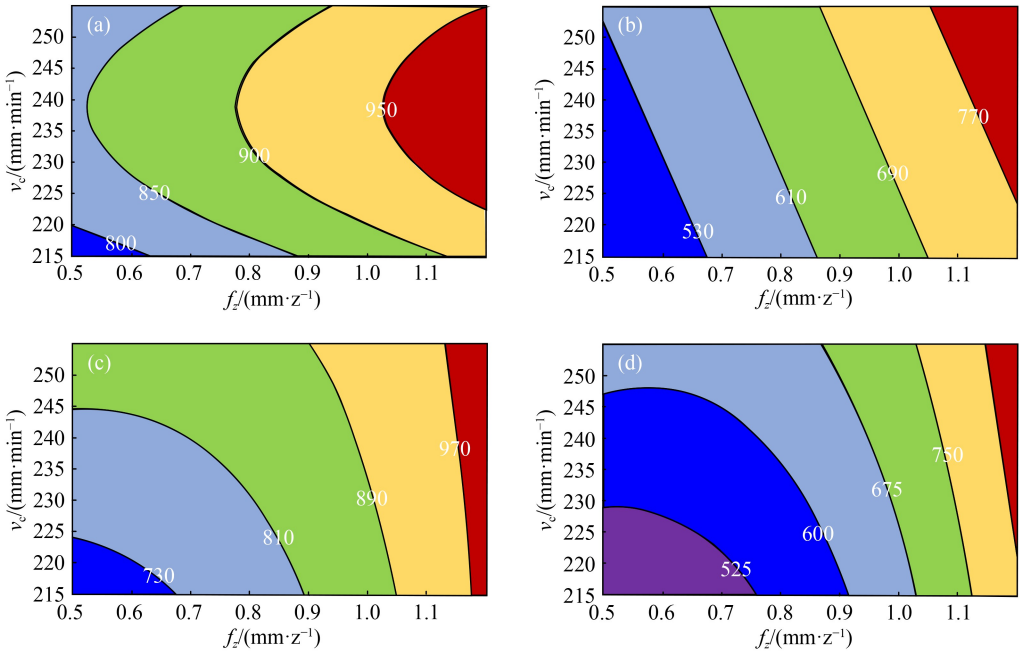

Fig. 44 Average residual stresses corresponding to different f_z and v_c: (a) conventional milling 0° residual stresses, (b) conventional milling 90° residual stresses, (c) cryogenic minimum quantity lubrication 0° residual stresses, and (d) cryogenic minimum quantity lubrication 90° residual stresses [209]. Reproduced with permission from Ref. [209] from Elsevier.

theoretical and experimental basis for the subsequent application of CMQL [211]. Furthermore, the team performed milling experiments on 300M steel under dry, CA, water mist cooling, oil mist friction reduction, and CMQL lubrication conditions using a CA pressure of 4.8 bar and an MQL flow rate of 150 mL/h. Through the results of single-factor and orthogonal experiments, it was found that, compared with other cooling and lubrication conditions, CMQL cutting conditions could obtain lower cutting forces and better surface smoothness [212].

The white layer affects the service performance of workpieces. Zhang et al. [213] studied the influence of tool wear on the formation of a white layer in dry milling and CMQLAM of H13 steel at a CA pressure of 1.5 bar and MQL flow rate of 20 mL/h. The results showed that CMQLAM could increase tool life by a factor of 1.78 compared with dry milling. Furthermore, the formation of the white layer was related to tool wear. The thickness of the white layer increased with increasing tool wear. According to the experimental results, the white layer could be partially or completely eliminated under CMQL conditions by optimizing the parameters, as shown in Fig. 46(a) [213]. This indicates that CMQL can improve the surface integrity [213]. The authors also conducted side-milling experiments on H13 steel. Under CMQL conditions using a CA pressure of 2 bar and an MQL flow rate of 15 to 20 mL/h, the effects of three types of internal cooling tools, namely, double helix channel (DHC), single straight channel (SSC), and DSC, on the cutting force and tool wear were analyzed. Flank wear and fracture were found to be the main factors affecting tool life. The cutting force increased with an increase in tool wear. Comparing the tool wear of three internal cooling tools under CMQL conditions (Fig. 46(b) [214]) revealed that the DSC tool achieved an effective reduction in tool wear and a life 1.59 times longer than that of the DHC tool, indicating that the DSC tool was better than the DHC tool. From the perspective of environmental protection and economy, CMQLAM using a DSC internal cooling tool had the best effect on machining [214].

5.4 Summary of CMQLAM of difficult-to-machine metal materials

Based on the research presented above, the flow rate range of MQL used in CM with CMQLAM varies according to the basic properties of the difficult-to-machine metal materials being used. The MQL flow rate ranges for nickel-based alloy, titanium alloy, and high-strength steel are 8–120 mL/h, 19.8–180 mL/h, and 15–256 mL/h, respectively. These values are consistent with the machinability of the three materials. In summary, CMQLAM of difficult-to-machine metal materials is depicted in Fig. 47. Compared to CM casting cutting, the types of low-temperature medium, gas pressure, MQL flow rate, atomizing nozzle type, coating tool type, and cutting parameters all affect the machining results. The advantages of CMQLAM include low cutting force, high material removal rate, long tool life, low cutting specific energy, low cutting temperature, low manufacturing costs, small chip size, and high surface quality. However,

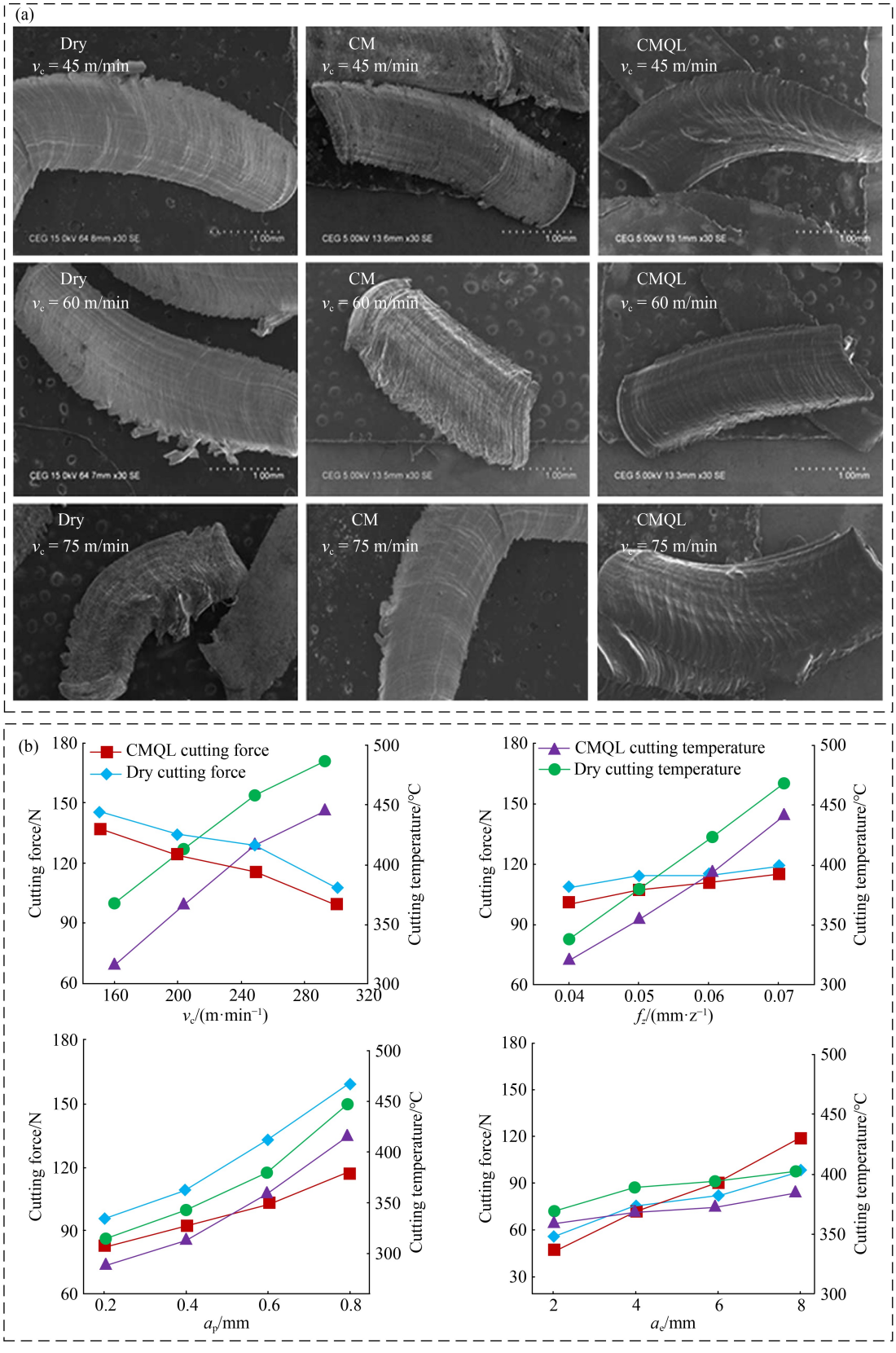

Fig. 45 Chip morphology, cutting force, and cutting temperature: (a) chip morphology under different lubrication environments [210] and (b) influence of cutting parameters on cutting force and cutting temperature [211]. CM: conventional milling; CMQL: cryogenic minimum quantity lubrication. Reproduced with permissions from Refs. [210,211] from ASTM and Springer Nature.

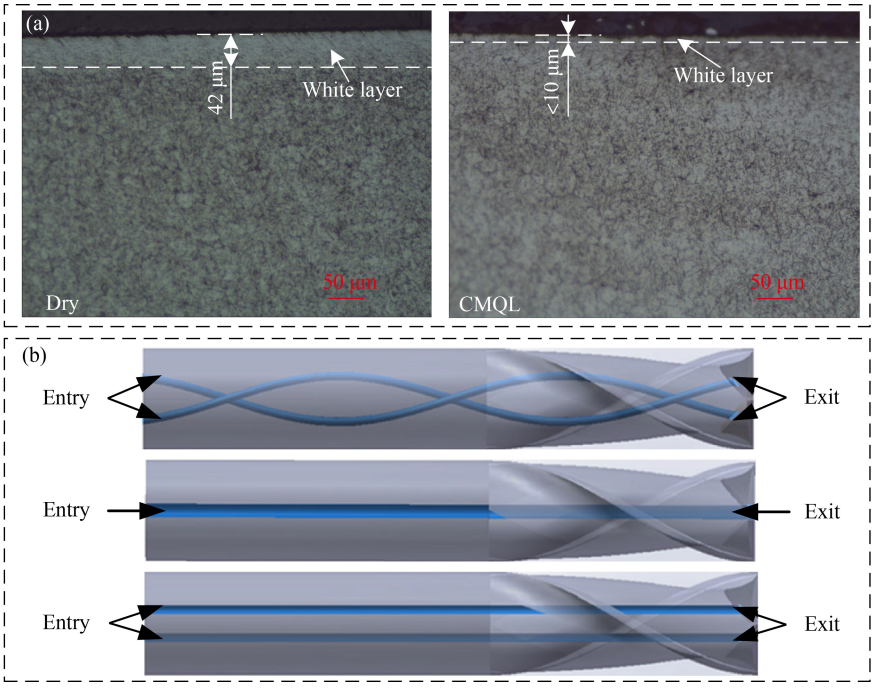

Fig. 46 Subsurface and channel structures: (a) white layer [213] and (b) three channel structures of internal cooling milling tools [214]. Reproduced with permissions from Refs. [213,214] from SAGE and Springer Nature.

there is currently no model available to obtain optimal parameters, and the FEM model of the machining process during cooling and lubrication and the predictive optimization algorithm model still require further research. Additionally, a normative guidance theory has not been developed for the lubrication mechanism of CMQLAM, and optimal processing parameters of CMQLAM have not been defined. In the future, it is necessary to design an intelligent matching system or database to establish a quantitative correspondence between the evaluation index level and the cooling medium parameters, to realize the most effective combination of lubricating oil types and process parameters under different processing conditions. Moreover, an intelligent nozzle and a multi-parameter coordinated control system that can automatically adjust the space attitude should be designed to guide the practical production environment for the purpose of accurately transporting the CMQL fluid to the cutting zone.

6 Conclusions

The discussed shortcomings, such as the large removal rate of titanium alloy, nickel-based alloy, high-strength steel, and other difficult-to-machine metal materials, the high energy consumption of machine tools, large tool consumption, low processing efficiency, large emissions of cutting oil mist and waste liquid, environmental pollution and health hazards, and the dependence on imported high-end tools and cutting oil, seriously restrict the green low-carbon and independent and controllable development of the manufacturing industry. With the increasing demand to address the issues of ‘carbon peak’, ‘carbon neutralization’, and ‘manufacturing power’, the concept of green manufacturing is becoming more important and will have a profound impact on the future development of the global manufacturing industry. It is, therefore, crucial to explore and address the limitations and defects of energy-field-assisted green processing technology for difficult-to-machine metal materials, and to provide innovative processing methods for global high-end manufacturing.

(1) Energy field-assisted machining mechanisms for difficult-to-machine metal materials

The use of LAM, UVAM, and CMQLAM technologies to process titanium alloys, nickel-based alloys, and high-strength steel can reduce the cutting force, improve the material removal rate, prolong the tool life, reduce the cutting specific energy, reduce manufacturing costs, decrease chip size, and improve surface quality. However, their processing mechanisms differ from one another. LAM softens the shear zone using the laser system before machining. UVAM applies ultrasonic frequency vibration to the workpiece or tool based on an ultrasonic system, which realizes a high-frequency periodic separation of the workpiece and tool in the cutting process. CMQLAM uses a jet device to spray a liquid/gaseous medium into the shear zone depending on the jet form, which can replace the CM cutting fluid for lubrication and cool the machining contact zone. Compared with the CM, the LAM has a greater influence

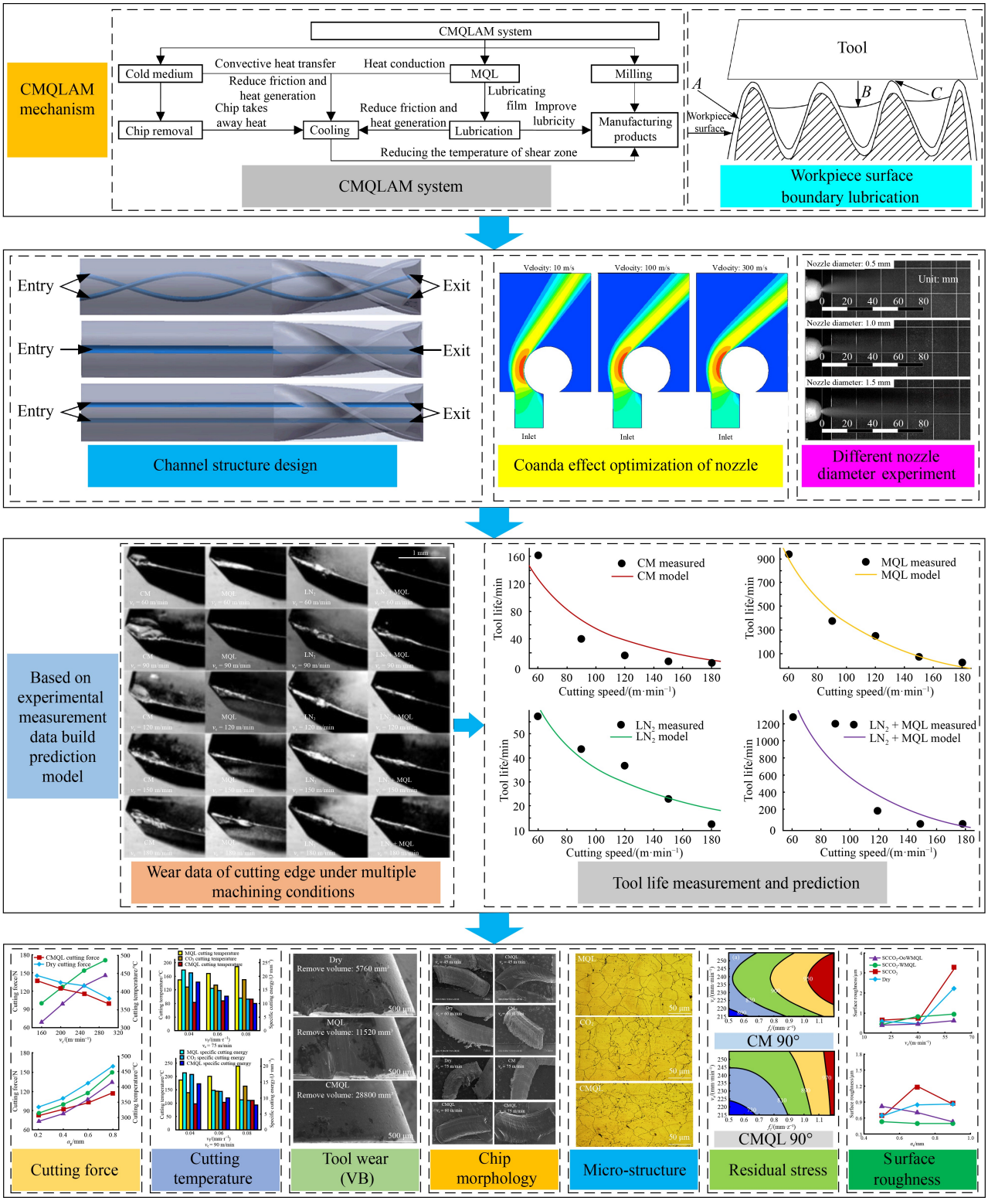

Fig. 47 Summary of cryogenic minimum quantity lubrication energy field-assisted milling (CMQLAM) machinability.

on the cutting force, and its limit value can be reduced by 70%. UVAM has the greatest effect on chips, making them thin and small. CMQLAM has the greatest influence on the tool life and cutting temperature, and its limit values can be reduced by 157% and 60%, respectively.

(2) Energy field-assisted machining methods for difficult-to-machine metal materials

Currently, the use of titanium alloys, nickel-based alloys, and high-strength steel is increasing. Traditional processing methods cause severe tool wear, low processing efficiency, and poor surface integrity. Therefore, new processing methods are required for this purpose. For the LAM process, this paper systematically illustrates the influence of laser and cutting parameters on the cutting force, material removal rate, tool life, cutting specific energy, manufacturing cost, chip morphology, and surface quality. To improve the data-driven processing effect, an intelligent algorithm should be established to predict the influence of the laser and cutting parameters on the corresponding parameters. For the UVAM process, in addition to exploring the effects of ultrasonic parameters, cutting parameters, and vibration direction changes on cutting force, surface morphology, surface roughness, residual stress, chip morphology, and tool wear, a prediction model of the influence of instantaneous cutting thickness change on the corresponding result parameters should be developed based on ultrasonic and cutting parameters. For the CMQLAM process, after exploring the effects of air pressure, flow rate, and cutting parameters on cutting force, material removal rate, tool life, cutting specific energy, cutting temperature, manufacturing cost, chip size, and surface quality, it is necessary to establish a CMQLAM specification guidance theory to define the optimal processing parameters.

(3) Difficulties in energy field-assisted machining of difficult-to-machine metal materials

A laser energy field can soften a material before machining. An ultrasonic energy field can improve chip-breaking ability. The CMQL energy field can reduce cutting fluid emissions and realize green machining. However, there are still difficulties restricting the application and development of energy fields, such as the long processing cycle of LAM, little effect of UVAM on reducing the temperature of the shear zone, and residual oil on the surface of the CMQLAM-processed workpieces. Therefore, the engineering application and development of energy field-assisted HSDM green machining technology requires combined global efforts. This review provides feasible ideas for realizing multi-energy field collaborative green machining of difficult-to-machine metal materials in the future.

7 Prospects

Difficult-to-machine metal materials will remain a global research hotspot in the future. However, there are still some limitations to the efficient and precise machining of difficult-to-machine metal materials. The above systematic summary shows that future research directions of energy field-assisted green machining technology for HSDM may mainly focus on the following points:

(1) For tool coatings with different application requirements, the elemental composition and thickness of coatings should be explored with three processing scenarios: rough machining, semi-finishing, and finishing. Thus, the optimum working conditions can be applied to the various processing methods of difficult-to-machine metal materials, which can prolong the tool life in the energy field-assisted HSDM process.

(2) It is necessary to utilize multi-energy field synergy to assist the manufacturing of difficult-to-machine metal materials, and cutting force, vibration, and temperature sensing technology can be used as signal input sources to control the ultrasonic and CMQL parameters in real time under different processing conditions, which can realize the adaptive intelligent control of difficult-to-machine metal materials in large-scale manufacturing.

(3) To address the problem of high carbon emissions in the machining process, a multi-energy field collaborative and multi-dimensional carbon-efficient concept for HSDM is proposed, which considers both efficient material removal and surface quality assurance and realizes green intelligent machining using multi-energy fields at a low total energy consumption of the process.

Nomenclature

Abbreviations

B&F	Back-and-forth
CA	Cold air
CCD	Central composite design
CFD	Computational fluid dynamics
CL	Conventional melting
CM	Conventional milling
CMQL	Cryogenic minimum quantity lubrication
CMQLAM	Cryogenic minimum quantity lubrication energy field-assisted milling
CVD	Chemical vapor deposition
DHC	Double helix channel
DSC	Double straight channel
FEM	Finite element method
HAZ	heat-affected zone
H.F	High feed milling
HM	Helical milling
HPDL	High-power semiconductor laser
HSDM	High-speed dry milling
LAM	Laser-assisted milling
LCO_2	Liquid carbon dioxide
L.F	Low feed milling
LMO	Local misorientation
LS	Single laser scanning

MQL	Minimum quantity lubrication
Nd:YAG	Neodymium-doped yttrium aluminum garnet
NMQL	Nanofluid minimum quantity lubrication
NURBS	Non-uniform rational B-spline
OoW	Oil-on-water
PCBN	Polycrystalline cubic boron nitride
PVD	Physical vapor deposition
$SCCO_2$	Supercritical carbon dioxide
SEM	Scanning electron microscope
SLM	Selective laser melting
SSC	Single straight channel
S&T	Spatial and temporal
TAM	Thermal-assisted machining
TC4	Ti–6Al–4V
UVAM	Ultrasonic vibration-assisted milling
XRD	X-ray diffraction

Variables

A	Vibration amplitude
d_L	Heat source size
f	Vibration frequency
f_z	Feed per tooth
N_z	Number of tips
P_{ci}	Coordinate tool point
P_{li}	Initial coordinate point
P_L	Laser power
P_{Li}	End coordinate point
r	Radius of the cutting tool
r_c	Sum of the radius of the cutting tool
R	Expected fillet radius
Sa	Average roughness
Sq	Surface root mean square roughness
t	Cutting time
v_c	Cutting speed
v_f	Feed speed
V_L	Laser scanning speed
x, y, z	Tip displacements
x_{cl}	Distance between the tool center and the laser heat source center
x_L	Distance between spot and tool
ω_r	Angular velocity of the spindle
α_i	Tool radius angle
α_p	Axial cutting depth
α_e	Radial cut width
β	Tool rotation angle
θ	Initial phase of the vibration signal
Δ_{xi}	Distance between the initial coordinate point of the heat source and the end coordinate point

Acknowledgements This work was supported by the National Key R&D Program of China (Grant No. 2020YFB2010500). The authors gratefully acknowledge the reviewers and editors for their insightful comments.

Conflict of Interest The authors declare that they have no conflict of interest.

References

1. Inasaki I. Grinding of hard and brittle materials. CIRP Annals, 1987, 36(2): 463–471
2. Dudzinski D, Devillez A, Moufki A, Larrouquère D, Zerrouki V, Vigneau J. A review of developments towards dry and high speed machining of Inconel 718 alloy. International Journal of Machine Tools and Manufacture, 2004, 44(4): 439–456
3. Bowden D, Krysiak Y, Palatinus L, Tsivoulas D, Plana-Ruiz S, Sarakinou E, Kolb U, Stewart D, Preuss M. A high-strength silicide phase in a stainless steel alloy designed for wear-resistant applications. Nature Communications, 2018, 9(1): 1374
4. Zhao W, Wang S Z, Li L, Yang Y F. Evaluation of cutting tool performance of end mills for titanium alloy components. Journal of South China University of Technology (Natural Science Edition), 2015, 43(9): 121–126 (in Chinese)
5. Li F. Wear of grinding wheels in high efficiency grinding of nickel-based superalloy. Thesis for the Master's Degree. Nanjing: Nanjing University of Aeronautics and Astronautics, 2012 (in Chinese)
6. Zhang X L. Investigation of mechanism in high speed machining of 40CrNi2Si2MoVA ultra high strength process. Thesis for the Master's Degree. Harbin: Harbin University of Science and Technology, 2016 (in Chinese)
7. He G H, Wu M Y, Li L X, Zou L L, Cheng C. Study on the formation mechanism of phase transformation and the influencing factors of cutting layer of the typical titanium alloy. Journal of Mechanical Engineering, 2018, 54(17): 133–141 (in Chinese)
8. Ding W F, Miao Q, Li B K, Xu J H. Review on grinding technology of nickel-based superalloys used for aero-engine. Journal of Mechanical Engineering, 2019, 55(1): 189–215 (in

Chinese)
9. Lin S. Modeling and experimental investigation on workpiece temperature field for turn-milling of high strength steel. Dissertation for the Doctoral Degree. Wuhan: Huazhong University of Science and Technology, 2014 (in Chinese)
10. He G H, Liu X L, Wu C H, Zhang S Q, Zou L L, Li D J. Study on the negative chamfered edge and its influence on the indexable cutting insert's lifetime and its strengthening mechanism. The International Journal of Advanced Manufacturing Technology, 2016, 84(5–8): 1229–1237
11. Liu L J, Lv M, Wu W G, Zhu X J. Experimental study on the chip morphology in high speed milling Ti–6Al–4V alloy. Journal of Mechanical Engineering, 2015, 51(3): 196–205 (in Chinese)
12. Ren J X, Hua D A. Principle of Grinding. Beijing: Electronic Industry Press, 2011 (in Chinese)
13. Putz M, Cardone M, Dix M, Wertheim R. Analysis of workpiece thermal behaviour in cut-off grinding of high-strength steel bars to control quality and efficiency. CIRP Annals, 2019, 68(1): 325–328
14. Kim S W, Lee D W, Kang M C, Kim J S. Evaluation of machinability by cutting environments in high-speed milling of difficult-to-cut materials. Journal of Materials Processing Technology, 2001, 111(1–3): 256–260
15. Koshy P, Dewes R C, Aspinwall D K. High speed end milling of hardened AISI D2 Tool Steel (~58HRC). Journal of Materials Processing Technology, 2002, 127(2): 266–273
16. Long Z H, Wang X B, Wang H C. Factorial study on nonlinear characteristics of difficult-to-cut materials in high-speed cutting process. Journal of Mechanical Engineering, 2006, 42(1): 30–34 (in Chinese)
17. Liu G L, Zou B, Huang C Z, Wang X Y, Wang J, Liu Z Q. Tool damage and its effect on the machined surface roughness in high-speed face milling the 17-4PH stainless steel. The International Journal of Advanced Manufacturing Technology, 2016, 83(1–4): 257–264
18. Marusich T D, Ortiz M. Modelling and simulation of high-speed machining. International Journal for Numerical Methods in Engineering, 1995, 38(21): 3675–3694
19. Umbrello D. Finite element simulation of conventional and high speed machining of Ti6Al4V alloy. Journal of Materials Processing Technology, 2008, 196(1–3): 79–87
20. Chen G, Ren C Z, Yang X Y, Jin X M, Guo T. Finite element simulation of high-speed machining of titanium alloy (Ti–6Al–4V) based on ductile failure model. The International Journal of Advanced Manufacturing Technology, 2011, 56(9–12): 1027–1038
21. Gong Q H, Sun C, Wang W. High speed and high efficiency machining research of titanium alloy aircraft structure part and its application. Aeronautical Manufacturing Technology, 2016, (7): 26–32 (in Chinese)
22. Liu M Z, Li C H, Cao H J, Zhang S, Chen Y, Liu B, Zhang N Q, Zhou Z M. Research progresses and applications of CMQL machining technology. China Mechanical Engineering, 2022, 33(5): 529–550 (in Chinese)
23. Baumeister K J, Simon F F. Leidenfrost temperature—its correlation for liquid metals, cryogens, hydrocarbons, and water. ASME Journal of Heat and Mass Transfer, 1973, 95(2): 166–173
24. Hu D H, Qiu H, Li Q. Study on bubble dynamics inside droplets under local boiling. Journal of Engineering Thermophysics, 2021, 42(4): 1026–1031 (in Chinese)
25. Rao P N, Srikant R R. Sustainable machining utilizing vegetable oil based nanofluids. In: Proceedings of 2015 International Conference on Smart Technologies and Management for Computing, Communication, Controls, Energy and Materials. Avadi: IEEE, 2015, 664–672
26. Adler D P, Hii W W S, Michalek D J, Sutherland J W. Examining the role of cutting fluids in machining and efforts to address associated environmental/health concerns. Machining Science and Technology, 2006, 10(1): 23–58
27. Anton S, Andreas S, Friedrich B. Heat dissipation in turning operations by means of internal cooling. Procedia Engineering, 2015, 100: 1116–1123
28. Pusavec F, Kramar D, Krajnik P, Kopac J. Transitioning to sustainable production—part II: evaluation of sustainable machining technologies. Journal of Cleaner Production, 2010, 18(12): 1211–1221
29. Sankaranarayanan R, Rajesh J H N, Senthil K J, Krolczyk G M. A comprehensive review on research developments of vegetable-oil based cutting fluids for sustainable machining challenges. Journal of Manufacturing Processes, 2021, 67: 286–313
30. Yang X, Cao H J, Chen Y P, Zhang C L, Zhou L. Whole process cutting heat transfer model for high-speed dry hobbing. Journal of Mechanical Engineering, 2015, 51(19): 189–196
31. Chen Y P, Cao H J, Yang X. Research on load distribution characteristic on the cutting edge in high-speed gear hobbing process. Journal of Mechanical Engineering, 2017, 53(15): 181–187
32. Zhang H, Dang J Q, Ming W W, Xu X W, Chen M, An Q L. Cutting responses of additive manufactured Ti6Al4V with solid ceramic tool under dry high-speed milling processes. Ceramics International, 2020, 46(10): 14536–14547
33. Salahshoor M, Guo Y B. Cutting mechanics in high speed dry machining of biomedical magnesium–calcium alloy using internal state variable plasticity model. International Journal of Machine Tools and Manufacture, 2011, 51(78): 579–590
34. Yang X, Cao H J, Du Y B, Xu L, Chen Y P. Regulation and control method for tool temperature in high-speed dry cutting processes based on specific cutting energy. China Mechanical Engineering, 2018, 29(21): 2559–2564 (in Chinese)
35. Liu G L. High-speed machinability evaluation method of difficult-to-machine material for fatigue and corrosion resistance. Dissertation for the Doctoral Degree. Jinan: Shandong University, 2019 (in Chinese)
36. Li B J. Research on exergy efficiency model and coordinative optimization method of spindle system of high-speed dry hobbing machine tool. Dissertation for the Doctoral Degree. Chongqing: Chongqing University, 2019 (in Chinese)
37. Lu L, Wang Q M, Chen B Z, Ao Y C, Yu D H, Wang C Y, Wu S H, Kim K H. Microstructure and cutting performance of CrTiAlN coating for high-speed dry milling. Transactions of Nonferrous Metals Society of China, 2014, 24(6): 1800–1806
38. Li X G. Study on green manufacturing operation model and its

main lines in machine tool industry. Dissertation for the Doctoral Degree. Chongqing: Chongqing University, 2012 (in Chinese)
39. Yang X. Transfer characteristics and quantification analysis method of the cutting heat in high-speed dry hobbing. Dissertation for the Doctoral Degree. Chongqing: Chongqing University, 2017 (in Chinese)
40. Li C H, Li J Y, Wang S, Zhang Q. Modeling and numerical simulation of the grinding temperature field with nanoparticle jet of MQL. Advances in Mechanical Engineering, 2013, 5: 986984
41. Arunachalam R, Mannan M A. Machinability of nickel-based high temperature alloys. Machining Science and Technology, 2000, 4(1): 127–168
42. Song H W. Research on cutting mechanism of laser assisted machining for fused silica with experiments. Dissertation for the Doctoral Degree. Wuhan: Huazhong University of Science and Technology, 2019 (in Chinese)
43. Lajis M A, Amin A K M N, Karim A N M, Radzi H C D M, Ginta T L. Hot Machining of hardened steels with coated carbide inserts. American Journal of Engineering and Applied Sciences, 2009, 2(2): 421–427
44. Rajagopal S, Plankenhorn D J, Hill V L. Machining aerospace alloys with the aid of a 15 kW laser. Journal of Applied Metalworking, 1982, 2(3): 170–184
45. Kim K S, Lee C M. A fundamental study on the prediction of preheating temperature of silicon nitride ceramics by using HPDL. Applied Mechanics and Materials, 2012, 229–231: 287–291
46. Özler L, İnan A, Özel C. Theoretical and experimental determination of tool life in hot machining of austenitic manganese steel. International Journal of Machine Tools and Manufacture, 2001, 41(2): 163–172
47. Tosun N, Özler L. A study of tool life in hot machining using artificial neural networks and regression analysis method. Journal of Materials Processing Technology, 2002, 124(1–2): 99–104
48. Ding H T, Shin Y C. Improving machinability of high chromium wear-resistant materials via laser-assisted machining. Machining Science and Technology, 2013, 17(2): 246–269
49. Anderson M, Patwa R, Shin Y C. Laser-assisted machining of Inconel 718 with an economic analysis. International Journal of Machine Tools and Manufacture, 2006, 46(14): 1879–1891
50. Ding H T, Shin Y C. Improvement of machinability of waspaloy via laser-assisted machining. The International Journal of Advanced Manufacturing Technology, 2013, 64(1–4): 475–486
51. Suthar K J, Patten J, Dong L, Abdel-Aal H. Estimation of temperature distribution in silicon during micro laser assisted machining. In: Proceedings of the ASME 2008 International Manufacturing Science and Engineering Conference. Evanston: ASME, 2008, 301–309
52. Sun S, Brandt M, Dargusch M S. Thermally enhanced machining of hard-to-machine materials—a review. International Journal of Machine Tools and Manufacture, 2010, 50(8): 663–680
53. Germain G, Dal Santo P, Lebrun J L. Comprehension of chip formation in laser assisted machining. International Journal of Machine Tools and Manufacture, 2011, 51(3): 230–238
54. Song P P. Key fundamental research on laser assisted machining of silicon nitride ceramics. Dissertation for the Doctoral Degree. Zibo: Shandong University of Technology, 2020
55. Fang S X, Zhao H L, Zhang Q J. The application status and development trends of ultrasonic machining technology. Journal of Mechanical Engineering, 2017, 53(19): 22–32
56. Cao F G. Ultrasonic Machining. Beijing: Chemical Industry Press, 2014 (in Chinese)
57. Zhang X Y, Lu Z H, Peng Z L, Zhang D Y. High quality and efficient ultrasonic vibration cutting of titanium alloys. Journal of Mechanical Engineering, 2021, 57(5): 133–147
58. Yılmaz B, Karabulut Ş, Güllü A. A review of the chip breaking methods for continuous chips in turning. Journal of Manufacturing Processes, 2020, 49: 50–69
59. Ma L J, Liu G J, Wang G C. Study on mechanism of breaking chip of axial vibration drilling. Chinese Machinery Design and Manufacture, 2009, (2): 228–230 (in Chinese)
60. Ni C B, Zhu L D, Ning J S, Yang Z C, Liu C F. Research on the characteristics of cutting force signal and chip in ultrasonic vibration-assisted milling of titanium alloys. Journal of Mechanical Engineering, 2019, 55(7): 207–216 (in Chinese)
61. Verma G C, Pandey P M, Dixit U S. Estimation of workpiece-temperature during ultrasonic-vibration assisted milling considering acoustic softening. International Journal of Mechanical Sciences, 2018, 140: 547–556
62. Xu X X, Mo Y L, Liu C S, Zhao B. Drilling force of SiC particle reinforced aluminum-matrix composites with ultrasonic vibration. Key Engineering Materials, 2009, 416(21): 243–247
63. Zhang L B, Wang L J, Liu X Y, Zhao H W, Wang X, Luo H Y. Mechanical model for predicting thrust and torque in vibration drilling fibre-reinforced composite materials. International Journal of Machine Tools and Manufacture, 2001, 41(5): 641–657
64. Zhao B, Chen F, Tong J L. Theoretical and experimental research on material removal rate under ultrasonic grinding. Journal of Henan Polytechnic University, 2013, 32(3): 302–307
65. Kaynak Y, Gharibi A, Yilmaz U, Köklü U, Aslantaş K. A comparison of flood cooling, minimum quantity lubrication and high pressure coolant on machining and surface integrity of titanium Ti-5553 alloy. Journal of Manufacturing Processes, 2018, 34: 503–512
66. Yan P, Rong Y M, Wang X B, Zhu J Y, Jiao L, Liang Z Q. Effect of cutting fluid on precision machined surface integrity of heat-resistant stainless steel. Proceedings of the Institution of Mechanical Engineers, Part B: Journal of Engineering Manufacture, 2018, 232(9): 1535–1548
67. Pecat O, Brinksmeier E. Tool wear analyses in low frequency vibration assisted drilling of CFRP/Ti6Al4V stack material. Procedia CIRP, 2014, 14: 142–147
68. Adithan M. Tool wear studies in ultrasonic drilling. Wear, 1974, 29(1): 81–93
69. Wang D Z, Wu S J, Lin J P, Guo G Q, Wang P. Research on ultrasonic elliptical vibration micro-cutting Inconel 718 based on minimum quantity lubrication. Journal of Mechanical Engineering, 2021, 57(9): 264–272 (in Chinese)
70. Verma G C, Pandey P M, Dixit U S. Modeling of static machining force in axial ultrasonic-vibration assisted milling considering acoustic softening. International Journal of

Mechanical Sciences, 2018, 136: 1–6
71. Cao Y, Yin J F, Ding W F, Xu J H. Alumina abrasive wheel wear in ultrasonic vibration-assisted creep-feed grinding of Inconel 718 nickel-based superalloy. Journal of Materials Processing Technology, 2021, 297: 117241
72. Klocke F, Eisenblätter G. Dry cutting. CIRP Annals, 1997, 46(2): 519–526
73. Yang J Z, Wang C Y, Yuan Y H, Yuan S M, Wang X B, Lang C L, Li W Q. State-of-the-art on MQL synergistic technologies and their applications. China Mechanical Engineering, 2022, 33(5): 506–528 (in Chinese)
74. Race A, Zwierzak I, Secker J, Walsh J, Carrell J, Slatter T, Maurotto A. Environmentally sustainable cooling strategies in milling of SA516: effects on surface integrity of dry, flood and MQL machining. Journal of Cleaner Production, 2021, 288: 125580
75. Gaitonde V N, Karnik R S, Davim J P. Minimum Quantity Lubrication in Machining. John Wiley & Sons, Inc., 2013
76. Höhn B R, Michaelis K. Influence of oil temperature on gear failures. Tribology International, 2004, 37(2): 103–109
77. Yuan S M, Han W L, Zhu G Y, Hou X B, Wang L. Recent progress on the efficiency increasing methods of minimum quantity lubrication technology in green cutting. Journal of Mechanical Engineering, 2019, 55(5): 175–185 (in Chinese)
78. Weinert K, Inasaki I, Sutherland J W, Wakabayashi T. Dry machining and minimum quantity lubrication. CIRP Annals, 2004, 53(2): 511–537
79. Shao Y M, Fergani O, Li B Z, Liang S Y. Residual stress modeling in minimum quantity lubrication grinding. The International Journal of Advanced Manufacturing Technology, 2016, 83(5–8): 743–751
80. Han C C. Research on single crystal diamond turning technology of titanium alloy under nanofluids minimum quantity lubrication. Dissertation for the Doctoral Degree. Harbin: Harbin Institute of Technology, 2019 (in Chinese)
81. Zhang Y B. Grinding mechanism,force prediction model and experimental validation of vegetable oil based nanofluids minimum quantity lubrication. Dissertation for the Doctoral Degree. Qingdao: Qingdao University of Technology, 2018 (in Chinese)
82. Yıldırım Ç V. Experimental comparison of the performance of nanofluids, cryogenic and hybrid cooling in turning of Inconel 625. Tribology International, 2019, 137: 366–378
83. Yıldırım Ç V, Sarıkaya M, Kıvak T, Şirin Ş. The effect of addition of hBN nanoparticles to nanofluid-MQL on tool wear patterns, tool life, roughness and temperature in turning of Ni-based Inconel 625. Tribology International, 2019, 134: 443–456
84. Singh T, Dureja J S, Dogra M, Bhatti M S. Machining performance investigation of AISI 304 austenitic stainless steel under different turning environments. International Journal of Automotive and Mechanical Engineering, 2018, 15(4): 5837–5862
85. Anand N, Kumar A S, Paul S. Effect of cutting fluids applied in MQCL mode on machinability of Ti–6Al–4V. Journal of Manufacturing Processes, 2019, 43: 154–163
86. Das A, Patel S K, Das S R. Performance comparison of vegetable oil based nanofluids towards machinability improvement in hard turning of HSLA steel using minimum quantity lubrication. Mechanics & Industry, 2019, 20(5): 506–526
87. Said Z, Gupta M, Hegab H, Arora N, Khan A M, Jamil M, Bellos E. A comprehensive review on minimum quantity lubrication (MQL) in machining processes using nano-cutting fluids. The International Journal of Advanced Manufacturing Technology, 2019, 105(5–6): 2057–2086
88. Roushan A, Rao U S, Patra K, Sahoo P. Performance evaluation of tool coatings and nanofluid MQL on the micro-machinability of Ti–6Al–4V. Journal of Manufacturing Processes, 2022, 73: 595–610
89. Kaynak Y. Evaluation of machining performance in cryogenic machining of Inconel 718 and comparison with dry and MQL machining. The International Journal of Advanced Manufacturing Technology, 2014, 72(5–8): 919–933
90. Ni J, Cui Z, Wu C, Sun J B, Zhou J H. Evaluation of MQL broaching AISI 1045 steel with sesame oil containing nano-particles under best concentration. Journal of Cleaner Production, 2021, 320: 128888
91. Gao D Q, Zeng X J, He N R, Jia J H, Gao S S. Application of low temperature cutting technology in the processing of difficult materials. Manufacturing Technology and Machine Tool, 2020(6), 39–43
92. Shokrani A, Dhokia V, Newman S T. Investigation of the effects of cryogenic machining on surface integrity in CNC end milling of Ti–6Al–4V titanium alloy. Journal of Manufacturing Processes, 2016, 21: 172–179
93. Fernández D, Sandá A, Bengoetxea I. Cryogenic milling: study of the effect of CO_2 cooling on tool wear when machining Inconel 718, Grade EAIN steel and Gamma TiAl. Lubricants, 2019, 7(1): 10
94. Mulyana T, Rahim E A, Md Yahaya S N. The influence of cryogenic supercritical carbon dioxide cooling on tool wear during machining high thermal conductivity steel. Journal of Cleaner Production, 2017, 164: 950–962
95. Jozić S, Bajić D, Celent L. Application of compressed cold air cooling: achieving multiple performance characteristics in end milling process. Journal of Cleaner Production, 2015, 100: 325–332
96. Chaabani S, Arrazola P J, Ayed Y, Madariaga A, Tidu A, Germain G. Comparison between cryogenic coolants effect on tool wear and surface integrity in finishing turning of Inconel 718. Journal of Materials Processing Technology, 2020, 285: 116780
97. Khan A M, Anwar S, Jamil M, Nasr M M, Gupta M K, Saleh M, Ahmad S, Mia M. Energy, environmental, economic, and technological analysis of Al-GnP nanofluid-and cryogenic LN_2-assisted sustainable machining of Ti–6Al–4V alloy. Metals, 2021, 11(1): 88
98. Khan A M, Zhao W, Li L, Alkahtani M, Hasnain S, Jamil M, He N. Assessment of cumulative energy demand, production cost, and CO_2 emission from hybrid CryoMQL assisted machining. Journal of Cleaner Production, 2021, 292: 125952
99. Liu M Z, Li C H, Zhang Y B, An Q L, Yang M, Gao T, Mao C, Liu B, Cao H J, Xu X F, Said Z, Debnath S, Jamil M, Ali H M,

Sharma S. Cryogenic minimum quantity lubrication machining: from mechanism to application. Frontiers of Mechanical Engineering, 2021, 16(4): 649–697

100. De Chiffre L, Andreasen J L, Lagerberg S, Thesken I B. Performance testing of cryogenic CO_2 as cutting fluid in parting/grooving and threading austenitic stainless steel. CIRP Annals, 2007, 56(1): 101–104
101. Chen B, Xiong F X, Tang H Q, He L, Hu S S. Effect of cooling method on small diameter blind-hole drilling of new β-type dental Ti-Zr-Nb alloy. Journal of Manufacturing Processes, 2020, 59: 421–431
102. Damir A, Shi B, Attia M H. Flow characteristics of optimized hybrid cryogenic-minimum quantity lubrication cooling in machining of aerospace materials. CIRP Annals, 2019, 68(1): 77–80
103. Schulz H, Moriwaki T. High-speed machining. CIRP Annals, 1992, 41(2): 637–643
104. Krishnaraj V, Samsudeensadham S, Sindhumathi R, Kuppan P. A study on high-speed end milling of titanium alloy. Procedia Engineering, 2014, 97: 251–257
105. Ginting A, Nouari M. Experimental and numerical studies on the performance of alloyed carbide tool in dry milling of aerospace material. International Journal of Machine Tools and Manufacture, 2006, 46(7–8): 758–768
106. Li A H, Zhao J, Luo H B, Pei Z Q, Wang Z M. Progressive tool failure in high-speed dry milling of Ti–6Al–4V alloy with coated carbide tools. The International Journal of Advanced Manufacturing Technology, 2012, 58(5–8): 465–478
107. Li A H, Zhao J, Luo H B, Zheng W. Machined surface analysis in high-speed dry milling of Ti–6Al–4V alloy with coated carbide inserts. Advanced Materials Research, 2011, 325: 412–417
108. Li A H, Zhao J, Zhou Y H, Chen X X, Wang D. Experimental investigation on chip morphologies in high-speed dry milling of titanium alloy Ti–6Al–4V. The International Journal of Advanced Manufacturing Technology, 2012, 62(9–12): 933–942
109. Safari H, Sharif S, Izman S, Jafari H. Surface integrity characterization in high-speed dry end milling of Ti–6Al–4V titanium alloy. The International Journal of Advanced Manufacturing Technology, 2015, 78(1–4): 651–657
110. Sharif S, Safari H, Izman S, Kurniawan D. Effect of high-speed dry end milling on surface roughness and cutting forces of Ti–6Al–4V ELI. Applied Mechanics and Materials, 2014, 493: 546–551
111. Niu Q L, Chen M, Ming W W, An Q L. Evaluation of the performance of coated carbide tools in face milling TC6 alloy under dry condition. The International Journal of Advanced Manufacturing Technology, 2013, 64(5–8): 623–631
112. Liu J, Zhu S S, Deng X, Liu J Y, Wang Z P, Qu Z. Cutting performance and wear behavior of AlTiN- and TiAlSiN-coated carbide tools during dry milling of Ti–6Al–4V. Acta Metallurgica Sinica, 2020, 33(3): 459–470
113. Zhou J. Research on correlation technique and mechanism of high-speed cutting Ni-based superalloy GH4169. Dissertation for the Doctoral Degree. Harbin: Harbin Institute of Technology, 2012 (in Chinese)
114. Huang W M, Zhao J, Wang S Y. Necessity of multidimensional evaluation of the high-speed ball-end milled surface of hardened AISI D2 steel from a wear resistance perspective. The International Journal of Advanced Manufacturing Technology, 2019, 103(9–12): 4085–4093
115. Zheng G M, Cheng X, Li L, Xu R F, Tian Y B. Experimental investigation of cutting force, surface roughness and tool wear in high-speed dry milling of AISI 4340 steel. Journal of Mechanical Science and Technology, 2019, 33(1): 341–349
116. Li Y, Zheng G M, Zhang X, Cheng X, Yang X H, Xu R F. Cutting force, tool wear and surface roughness in high-speed milling of high-strength steel with coated tools. Journal of Mechanical Science and Technology, 2019, 33(11): 5393–5398
117. Zheng G M, Cheng X, Dong Y J, Liu H B, Yu Y Z. Surface integrity evaluation of high-strength steel with a TiCN-NbC composite coated tool by dry milling. Measurement, 2020, 166: 108204
118. Li H Z, Wang J. A study of cutting forces in high-speed dry milling of Inconel 718. Advanced Materials Research, 2012, 500: 105–110
119. Zhao B. Study on fabrication and properties of ceramic cutting tools for high-speed machining nickel-based superalloys. Dissertation for the Doctoral Degree. Jinan: Shandong University, 2018 (in Chinese)
120. Kamdani K, Hasan S, Ashaary A F I A, Lajis M A, Rahim E A. Study on tool wear and wear mechanisms of end milling nickel-based alloy. Jurnal Tribologi, 2019, 21: 82–92
121. Molaiekiya F, Stolf P, Paiva J M, Bose B, Goldsmith J, Gey C, Engin S, Fox-Rabinovich G, Veldhuis S C. Influence of process parameters on the cutting performance of SiAlON ceramic tools during high-speed dry face milling of hardened Inconel 718. The International Journal of Advanced Manufacturing Technology, 2019, 105(1–4): 1083–1098
122. Zhang Y L, Sun J F, Shen X, Chen W Y. Performance of PCBN tools in high-speed milling nickel-based superalloy. Materials Research Innovations, 2015, 19(sup1): S1-118–S1-125
123. Qiao Y, Fu X L, Yang X F. An experimental research of dry milling powder metallurgy nickel-based superalloy with coated carbide tools. Advanced Materials Research, 2012, 500: 38–43
124. Molaiekiya F, Aliakbari Khoei A, Aramesh M, Veldhuis S C. Machined surface integrity of Inconel 718 in high-speed dry milling using SiAlON ceramic tools. The International Journal of Advanced Manufacturing Technology, 2021, 112(7–8): 1941–1950
125. Şirin Ş, Sarıkaya M, Yıldırım Ç V, Kıvak T. Machinability performance of nickel alloy X-750 with SiAlON ceramic cutting tool under dry, MQL and hBN mixed nanofluid-MQL. Tribology International, 2021, 153: 106673
126. Zha J, Yuan Z L, Zhang H C, Li Y P, Chen Y L. Nickel-based alloy dry milling process induced material softening effect. Materials, 2020, 13(17): 3758
127. Lee C M, Kim D H, Baek J T, Kim E J. Laser assisted milling device: a review. International Journal of Precision Engineering and Manufacturing-Green Technology, 2016, 3(2): 199–208
128. Zeng H H. Research on the mechanism and surface integrity in laser-assisted milling of AerMet100 steel. Dissertation for the Doctoral Degree. Wuhan: Huazhong University of Science and

Technology, 2019 (in Chinese)
129. Singh R, Melkote S N. Hybrid laser-assisted mechanical micromachining (LAMM) process for hard-to-machine materials. Journal of Laser Micro Nanoengineering, 2007, 2(2): 156–161
130. Singh R, Melkote S N. Experimental characterization of laser-assisted mechanical micromachining (LAMM) process. In: Proceedings of the ASME 2005 International Mechanical Engineering Congress and Exposition. Orlando: ASME, 2005, 957–964
131. Jeon Y H, Pfefferkorn F. Effect of laser preheating the workpiece on micro end milling of metals. Journal of Manufacturing Science and Engineering, 2008, 130(1): 011004
132. Özel T, Pfefferkorn F. Pulsed laser assisted micromilling for die/mold manufacturing. In: Proceedings of the ASME 2007 International Manufacturing Science and Engineering Conference. Atlanta: ASME, 2007, 337–342
133. Cao X F, Woo W S, Lee C M. A study on the laser-assisted milling of 13-8 stainless steel for optimal machining. Optics & Laser Technology, 2020, 132: 106473
134. Bermingham M J, Kent D, Dargusch M S. Dargusch. A new understanding of the wear processes during laser assisted milling 17-4 precipitation hardened stainless steel. Wear, 2015, 328–329: 518–530
135. Meikote S, Kumar M, Hashimoto F, Lahoti G. Laser assisted micro-milling of hard-to-machine materials. CIRP Annals, 2009, 58(1): 45–48
136. Kumar M, Chang C J, Melkote S N, Roshan Joseph V. Modeling and analysis of forces in laser assisted micro milling. Journal of Manufacturing Science and Engineering, 2013, 135(4): 041018
137. Kadivar M, Azrhoushang B, Zahedi A, Müller C. Laser-assisted micro-milling of austenitic stainless steel X5CrNi18-10. Journal of Manufacturing Processes, 2019, 48: 174–184
138. Zeng H H, Yan R, Wang W, Zhang H, Yan J N, Peng F Y. Analytical modeling of the heat-affected zone in laser-assisted milling of AerMet100 steel. The International Journal of Advanced Manufacturing Technology, 2020, 109(9–12): 2481–2490
139. Kim D H, Lee C M. Experimental investigation on machinability of titanium alloy by laser-assisted end milling. Metals, 2021, 11(10): 1552
140. Sim M S, Lee C M. Determination of optimal laser power according to the tool path inclination angle of a titanium alloy workpiece in laser-assisted machining. The International Journal of Advanced Manufacturing Technology, 2016, 83(9–12): 1717–1724
141. Woo W S, Lee C M. A study on the optimum machining conditions and energy efficiency of a laser-assisted fillet milling. International Journal of Precision Engineering and Manufacturing-Green Technology, 2018, 5(5): 593–604
142. Woo W S, Lee C M. Laser-assisted milling of turbine blade using five-axis hybrid machine tool with laser module. International Journal of Precision Engineering and Manufacturing-Green Technology, 2021, 8(3): 783–793
143. Oh N S, Woo W S, Lee C M. A study on the machining characteristics and energy efficiency of Ti–6Al–4V in laser-assisted trochoidal milling. International Journal of Precision Engineering and Manufacturing-Green Technology, 2018, 5(1): 37–45
144. Hedberg G K, Shin Y C, Xu L. Laser-assisted milling of Ti–6Al–4V with the consideration of surface integrity. The International Journal of Advanced Manufacturing Technology, 2015, 79(9–12): 1645–1658
145. Wiedenmann R, Zaeh M F. Laser-assisted milling—process modeling and experimental validation. CIRP Journal of Manufacturing Science and Technology, 2015, 8: 70–77
146. Hedberg G K, Shin Y C. Laser assisted milling of Ti–6Al–4V ELI with the analysis of surface integrity and its economics. Lasers in Manufacturing and Materials Processing, 2015, 2(3): 164–185
147. Wiedenmann R, Liebl S, Zaeh M F. Influencing factors and workpiece's microstructure in laser-assisted milling of titanium. Physics Procedia, 2012, 39: 265–276
148. Kong X J, Yang L J, Zhang H Z, Zhou K, Wang Y. Cutting performance and coated tool wear mechanisms in laser-assisted milling K24 nickel-based superalloy. The International Journal of Advanced Manufacturing Technology, 2015, 77(9–12): 2151–2163
149. Tian Y G, Wu B X, Anderson M, Shin Y C. Laser-assisted milling of silicon nitride ceramics and Inconel 718. Journal of Manufacturing Science and Engineering, 2008, 130(3): 031013
150. Kim T W, Lee C M. Determination of the machining parameters of nickel-based alloys by high-power diode laser. International Journal of Precision Engineering and Manufacturing, 2015, 16(2): 309–314
151. Kim D H, Lee C M. A study on the laser-assisted ball-end milling of difficult-to-cut materials using a new back-and-forth preheating method. The International Journal of Advanced Manufacturing Technology, 2016, 85(5–8): 1825–1834
152. Kim E J, Lee C M. A study on the machining characteristics of curved workpiece using laser-assisted milling with different tool paths in Inconel 718. Metals, 2018, 8(11): 968
153. Wu X F, Zhu W B, Chen J F. Tool wear mechanisms in laser-assisted milling of nickel-based superalloys. Journal of the Brazilian Society of Mechanical Sciences and Engineering, 2021, 43(3): 151
154. Wu X F, Chen J F. The temperature process analysis and control on laser-assisted milling of nickel-based superalloy. The International Journal of Advanced Manufacturing Technology, 2018, 98(1–4): 223–235
155. Shang Z D, Liao Z R, Sarasua J A, Billingham J, Axinte D. On modelling of laser assisted machining: forward and inverse problems for heat placement control. International Journal of Machine Tools and Manufacture, 2019, 138: 36–50
156. Xu D D, Liao Z R, Axinte D, Sarasua J A, M'Saoubi R, Wretland A. Investigation of surface integrity in laser-assisted machining of nickel based superalloy. Materials & Design, 2020, 194: 108851
157. Brecher C, Emonts M, Rosen C J, Hermani J P. Laser-assisted milling of advanced materials. Physics Procedia, 2011, 12: 599–606
158. Zhang X Y, Lu Z H, Peng Z L, Zhang D Y. High quality and efficient ultrasonic vibration cutting of titanium alloys. Journal of Mechanical Engineering, 2021, 57(5): 133–147 (in Chinese)

159. Xue F, Zheng K, Liao W H, Shu J, Dong S. Investigation on fiber fracture mechanism of C/SiC composites by rotary ultrasonic milling. International Journal of Mechanical Sciences, 2021, 191: 106054
160. Chen W Q, Zheng L, Xie W K, Yang K, Huo D H. Modelling and experimental investigation on textured surface generation in vibration-assisted micro-milling. Journal of Materials Processing Technology, 2019, 266: 339–350
161. Zhang X Y, Zhang D Y, Sui H, Jiang X G. Influence of depth of cut on elliptical ultrasonic vibration cutting mechanism. ACTA Aeronauticaet Astronautica Sinica, 2017, 38(4): 420567
162. Lv D S, Xu J H, Ding W F, Fu Y C, Yang C Y, Su H H. Tool wear in milling Ti40 burn-resistant titanium alloy using pneumatic mist jet impinging cooling. Journal of Materials Processing Technology, 2016, 229: 641–650
163. Hsu C Y, Huang C K, Wu C Y. Milling of MAR-M247 nickel-based superalloy with high temperature and ultrasonic aiding. The International Journal of Advanced Manufacturing Technology, 2007, 34(9–10): 857–866
164. Fang B, Yuan Z H, Li D P, Gao L Y. Effect of ultrasonic vibration on finished quality in ultrasonic vibration assisted micromilling of Inconel 718. Chinese Journal of Aeronautics, 2021, 34(6): 209–219
165. Yuan Z H, Fang B, Zhang Y B, Wang F. Effect of cutting parameters on chips and burrs formation with traditional micromilling and ultrasonic vibration assisted micromilling. The International Journal of Advanced Manufacturing Technology, 2022, 119(3–4): 2615–2628
166. Suárez A, Veiga F, de Lacalle L N L, Polvorosa R, Lutze S, Wretland A. Effects of ultrasonics-assisted face milling on surface integrity and fatigue life of Ni-alloy 718. Journal of Materials Engineering and Performance, 2016, 25(11): 5076–5086
167. Suárez A, Veiga F, Polvorosa R, Artaza T, Holmberg J, de Lacalle L N L, Wretland A. Surface integrity and fatigue of non-conventional machined alloy 718. Journal of Manufacturing Processes, 2019, 48: 44–50
168. Su Y S, Li L. An investigation of cutting performance and action mechanism in ultrasonic vibration-assisted milling of Ti6Al4V using a PCD tool. Micromachines, 2021, 12(11): 1319
169. Su Y S, Li L. Surface integrity of ultrasonic-assisted dry milling of SLM Ti6Al4V using polycrystalline diamond tool. The International Journal of Advanced Manufacturing Technology, 2022, 119(9–10): 5947–5956
170. Gao H H, Ma B J, Zhu Y P, Yang H. Enhancement of machinability and surface quality of Ti–6Al–4V by longitudinal ultrasonic vibration-assisted milling under dry conditions. Measurement, 2022, 187: 110324
171. Xie W B, Wang X K, Liu E B, Wang J, Tang X B, Li G X, Zhang J, Yang L Q, Chai Y B, Zhao B. Research on cutting force and surface integrity of TC18 titanium alloy by longitudinal ultrasonic vibration assisted milling. The International Journal of Advanced Manufacturing Technology, 2022, 119(7–8): 4745–4755
172. Zhang C Y, Zhao B, Zhao C Y. Effect of ultrasonic vibration-assisted face milling on the surface microstructure and tribological properties. Journal of Vibroengineering, 2022, 24(1): 1–17
173. Xu L H, Na H B, Han G C. Machinablity improvement with ultrasonic vibration-assisted micro-milling. Advances in Mechanical Engineering, 2018, 10(12): 1687814018812531
174. Zhu L D, Ni C B, Yang Z C, Liu C F. Investigations of micro-textured surface generation mechanism and tribological properties in ultrasonic vibration-assisted milling of Ti–6Al–4V. Precision Engineering, 2019, 57: 229–243
175. Wang X B, Jiao F, Zhao C Y, Zhao B. Modeling and experimental analysis of cutting force in longitudinal–torsional ultrasonic-assisted milling of titanium. Advances in Mechanical Engineering, 2019, 11(4): 1687814019835107
176. Gao G F, Xia Z W, Su T T, Xiang D H, Zhao B. Cutting force model of longitudinal–torsional ultrasonic-assisted milling Ti–6Al–4V based on tool flank wear. Journal of Materials Processing Technology, 2021, 291: 117042
177. Rinck P M, Gueray A, Kleinwort R, Zaeh M F. Experimental investigations on longitudinal–torsional vibration-assisted milling of Ti–6Al–4V. The International Journal of Advanced Manufacturing Technology, 2020, 108(11–12): 3607–3618
178. Ren W F, Xu J K, Lin J Q, Yu Z J, Yu P, Lian Z X, Yu H D. Research on homogenization and surface morphology of Ti–6Al–4V alloy by longitudinal–torsional coupled ultrasonic vibration ball-end milling. The International Journal of Advanced Manufacturing Technology, 2019, 104(1–4): 301–313
179. Ahmed F, Ko T J, Kurniawan R, Kwack Y. Machinability analysis of difficult-to-cut material during ultrasonic vibration-assisted ball end milling. Materials and Manufacturing Processes, 2021, 36(15): 1734–1745
180. Tsai M Y, Chang C T, Ho J K. The machining of hard mold steel by ultrasonic assisted end milling. Applied Sciences, 2016, 6(11): 373
181. Maurotto A, Wickramarachchi C T. Experimental investigations on effects of frequency in ultrasonically-assisted end-milling of AISI 316L: a feasibility study. Ultrasonics, 2016, 65: 113–120
182. Razfar M R, Sarvi P, Zarchi M M A. Experimental investigation of the surface roughness in ultrasonic-assisted milling. Proceedings of the Institution of Mechanical Engineers, Part B: Journal of Engineering Manufacture, 2011, 225(9): 1615–1620
183. Sarvi Hampa P, Razfar M R, Malaki M, Maleki A. The role of dry aero-acoustical lubrication and material softening in ultrasonically assisted milling of difficult-to-cut AISI 304 steels. Transactions of the Indian Institute of Metals, 2015, 68(1): 43–49
184. Abootorabi Zarchi M M, Razfar M R, Abdullah A. Experimental investigation of chip formation and surface topology in ultrasonic-assisted milling of X20Cr13 stainless steel. In: Proceedings of the ASME 2013 International Manufacturing Science and Engineering Conference collocated with the 41st North American Manufacturing Research Conference. Madison: ASAM, 2013, V001T01A042
185. Ding H, Ibrahim R, Cheng K, Chen S J. Experimental study on machinability improvement of hardened tool steel using two dimensional vibration-assisted micro-end-milling. International Journal of Machine Tools and Manufacture, 2010, 50(12): 1115–1118
186. Abootorabi Zarchi M M, Razfar M R, Abdullah A. Influence of ultrasonic vibrations on side milling of AISI 420 stainless steel. The International Journal of Advanced Manufacturing Technology, 2013, 66(1–4): 83–89
187. Rao K V, Prasad V U S V, Ben B S. A comparative study on

cutting forces and power consumption in plain and ultrasonic vibration helical milling of AISI 1020 steel. Proceedings of the Institution of Mechanical Engineers, Part B: Journal of Engineering Manufacture, 2022, 236(13): 1726–1737

188. Ding H, Chen S J, Cheng K. Two dimensional vibration-assisted micro-milling: kinematics simulation, chip thickness computation and analysis. Advanced Materials Research, 2010, 97–101: 2779–2784
189. Qi B Y, He N, Li L, Zhao W, Bian R. Cryogenic minimum quantity lubrication technology and its action mechanism. Mechanical Science and Technology for Aerospace Engineering, 2010, 29(6): 826–831, 835 (in Chinese)
190. Pereira O, Rodríguez A, Barreiro J, Fernández-Abia A I, López-de-Lacalle L N. Nozzle design for combined use of MQL and cryogenic gas in machining. International Journal of Precision Engineering and Manufacturing-Green Technology, 2017, 4(1): 87–95
191. Ross N S, Gopinath C, Nagarajan S, Gupta M K, Shanmugam R, Kumar M S, Boy M, Korkmaz M E. Impact of hybrid cooling approach on milling and surface morphological characteristics of Nimonic 80A alloy. Journal of Manufacturing Processes, 2022, 73: 428–439
192. Pereira O, Català P, Rodríguez A, Ostra T, Vivancos J, Rivero A, López-de-Lacalle L N. The use of hybrid CO_2 + MQL in machining operations. Procedia Engineering, 2015, 132: 492–499
193. Nimel Sworna Ross K, Manimaran G, Anwar S, Rahman M A, Korkmaz M E, Gupta M K, Alfaify A, Mia M. Investigation of surface modification and tool wear on milling Nimonic 80A under hybrid lubrication. Tribology International, 2021, 155: 106762
194. Sterle L, Mallipeddi D, Krajnik P, Pušavec F. The influence of single-channel liquid CO_2 and MQL delivery on surface integrity in machining of Inconel 718. Procedia CIRP, 2020, 87: 164–169
195. Shokrani A, Dhokia V, Newman S T. Hybrid cooling and lubricating technology for CNC milling of Inconel 718 nickel alloy. Procedia Manufacturing, 2017, 11: 625–632
196. Shokrani A, Newman S T. Hybrid cooling and lubricating technology for CNC milling of Inconel 718 nickel alloy. Procedia CIRP, 2018, 77: 215–218
197. Şirin S, Yıldırım Ç V, Kıvak T, Sarıkaya M. Performance of cryogenically treated carbide inserts under sustainable cryo-lubrication assisted milling of Inconel X750 alloy. Sustainable Materials and Technologies, 2021, 29: e00314
198. Zhang S, Li J F, Wang Y W. Tool life and cutting forces in end milling Inconel 718 under dry and minimum quantity cooling lubrication cutting conditions. Journal of Cleaner Production, 2012, 32: 81–87
199. Bagherzadeh A, Kuram E, Budak E. Experimental evaluation of eco-friendly hybrid cooling methods in slot milling of titanium alloy. Journal of Cleaner Production, 2021, 289: 125817
200. Hanenkamp N, Amon S, Gross D. Hybrid supply system for conventional and CO_2/MQL-based cryogenic cooling. Procedia CIRP, 2018, 77: 219–222
201. Cai C Y, Liang X, An Q L, Tao Z R, Ming W W, Chen M. Cooling/lubrication performance of dry and supercritical CO_2-based minimum quantity lubrication in peripheral milling Ti–6Al–4V. International Journal of Precision Engineering and Manufacturing-Green Technology, 2021, 8(2): 405–421
202. Suhaimi M A, Yang G D, Park K H, Hisam M J, Sharif S, Kim D W. Effect of cryogenic machining for titanium alloy based on indirect, internal and external spray system. Procedia Manufacturing, 2018, 17: 158–165
203. Park K H, Yang G D, Suhaimi M A, Lee D Y, Kim T G, Kim D W, Lee S W. The effect of cryogenic cooling and minimum quantity lubrication on end milling of titanium alloy Ti–6Al–4V. Journal of Mechanical Science and Technology, 2015, 29(12): 5121–5126
204. Shokrani A, Al-Samarrai I, Newman S T. Hybrid cryogenic MQL for improving tool life in machining of Ti–6Al–4V titanium alloy. Journal of Manufacturing Processes, 2019, 43: 229–243
205. Su Y, He N, Li L. Effect of cryogenic minimum quantity lubrication (CMQL) on cutting temperature and tool wear in high-speed end milling of titanium alloys. Applied Mechanics and Materials, 2010, 34–35: 1816–1821
206. Song K H, Lim D W, Park J Y, Ha S J, Yoon G S. Investigation on influence of hybrid nozzle of CryoMQL on tool wear, cutting force, and cutting temperature in milling of titanium alloys. The International Journal of Advanced Manufacturing Technology, 2020, 110(7–8): 2093–2103
207. Ha S J, Kim D W, Kim J H, Park J Y, Song K H. Economic evaluation and machining performance in Ti–6Al–4V titanium alloy milling by integrated CO_2 & MQL injection system. Journal of Mechanical Science and Technology, 2021, 35(9): 4135–4142
208. Yuan Y H, Wang C Y, Yang J Z, Zheng L J, Xiong W Q. Performance of supercritical carbon dioxide ($scCO_2$) mixed with oil-on-water (OoW) cooling in high-speed milling of 316L stainless steel. Procedia CIRP, 2018, 77: 391–396
209. Wika K K, Litwa P, Hitchens C. Impact of supercritical carbon dioxide cooling with minimum quantity lubrication on tool wear and surface integrity in the milling of AISI 304L stainless steel. Wear, 2019, 426–427: 1691–1701
210. Manimaran G, Nimel Sworna Ross K. Surface behavior of AISI H13 alloy steel machining under environmentally friendly cryogenic MQL with PVD-coated tool. Journal of Testing and Evaluation, 2020, 48(4): 3269–3280
211. Zhang H P, Zhang Q Y, Ren Y, Shay T, Liu G L. Simulation and experiments on cutting forces and cutting temperature in high speed milling of 300M steel under CMQL and dry conditions. International Journal of Precision Engineering and Manufacturing, 2018, 19(8): 1245–1251
212. Zhang H P, Ding C L, Shi R X, Liu R H. Optimization of technological parameters and application conditions of CMQL in high-speed milling 300M steel. Integrated Ferroelectrics, 2021, 217(1): 141–153
213. Zhang S, Li J F, Lv H G. Tool wear and formation mechanism of white layer when hard milling H13 steel under different cooling/lubrication conditions. Advances in Mechanical Engineering, 2014, 6: 949308
214. Zhang C L, Zhang S, Yan X F, Zhang Q. Effects of internal cooling channel structures on cutting forces and tool life in side milling of H13 steel under cryogenic minimum quantity lubrication condition. The International Journal of Advanced Manufacturing Technology, 2016, 83(5–8): 975–984